4D Mapping of Network-Specific Pathological Propagation in Alzheimer's Disease

by

Rebecca Gail Canter
B.S. The Johns Hopkins University (2009)

Submitted to the Department of Brain and Cognitive Sciences
in Partial Fulfillment of the Requirements for the Degree of

Doctor of Philosophy

at the

MASSACHUSETTS INSTITUTE OF TECHNOLOGY

September 2016

Signature of Author Signature redacted
Department of Brain and Cognitive Sciences
June, 2013

Certified By Signature redacted
Li-Huei Tsai, Ph.D., D.V.M.
Director, The Picower Institute for Learning and Memory
Picower Professor of Neuroscience
Thesis Supervisor

Accepted By Signature redacted
Matthew A. Wilson, Ph.D.
Sherman Fairchild Professor of Neuroscience
Director of Graduate Education for Brain and Cognitive Sciences

4D Mapping of Network-Specific Pathological Propagation in Alzheimer's Disease

By

Rebecca Gail Canter

Submitted to the Department of Brain and Cognitive Sciences on June 13, 2016
in Partial Fulfillment of the Requirements for the Degree of
Doctor of Philosophy in Neuroscience

Abstract

Alzheimer's disease (AD) causes a devastating loss of memory and cognition for which there is no cure. Without effective treatments that slow or reverse the course of the disease, the rapidly aging population will require astronomical investment from society to care for the increasing numbers of AD patients. Additionally, the financial and emotional burden on families of affected individuals will be profound. Traditional approaches to the study of AD use either biochemical assays to probe cellular pathophysiology or non-invasive imaging platforms to investigate brain-wide network alterations. Though decades of research using these tools have advanced the field significantly, our increased understanding of AD has not led to successful interventions. One reason for this impediment may be that the tools used in neither approach can achieve the spatial and temporal precision necessary to study the consequences of molecular insults across the brain over time. In this thesis, I capitalize on recent advances in tissue processing technologies to gain a network-level perspective on the molecular and cellular progression of AD. First, I present optimized methods for *in situ* proteomic phenotyping of large-volume tissue specimens. Then, I use the techniques to map amyloid-beta (Aβ) aggregates at the whole-brain scale across disease stages in a mouse model of AD. The spatially-unbiased, temporally-precise map demonstrates hierarchical susceptibility of increasingly large, memory-related brain networks to Aβ deposition. Importantly, the 4D nature of the map reveals that subcortical nodes and white matter tracts of the Papez memory circuit exhibit unique, early vulnerability to Aβ aggregates. Finally, using large-volume labeling approaches, I confirm the molecular findings by showing disease-specific Aβ aggregation in human samples from the early hub regions. Together, this data unites desperate observations of network-level deficits and identifies critical locations of early Aβ deposition in the brain. By linking molecular and network observations, I begin to provide biological explanations for the clinical manifestation of AD. This perspective can guide earlier patient identification and refine experimental approaches to developing cognitively efficacious treatments. These discoveries emphasize the necessity of multi-level investigations in neuroscience research and highlight the potential impacts of tools that enable researchers to bridge the gap.

Thesis supervisor: Li-Huei Tsai, Ph.D., D.V.M.
Title: Director, The Picower Institute for Learning and Memory
Picower Professor of Neuroscience

“Then leaf subsides to leaf.
-Robert Frost

TABLE OF CONTENTS

Acknowledgements

This thesis culminates years of work, not only my own and my colleagues within the laboratories at MIT, but also on behalf of my teachers, mentors, friends, and family who have supported me in getting to this point. Without them, I would not be the researcher, thinker, or person that I am today, and I am eternally grateful for their contributions to this work.

First and foremost I must acknowledge Dr. Li-Huei Tsai, my advisor and mentor and without whom I would not have been able to write this thesis on multiple levels. I wish I could acknowledge each way in which Li-Huei has significantly impacted my life, but it would take too many pages to list each of the things I have learned from her mentorship, advice, and example. To Li-Huei – thank you for taking me in when I thought there was nothing left for me in science, and helping to rekindle the love of exploration and investigation that drove me to research. Thank you for your enthusiasm for science, your visionary questions, and your courage to pursue the most challenging projects. Working with you has changed my life. I cannot express how profound and important your mentorship has been throughout the journey to this thesis and how much I will cherish your influence as I move through my scientific career.

Next, I must acknowledge my family for their continual support of my exploration and wacky endeavors. They encouraged my earliest scientific inquiries (if you can call them that) and have endured the stress of my personal adventures as I've grown. Mom, Dad, and Matt – you are the best. No words written here can acknowledge what you have done for me. Thank you for always reminding me who I am and where I came from. To my 'extended' family who have always been a huge part of my life and championed my nerdiness since I was young – Nanny, Aunt Marsha, Uncle Michael, Uncle Mark, Aunt Nancy, Aunt Gail, Uncle Rob, Uncle Jimmy, and Aunt Sheila, and all of my cousins – it just doesn't get any better than this. And to Poppy who is always listening in – thank you for providing the motivation to keep going when things got hard.

Throughout my life I have the privilege of learning from some amazing teachers. In my earliest years Elaine Russeniello and Deborah V.H. Cook helped foster the sensitivity, inquisitiveness, and creativity that have influenced my character and love of science in immeasurable ways. In high school, two teachers in particular – Jennifer Mockensturm and Zachary Marks – took me under their wings and encouraged my curiosity. They let me explore areas outside our coursework and encouraged me to work beyond the books. Thank you for your continued confidence that I could accomplish anything I tried.

My undergraduate mentors set me off on the path of science. Dr. Gregory Ball, Dr. Peter Holland, and Dr. Alexander Johnson – thank you for providing me the opportunity, tools, and vocabulary to ask questions I never thought tractable and introducing me to neuroscience and behavioral research. The unique resources, ideas and information you taught me have truly shaped my intellectual interests and instilled the questions that have driven my pursuit of neuroscience.

At MIT, I have been fortunate to work with some of the best scientific minds. Learning from these incredible and accomplished professors how to ask and answer groundbreaking questions,

Acknowledgements

while also observing the personal and professional fortitude it takes to be successful has been invaluable. Thank you to Dr. Matthew Wilson, Dr. Kay Tye, Dr. Ivana Delalle, and Dr. Dava Newman for these lessons. Also, I must add a special acknowledgement to Dr. Kwanghun Chung whose mentorship contributed to my scientific and personal growth at MIT, and who taught me that positivity, optimism, and perseverance pay off.

In addition to working with Li-Huei, I have been fortunate to work in her laboratory filled with some of the most brilliant scientists on the planet. The Tsai lab is full of dedicated researchers who are also fun, thoughtful, and engaging colleagues. Without the technical advice, moral support, and insightful discussions from the entire lab, this thesis would have been an unconquerable beast. Ram, Jinsoo, Elizabeth, Ashley, Nina, Alison, Ying, Susan, Matt, Fatema, Jay, Chinna, Marco, and Hiruy deserve a special acknowledgement for their friendship and help. As do the incredible undergraduate women who worked with me – Christine Yao, Stephanie Bousleiman, and Kamilla Tekiela – your dedication, company, and insight have helped bring the findings in this thesis from ideas to fruition.

My graduate student friends and colleagues have been there every step of the way and made MIT a home away from home. I am lucky to have lived, played, and worked with you all. Meg, Joe, Stetner, Eitan, and Kean – it was a great run together. To Evan and Naveed, thank you for working long nights alongside me so I was rarely alone. To Corey and Zach – thank you for letting me word-vomit my day when I came home stressed and for expanding my culinary horizons. To Amy, Jo, Larissa, Shuyu, Dale, John, Glenn and the rest of the MIT Rowing Club – the camaraderie of the sport got me through the most difficult times in my life. I am lucky to have been a part of the team. To Leyla and Dan -- as fellow Blue Jays, Baker House GRTs, and friends, I may be most thankful to you for introducing me to CrossFit. To Susana, Tyler, Dom, and Tracy – although you haven't been graduate students for most (all) of the time I have known you, your support and our adventures and celebrations are some of my best memories from my time at MIT.

I am lucky to have made many great friends outside of MIT. Sarah, Andrea, and Katie – thank you for accepting my grad student lifestyle, sending constant encouragement and support, and providing a respite to normal life. You have kept me sane throughout. Amrit and Eddie – thank you for your wisdom, fun times, and good conversations that kept me grounded.

Living in Boston away from home I have also been lucky enough to stumble on to a family-away-from-home. Retsina and Reuben– thank you for everything. I could not have gotten here without you. Thank you for your support, encouragement, advice, adventures, and everything else I've missed.

Last, but certainly not least, Andrea. You are everything. Thank you for your optimism, for keeping it silly, and for your tactical and emotional support. Your love encourages me to be stronger, smarter, and more capable than I ever thought possible. Your inspiration helps me strive to make the world a better place each day.

Preface

The Costs of Mental Illness

In 2011, the World Economic Forum commissioned a report that indicated non-communicable diseases will cost the world nearly $47 trillion by 2030. Of this economic loss, the largest portion -- nearly 35% -- will be due to mental illnesses.[1] These diseases can occur in any stage of life and are often chronic, impacting affected individuals' abilities to function in society for long periods of time. Fortunately, the development of treatments for depression, anxiety, and schizophrenia[2] that can ameliorate disease symptoms has brought relief to many patients.[3] Though more work must be done to find drugs with better efficacy and specificity, especially for patients that do not respond to the currently available treatments, the success has affirmed that many mental illnesses are biologically tractable diseases for which there may be cures. However beyond the diseases for which drugs exist, there remain other mental illnesses that have no treatments or cures, and with mounting failures to develop efficacious drugs, the potential grows increasingly less certain.[4]

Dementias are a group of diseases that cause cognitive impairment and memory loss and have become the most costly mental illness for which there are no treatments or cures.[1,5] In 2010, nearly 15% of the US population had dementia at a cost of over $55,000 per affected individual. By 2040, conservative predictions estimate that dementias alone will cost the US nearly $400 billion[6], and although there are several types of dementia, including frontotemporal dementia, vascular dementia, Creutzfeldt-Jakob disease, and dementia with Lewy bodies, Alzheimer's disease (AD) is the most prevalent and will account for most of that cost.[7] Though the calculated economic costs of AD include care and account for the time spent by non-compensated caregivers (e.g. family members), they often do not reflect the emotional and physical toll that these diseases wreak on individuals throughout society.[7] These unquantifiable consequences of AD not only impact families, but also can lead to or exacerbate mental illnesses amongst the caregiving population. With few drug prospects and an aging population, the burden of AD will rise, and it is likely society has yet to fully realize the costs of rising AD prevalence. For neuroscientists, the wide-reaching impact of AD, alongside failed drug trails and mounting individual and societal costs, presents an opportunity to review our approach dementia research and potentially revolutionize the way medicine considers AD.

Traditional Approaches to AD Research

Since the discovery of AD-causative genes, research has focused on finding heritable mutations that predispose individuals to AD and the cellular consequences of those mutations.[8,9] Though this approach has provided insight to the molecular climates that drive neurodegeneration in AD, they have largely highlighted the role of observable hallmark pathologies and failed to explain cognitive deficits.[10] Furthermore, these studies have yet to account for variable correlations between pathology and memory loss, especially at the earliest clinical stages.[11] With increasing evidence that observable AD pathology is not informative for cognitive decline,[11] and that therapeutically rescuing burden does not improve cognition,[12,13] research has shifted to examine the cellular changes that underlie the disease.[14] Indeed,

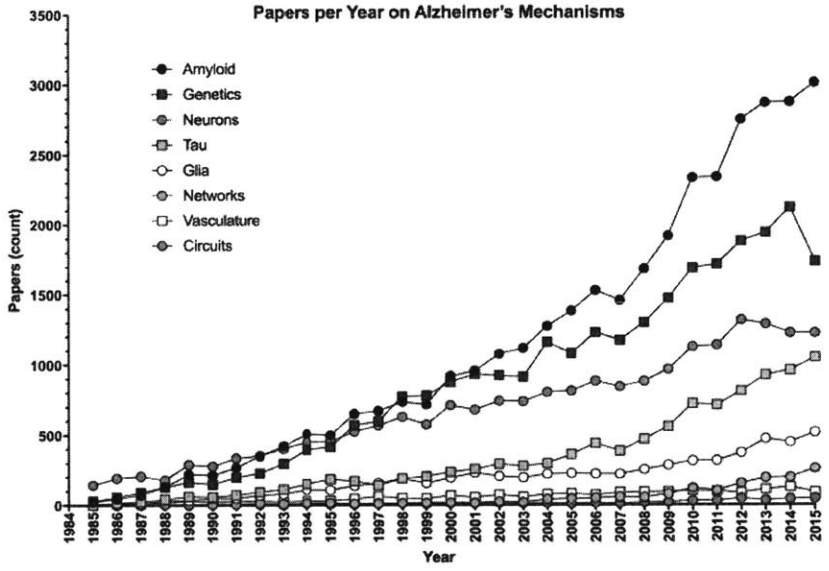

Figure 1. Papers published per year on putative mechanisms of Alzheimer's disease pathogenesis. Numbers were taken from 'Results by year' graph that accompanies Pubmed.gov search results of "Alzheimer's [xx]". [xx] is the search term indicated in the legend. If the 'Results by year' data were not available, numbers were tabulated from the search data. Papers including multiple search terms will be represented in each category.

while investigation of AD genetics and the hallmark AD pathologies – amyloid beta (Aβ) aggregates and hyperphosphorylated neurofibrillary tau tangles (NFT) – by number of papers published per year remains high (Fig. 1), studies looking at the cellular contributions to disease progression are increasing (Fig. 1), largely due to renewed interest in glia over the last decade. Studies of cellular mechanisms together surpass examinations of AD genetics (Fig. 2). Though this is a promising shift towards a functional

understanding of AD-related pathophysiological processes, an understanding of how cellular-level alterations impact cognition is still untenable. Instead, circuit- and network-based studies are beginning to

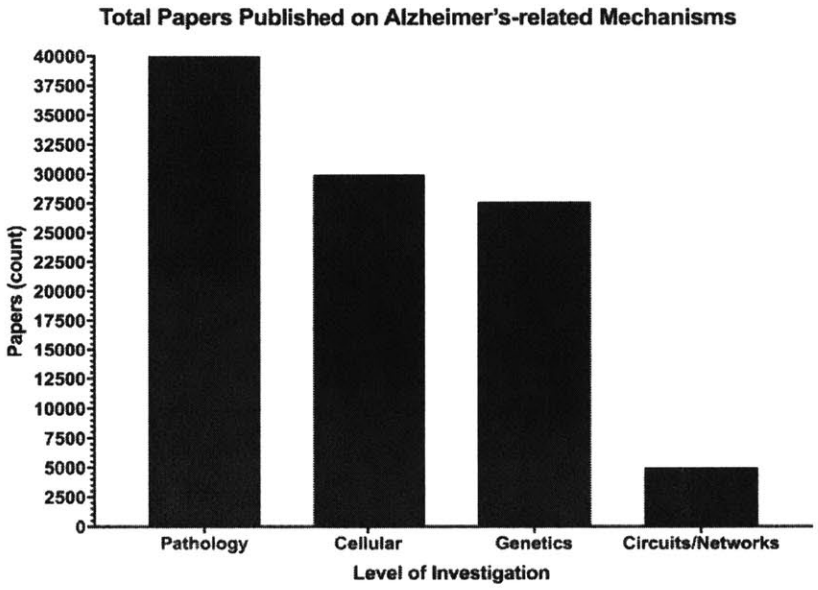

Figure 2. Total papers published on AD-related mechanisms at each level of basic neuroscience investigation. Pathology: tau, amyloid; Cellular: neurons, glia, vasculature; Genetics: genetics; Circuits/Networks: circuits, networks, white matter.

illuminate how brain activity drives memory and behavior. Unfortunately, network- and cellular-level studies are lacking in the AD field, with nearly 5-fold fewer papers published on the topic (Fig. 2).

A Circuit and Network Perspective of AD

At its core, AD is episodic memory impairment.[15] This impairment starts as an anterograde amnesia for specific events, and progresses to a loss of long-term memory recall. The loss of cognitive function and progression are core criteria for diagnosis,[5] and importantly, the loss of episodic recall (remembering details of the event) seems to be specific for AD, whereas recognition memory (familiarity with an event or person) impairments are typical of multiple amnesic dementias.[15–17] This is important because in humans, identifying which brain regions is possible with high resolution magnetic resonance imaging (MRI), and studies of structural connectivity in patients with mild cognitive impairment (MCI), a

prodromal stage of AD, suggest that neural connections shifts to compensate when recall circuits have damage.[18] Thus, unlike pathological burden which occurs non-specifically across dementias and poorly correlates to memory function,[19] network-level investigations are beginning to reveal disease-specific alterations that do correspond to observed patient deficits.

There is a lot of evidence for circuit and network disruption in AD, and increasing studies suggest that network deficits are consistent between human patient observations and preclinical murine models. For example, in AD-like mouse models of amyloidosis, a core region of learning and memory, the hippocampus (HPC), demonstrates marked hyperexcitability.[20] This effect recapitulates seizure-like activity seen in AD patients[21], and rescue of this hyperexcitability in both mice and humans improved cognition.[22,23] Although these experiments lack the molecular specificity of targeted cellular interventions, it is likely that the physiological changes in AD result from complex and widespread alterations that are not amenable to such specific treatments. This is likely to be particularly true at the later stages of memory loss, before which pathological burden had plateaued for many years.[24] Moving towards a network-understanding of AD may provide avenues for interventions that bypass the need for molecular specificity, and with emerging technologies it is possible that these can be targeted directly to the brain with high chances for cognitive efficacy in the absence of off-target systemic side effects. Furthermore, because network dysfunction results from and drives cellular and molecular changes, optimizing this framework will inevitably provide new information on specific, druggable molecular targets, bringing the field closer to treatments and cures.

Addressing the Multifaceted Etiology of AD

In addition to long-range networks within the brain, understanding how peripheral biological influences and lifestyle factors contribute to AD is critical. Lifetime experience factors like education, diet, and socioeconomic status greatly impact cognition with aging, and may increase risk for AD.[6,25,26] Additionally, studies demonstrating links between peripheral inflammation and AD suggest that despite its relative immune privilege from the blood brain barrier, factors outside of the brain influence its function. This is not surprising, as research into neuroendocrinology and metabolism demonstrate clear roles for peripheral signals in controlling brain function, however how these influences related to AD remain uncertain. Some evidence for the role of these factors in AD susceptibility comes from insulin and obesity studies, which suggest that diabetes and high adiposity increase AD risk[27], however causal links between these factors and cognitive decline are lacking.

Thesis Overview

This thesis seeks to establish the importance of network-specific investigations in AD by developing tools for their unbiased characterization and using those tools to identify specific circuits that are vulnerable to novel pathologies. The first chapter presents a perspective that elaborates on the role of pathological observations and circuit and network research to progress AD therapeutic goals. Then, the second chapter outlines the technical specifications for large tissue specimen proteomic analyses techniques we worked to develop and optimize including: sample preparation, imaging, and quantification techniques. The concluding work highlights the utility of the tools for both preclinical and patient research, and uses the protocols to create an unbiased map of AD pathological progression. The data demonstrates network-specific spread of AD pathology and identifies novel diencephalic regions of the Papez long-term memory circuit as particularly vulnerable to early pathological burden, and that this susceptibility results in physiological impairment. Furthermore, the 3D nature of the data show, for the first time, specific white matter affliction of a particular long-range tract, the fornix, which connects the major nodes of the Papez circuit. This data is confirmed in human postmortem specimens, which demonstrate that the regions identified in the murine models also show disease-specific pathology throughout the AD progression spectrum, indicating this may be a useful biomarker of early AD in the patient population. The thesis concludes with a summary of the potential impact and a hypothesis that future work to understand the contributions of the Papez circuit hubs (particularly the mammillary bodies and fornix) to memory and mechanisms of pathological AD propagation in this system will shed light on the earliest stages of the disease and may provide a unifying framework onto which researchers can map the increasingly complex pathophysiology of AD.

Chapter 1: Introduction

The complex road to restoring circuits for the treatment of Alzheimer's disease.[a]

Preface

Alzheimer's disease (AD) is a progressive loss of memory and cognition for which there is no cure. While genetic studies initially suggested a primary role for amyloid-beta (Aβ) in AD, Aβ-targeted treatment strategies have failed to ameliorate cognitive symptoms. These clinical results suggest cognitive decline results from complex pathophysiology, and Aβ treatment alone may not be sufficient to treat the disease. This review discusses evidence that pathophysiological mechanisms outside the amyloidogenic pathway contribute to systemic dysfunction, cognitive decline, and Aβ accumulation and proposes that a broad outlook on circuit-damaging pathologies in AD will yield new insights to therapeutic strategies.

Contributions:
R.G.C & L-H.T. came up with the idea and curated the content.
R.G.C wrote the initial draft of the document and generated the figures.
J.P. helped edit the manuscript and wrote the initial draft of the HDAC2 paragraph.

[a] This chapter was accepted as a review article in the journal Nature on August 3, 2016. The citation for this publication is: Canter, RG, Penney, J, Tsai, L-H. The complex road to restoring circuits for the treatment of Alzheimer's disease. Nature. *In Press.*

Introduction

Age related dementias will affect almost 10% of the population, and place a tremendous burden on affected individuals and their families.[6] The most prevalent type of dementia, Alzheimer's disease (AD), is a devastating, progressive loss of cognition for which there is no treatment or cure. Analyses of AD patients' brains suggest that extracellular aggregates of amyloid beta peptides (Aβ), intracellular inclusions of tau-rich neurofibrillary tangles (NFT), and the appearance of neuritic plaques (NP) are pathological hallmarks of the disease, yet there is no conclusive link between these observations and the cognitive symptoms[28]. The inability to definitively connect progressive memory loss to pathological biomarkers is a huge impediment in the quest for effective AD therapeutics, but enhanced efforts to understand mechanisms of cognitive decline are beginning to reveal new avenues for intervention.

The insidious onset of AD-related memory loss has hampered etiological studies because cognitive symptoms emerge late in disease progression when there is already rampant Aβ deposition, NFT formation, and cellular death; each of which might contribute to memory loss.[10] Early genetic studies implicated Aβ as the primary causative factor because mutations in or duplications of amyloid precursor protein (*APP*)[29–32] and its processing pathway components presenilins 1 & 2 (*PS1, PS2*)[33–35] lead to inherited, early-onset AD. These breakthroughs laid the foundation for the amyloid cascade hypothesis, which postulates that the accumulation of Aβ peptides is the proximal event in the development of AD, that in turn leads to NFT pathology, neurodegeneration, and memory loss.[8] Corollary to this hypothesis, increased levels of Aβ in the brain-- due to excessive peptide generation or an inability to clear it-- underlie cognitive dysfunction, thus treatments to reduce Aβ load should improve cognition.[9] Surprisingly, despite extensive evidence for Aβ-driven neurodegeneration, all Aβ-targeted therapeutics have failed to reverse memory deficits or halt cognitive decline, even alongside significant Aβ reduction.[12] As the Aβ-modifying strategies for treating AD shift to preventing accumulation, refining drug targets, and improving compound design,[36,37] conceptual advances in functional AD pathophysiology, coupled with data from -omics technologies and brain imaging platforms, are highlighting other promising avenues.

Beyond the genes in the Aβ pathway, additional newly identified human genomic loci significantly increase the risk of AD. While studies link some of the genes to amyloid metabolism, many appear to function in cellular signaling pathways and the brain's immune system,[38] indicating the importance of atypical cellular responses to changing brain states in AD. Emerging functional data also shifts etiological focus from a neuron-centric view of the disease to an integrated outlook that acknowledges the synergistic

functions of the different cell types that make up the brain. Consistent with this holistic view, multiple pathophysiological processes in AD are interconnected and feedback and feed-forward to provoke a cycle dysfunction as the disease progresses.[14] The array of dysfunctional cellular processes ultimately affects neural circuit function and network connectivity,[39] and the aberrant circuit activity not only triggers additional cellular coping mechanisms, but may also propagate pathological spread to connected brain regions.

The complexity of the various interactions makes disentangling AD etiology a daunting task, however systematic examination of the genetic and cellular changes can provide mechanistic insight into the cascade of pathological events that occur during AD.[14] Importantly, however, only an understanding of how these alterations contribute to progressive network and circuit dysfunction will connect observable pathophysiology to biologically-abstract cognitive impairment. Additionally, identifying vulnerable networks and susceptibility nodes within them may hold clues to the disease origins and progression. This review will briefly explore the role of Aβ driven pathogenesis in AD. Then, rooted in the newly identified genetic risk factors, will examine growing evidence for genetic, cellular, and circuit dysregulation as pathophysiological mechanisms that not only result from, but can also lead to, Ab accumulation, tau aggregation, and cognitive impairment. With this perspective, the field can move past unsuccessful Aβ-targeted clinical trials towards implementing a multipronged approach to treatment including cellular- and circuit-level therapeutic strategies.

AD through the amyloid hypothesis lens.

Familial genetics implicate Aβ in AD pathogenesis.

The most compelling evidence for the central role of Aβ in AD comes from studies of familial Alzheimer's disease (FAD). FAD cases account for 5%[40] of the patient population and results from pathogenic, autosomal dominant mutations or duplications in *APP*, or mutations in genes for γ-secretase components presenilin-1 (*PS1*) and presenilin-2 (*PS2*)[30,33,34]. *APP*, *PS1*, and *PS2* mutations shift APP processing (see Box 1) to the amyloidogenic pathway and bias cleavage towards the longer, toxic Aβ species[41,42]. The mechanism of *APP* duplication toxicity is less clear, however FAD-related *APP* duplications exist[43,44], and individuals with Down syndrome (DS), who have 3 copies of the *APP* gene, also develop early onset AD[45,46]. Thus, despite differences in the specific location, mutation, or gene, heritable changes that either qualitatively or quantitatively increase longer Aβ species cause AD. Alternatively, mutations in the *MAPT* gene encoding tau, the other major pathological feature of AD, usually result in frontotemporal dementia, a similar but ultimately different disease.[47–49] Further implicating Aβ, mutations in *APP* that do not increase Aβ do not appear to be pathogenic, and may confer

protection from AD. One recently identified *APP* variant in the Icelandic population reduces amyloidogenic processing and protects against AD and normal age-related cognitive decline[50]. This suggests the relationship between Aβ levels and cognitive impairment is bidirectional, and the genetic data strongly support the idea that accumulation of Aβ, especially the longer forms, plays an important etiological role in AD-related cognitive decline.

Aβ impairs synapses and destabilizes circuits.

Aβ peptides can exert multiple detrimental effects on neurons as well as the other cell types that make up the brain (Figure 1)[14]. Though neurons primarily transmit information throughout the brain, glia also make significant contributions to signal propagation and modulation, especially at the synapse; thus any discussion of circuit changes in AD must incorporate activities of these cells too[51,52]. In addition to modifying communication, many non-neural cells support neuronal health and thus participate in Aβ clearance to protect neuronal function during disease progression. For example, astrocytes and microglia are the major source of apolipoprotein E (ApoE)[53–55], a protein for which allelic variation confers risk of developing AD. ApoE isoforms differentially facilitate Aβ clearance into astrocytes or through the vasculature, and the ε4 variant impairs this ability and reduces Aβ clearance, which augments its parenchymal levels[56,57]. Similarly, microglia are brain-resident myeloid-lineage cells that have phagocytotic capability[58]. Though it remains controversial whether microglia or blood-derived macrophages degrade Aβ in AD (but see ref [59]), microglial responses seem to affect aggregate levels and the cells themselves are capable of uptaking Aβ, suggesting they play a role[60,61]. Though oligodendrocyte fate in AD is less certain, the main component of the myelin they produce to ensheathe axons, myelin basic protein (MBP), may aid Aβ clearance.[62] Ultimately a complete characterization of non-neural Aβ–induced AD pathophysiology is lacking, however it is likely that disruptions in the normal functions of these cells impact neuronal health and circuit dynamics.

As an acutely toxic species, oligomeric Aβ (oAβ) directly incites neuronal apoptosis via interactions with cell surface receptors, and Aβ accumulation indirectly leads to oxidative damage of DNA and proteins, injured organelles, and dysregulated internal calcium (Ca^{2+}) levels, which can also provoke cellular death. *In vitro*, Aβ exposure induces neuronal dysfunction and can cause death within hours[63]. Although *in vivo* these pathogenic processes take years to have detectable consequences, widespread neuronal loss in the brain accompanies the onset of severe cognitive decline[24]. Though neuronal death has profound impacts on memory performance, deficits in synaptic plasticity, circuit function, and cognition all develop well before cellular loss occurs[39]. Indeed, synapse loss occurs before overt pathological aggregates develop[64,65], and this loss demonstrably contributes to circuit dysfunction and cognitive decline in AD[20,66].

A large body of evidence indicates that amyloid plays an important physiological role at the synapse and that synaptic activity is a major source of parenchymal Aβ[67,68]. Excitatory activity promotes APP proteolysis and release into the extracellular space.[67–71] Once there, the effects of synaptic Aβ on excitatory activity vary with its extracellular concentration: low Aβ levels promote excitatory activity and higher levels depress it. Small elevations in Aβ promote activity via presynaptic acetylcholine receptors, which elevate internal Ca^{2+} concentrations to increase glutamate release probability.[72,73] Though the resulting postsynaptic excitation could result in positive feedback whereby additional Aβ release increases synaptic excitability, increasingly high levels actually depress activity through a number of synaptic-strength modifying mechanisms, including glutamate receptor internalization[74,75] (Figure 1). While acute elevations in synaptic Aβ can impair potentiation of synaptic strength (LTP) and promote depression (LTD)[76–79], long-term elevations can weaken connectivity, alter dendritic spine dynamics, promote synapse loss, and impair the processes that shape circuits and underlie learning and memory[69]. The loss of spines can lead to neuron-intrinsic hyperexcitability[66], and Aβ also alters excitatory tone by impairing inhibitory interneurons' abilities to affect excitatory cells. Loss of inhibition occurs through multiple pathways, including down-regulation of cell-surface voltage-gated sodium channel subunits. Indeed, lower Nav1.1 sodium channel subunit expression in AD-model mice hinders action potential propagation through inhibitory parvalbumin interneurons, resulting in reduced release of the primary inhibitory neurotransmitter, GABA, and the loss of inhibition on excitatory neurons[22].

With long-term pathological accumulation of Aβ, disinhibition of excitatory cells and synaptic loss result in hyperactivity, which occurs in some pre-symptomatic patients in brain regions associated with learning and memory[21]. Over time, this may lead to epileptiform activity and compensatory inhibitory sprouting, which can impair learning processes[20]. AD patients that have seizures exhibit worse cognitive outcomes[80]. Treating patients with inhibitory receptor agonists can reduce the abnormal activity and restore cognition, suggesting aberrant spiking is directly related to memory loss[23]. Interestingly, restoring inhibition in mouse models not only rescues local circuit dynamics, but also reinstates the observed loss of long-range network coherence to enhance learning[81].

Network susceptibility is key to Aβ pathogenesis.

Amyloid deposition is a critical event in AD pathogenesis therefore identifying the brain networks that are susceptible to Aβ-induced dysfunction should reveal how the disease propagates through the brain, and may explain how spreading Aβ accumulation contributes to cognitive symptoms. Initial cross-sectional studies of postmortem tissue created a hierarchical map of Aβ advance through the brain. This

led to the observation that Aβ deposition initiated within the neocortical regions involved in cognition, spread to neural hubs underlying learning and memory, and finally progressed to motor and sensory structures, and also provided a framework for understanding the successive deterioration of cognitive and sensory impairments[82]. Because they suggested the serial involvement of interconnected brain regions, but could not functionally demonstrate propagation through networks or provide critical insight to mechanisms of Aβ propagation, these observations paved the way for longitudinal studies of Aβ accumulation in patients.

The development of Aβ binding tracers, like [^{11}C]-Pittsburgh Compound B (PiB) and [^{17}F]-florbetapir, for positron emission tomography (PET) has enabled researchers to assess the pattern of Aβ deposition across the course of the disease[83,84] (Figure 2). Cross-sectional PET studies of AD patients confirm the neuropathological findings of significant Aβ throughout the neocortex, and importantly demonstrate the amount of cortical retention is predictive of cognitive decline[24,85]. This indicates that Aβ levels may be a good biomarker for AD.[86] The consistent locations of tracer retention across studies suggest that an AD-specific pattern of Aβ accumulation is a fundamental and necessary change to effect cognitive symptoms, and correlational and functional studies suggest that memory decline may relate to Aβ within regions of the Default Mode Network (DMN).[87] The DMN is a group of functionally connected brain regions that co-activate during passive thinking, remembering, and planning, and early investigations with PiB-PET demonstrated overlap between areas of high Aβ and DMN regions, suggesting the network may be vulnerable in AD.[88] Studies using functional connectivity magnetic resonance imaging (MRI) demonstrated DMN susceptibility by showing reduced connectivity within the network[87]. Interestingly, ~25% of cognitively healthy individuals highly retain PiB, and this correlates with reductions in DMN connectivity, worse episodic memory, and predicts dementia in follow up studies[89–91]. Together this evidence suggests that DMN alterations may be a proximal network dysfunction underlying cognitive impairment. Surprisingly, despite cognitive deterioration, further increases in Aβ levels over the conversion period from aMCI to AD are relatively modest, which is consistent with observations that AD patients show little retention differences throughout disease progression[92–95]. This data suggests that amyloid deposition may plateau at pathological levels long before the onset of cognitive symptoms.

Though human imaging studies suggest Aβ pathology precedes cortical network dysfunction, the techniques have yet to reveal precipitating patterns of amyloid accumulation or give insight to mechanisms of propagation. Some preclinical studies suggest Aβ may propagate in a prion-like manner and undergo cell-cell transmission[96,97], yet other studies suggest that Aβ-induced circuit dysfunction

affects network connectivity[81], and local aberrant activity may result in Aβ accumulation at projection target structures, creating the appearance of sequential spread through these networks. Whichever mechanism contributes to Aβ progression, the realization that Aβ pathology begins many years before overt memory loss and spreads through the brain increases the urgency of identifying the key nodes for early intervention.

Aβ-based treatments have yet to restore cognition.

Despite the complexities, it is clear that Aβ contributes to AD pathogenesis and its probable contributions to AD progression make it a prime target for therapeutic intervention (Figure 2). Because elevated Aβ levels likely underlie its pathogenicity, treatment strategies have emerged targeting the two determinants of Aβ load: aberrant generation and faulty clearance mechanisms.

Drugs to modulate β- or γ- secretase activity are primary therapeutic strategies to reduce Aβ generation by limiting amyloidogenic proteolysis, and phase II trials have identified a few safe first-generation pharmacologics for each enzyme.[98,99] However, these trials have mostly failed due to problems with target specificity, brain permeability, or study design without testing cognitive or Aβ outcomes[36,100]. The few trials that have reported primary outcomes show reductions in CSF markers of Aβ, but have conflicting cognitive results with some showing hastened decline[101]. Given the pharmacological setbacks and uninformative memory outcomes, it is difficult to conclude the feasibility of Aβ proteolytic targets as AD treatments. However, with redesigned clinical trials that utilize updated dosing and outcome design, and increased understanding of the complexity of the enzymatic functions of the targets, hope remains that the next generation of compounds will be safe and effective.

Enhancing Aβ clearance from the parenchyma is an alternative approach to modifying Aβ levels. The primary avenue to affect these processes has been immunization, employing both active and passive strategies. Early clinical trials investigating active immunization successfully reduced amyloid burden, but also caused severe side effects like brain swelling and hemorrhage[102]. The promising effects on Aβ levels has led to new generations of immunotherapies, which have advanced quickly through clinical trials. Patients generally tolerate the newer immunotherapies well and phase I/II clinical trials indicate successful Aβ reductions[103]. These significant Aβ clearance results are unfortunately tempered by cognitive performance outcomes that suggest these treatments may only successfully slow decline in prodromal or mild AD, and across different therapeutics, the efficacy even within this population is mixed[12,104]. Trails that performed extensive participant screening to select for patients that may be most responsive to Aβ therapies have been more successful, indicating that stratification of patient populations

may be necessary for testing treatments with different mechanisms of action[105]. As clinical trials advance through stages III/IV, more insight into the long-term cognitive outcomes may provide a better understanding of the efficacy of these strategies for long-term prognosis. Additionally, preventative trials to hinder early Aβ accumulation are underway, and should be informative of the primacy of Aβ toxicity to AD-related cognitive impairment.

Together, the results from Aβ-modifying clinical trials herald significant progress towards reducing Aβ burden. Though variable and slight, the cognitive benefits of these therapeutics suggest that decreasing Aβ levels slows AD progression. However, because the effects are seen early in the disease, and many patients seek treatment only once they experience memory loss, preventing further deterioration is only the first step in an effective treatment regimen. The identification of additional interventions that can restore cognitive function and treat cellular pathophysiology late in the disease will be critical to improve quality of life for AD patients and to avert the looming public health crisis.

Multiple factors induce network dysfunction in AD.

Genetic risk and dysregulation prime AD pathology.

AD cases that have no identifiable genetic cause account for >90% of patients and they usually develop symptoms late in life[40]. 'Sporadic' or late-onset AD (LOAD) patients experience amnesic memory loss and develop Aβ aggregates and NFTs similarly to FAD; however the levels of pathology in LOAD patients vary considerably[19,28]. Because individual variation is high, and multiple complex and interrelated processes can lead to Aβ accumulation and tau aggregation, understanding the mechanisms behind LOAD pathology has proven even more difficult than making sense of FAD dysfunction[14]. While functional studies of the Aβ protein in FAD models have yielded insight into the pathologic mechanisms of peptide accumulation, the description of additional intracellular functions for APP and PS, alongside the identification of increasing numbers of genetic risk alleles and regulatory mechanisms, has shed light on additional pathophysiological processes that may precipitate Aβ accumulation and NFT formation, and contribute to cognitive decline in AD.

Though FAD-related protein changes directly increase Aβ levels, they may also have consequences outside of altered APP proteolysis. Mutations in *APP*, *PS1*, and *PS2* may affect the proteins' other roles in cholesterol binding, cellular adhesion, cytoskeletal dynamics, ion homeostasis, endocytosis, and synaptic plasticity (for review: [106,107]) - all processes which can affect circuit properties. Mice lacking APP exhibit deficits in LTP induction, and also show age dependent cognitive decline[108,109]. Similarly, deletion of presenilins suggests they play critical roles in neural development, synaptic plasticity, and

memory performance, while FAD mutations affect their function as calcium leak channels in the endoplasmic reticulum[110,111]. Thus, though FAD-linked mutations in these proteins do clearly affect Aβ production, it is possible that disruption of their additional physiological functions also contributes to circuit dysfunction and memory impairment in AD.

The early identification of FAD-causative mutations intensified the search for additional genetic factors. Though no additional causative genes arose, multiple genetic loci do contribute to disease susceptibility. The most significant among these, and the earliest identified, was the ε4 allelic variant of apolipoprotein E (*ApoE*), which leads to at least ~3-4 fold increase in the likelihood of developing AD[112,113]. *ApoE4* carriers also show more profound amyloid pathology than non-carrier LOAD patients, clearly demonstrating that ApoE participates in Aβ regulation[114]. The initial association of ApoE and Aβ drew focus away from investigations into the contribution of variable ApoE lipid functions to cellular health and cognitive decline; however changes in membrane cholesterol content and lipid rafts in AD patient brains suggest alterations in these processes may be a major pathogenic mechanism[115]. The identification of additional genetic risk factors in recent years has underscored the potential relevance of these processes to cognitive decline.

The establishment of *ApoE* as a heritable, but not causative, genetic factor paved the way for large-scale patient screens to identify additional risk loci that increase individual susceptibility to AD. These studies strongly implicate genes involved in lipid metabolism and cholesterol homeostasis, cellular adhesion, cytoskeletal dynamics, ion regulation, vascularization and maintenance, transcriptional regulation, inflammation, and endocytosis[38,116–122]. To date, confirmation of a subset of the hits in functional experiments demonstrates that lipid processing, endocytosis, and inflammation may contribute substantially to AD pathogenesis[123–125]. Unlike *ApoE*, *APP*, and *PS*, the exact pathogenic gene variants and cellular consequences of alterations in these loci are largely unknown[38]; however the processes the genes support are important for maintenance of normal cellular function[126–128]. Though many of the implicated proteins appear to play roles in Aβ processing or clearance[38], they may also be important for molecular homeostasis, cellular function, and synaptic dynamics, all of which influence circuit activity and network connectivity[14,39].

In addition to encoded genetic risk factors, epigenetic mechanisms such as DNA methylation and histone acetylation can also alter gene expression, and can respond to both environmental influences and intrinsic factors that affect cellular metabolism or health. Indeed, LOAD patients show altered DNA methylation,

affecting multiple different AD risk loci[129,130]. The further association of methylation status at some of these loci with disease risk and cellular pathology confirms the functional significance of such alterations[131]. Studies in AD model mice suggest that disease progression is also associated with widespread shifts in epigenetic histone modifications in cells from the hippocampus, which is correlated with transcriptional repression of synaptic genes and an induction of immune genes.[132] Importantly, evolutionarily conserved immune gene regulatory regions with altered histone modification profiles are enriched for AD patient-identified genetic variants, supporting the genetic links between immune processes and AD risk[132]. Further insight into the basis of epigenetic changes associated with neuronal genes in AD comes from the observation of increased levels of histone deacetylase 2 (HDAC2), a critical negative regulator of synaptic plasticity, in both AD model mice and human patients.[133,134]

Beyond epigenetic regulation, other experiential factors like circuit activity and peripheral signaling can modulate genetic risk by acting on transcriptional components, which may also lead to fundamental changes in cellular homeostasis. One example of a protective transcription factor is repressor element 1-silencing transcription factor (REST, aka NRSF), which upregulates cellular protection pathways in aging[135]. Higher REST expression levels correlate with increased hippocampal volume, improved cognitive outcomes with age, and protection against Aβ toxicity; but levels decline with age. Though the reason for age-related decline of REST remains unclear, its time-dependent expression kinetics may provide clues to the influence of circuits in healthy aging because the protein itself is regulated by non-cell autonomous signaling, indicating an important role for neuronal communication and circuit function in neuroprotection against AD[135,136].

Intracellular pathophysiology impairs circuits.
Recently identified genetic loci pinpoint cellular processes that may be involved in AD pathogenesis, and highlight the importance of not only neurons, but also non-neuronal cells, in disease progression[14]. Considerable evidence supports the idea that loss of cellular homeostasis across brain-resident cell types can result in circuit dysfunction and cognitive impairment. The 'cellular phase' of AD refers to the time during which processes that participate in feedback and feed-forward loops result in cellular pathology, and aligns with the observation that Aβ deposition plateaus before the onset of memory symptoms.[14] Though cognition remains largely intact at the initiation of pathological deposition, it is likely that progressive changes during and following the cellular phase alter network connections and circuit activity to produce cognitive decline[39]. Because the events leading to Aβ aggregation in the absence of causative mutations remain vague, understanding the convergent cellular factors that affect circuit activity and

contribute to cognitive impairment, and which may also initiate Aβ accumulation, is crucial to restoring memory capacity in advanced AD.

Metabolic and mitochondrial functions are major determinants of brain health that play central roles in multiple neurodegenerative disorders, including AD[19]. Glucose-metabolizing mitochondria accumulate age-related damage that can reduce metabolic efficiency, increase reactive oxygen species (ROS) production, and induce cellular dysfunction. ROS oxidize proteins, induce lipid peroxidation, and increase levels of BACE1, which hinder gene expression, alter membrane content, and increase Aβ generation, respectively[137–140]. Another major effect of ROS is the induction of oxidative DNA damage, which can directly perturb gene expression and induce broad changes in chromatin structure[141]. Indeed, aging is associated with reduced expression and increased oxidative damage to the promoters of a subset of genes in the human brain, effects that are mimicked by direct induction of oxidative stress *in vitro*[142]. Furthermore, ROS can cause widespread relaxation of heterochromatin, a tightly packaged form of DNA that functions to repress certain portions of the genome.[143] A reduction in heterochromatin-associated marks was observed in AD patient brains, as well as in animals overexpressing tau protein, and correlated with expression of genes normally repressed in healthy individuals[143]. In addition to oxidative damage, DNA strand breaks can also be detected at very early stages of disease progression in AD mouse models and patients[144,145]. Interestingly, recent evidence suggests physiological breaks in DNA arise in response to neuronal activity and Aβ can exacerbate such damage.[146] Breaks that form during a learning event initiate transcription of genes important for learning and memory, suggesting the possibility that as DNA repair mechanisms fail with age, mutations and breaks may accumulate at plasticity-related loci to stunt cognition.[142,147] This suggests a direct link between neural circuit activity, DNA integrity, and memory. In addition to effects on DNA, mitochondria affect cellular energetics and damage to mitochondrial membranes can dysregulate cytosolic calcium levels[148]. These alterations perturb the intracellular milieu and can induce deficits in synaptic plasticity in neurons, and reactivity and excitability across all cell types.

Calcium (Ca^{2+}) critically mediates many intracellular events and its levels regulate synaptic plasticity and signal propagation[127]. Brain cells tightly regulate cytosolic Ca^{2+} levels via influx through cell surface Ca^{2+} channels and certain neurotransmitter receptors, and from Ca^{2+} stores in the endoplasmic reticulum (ER)[127]. In AD, multiple processes ranging from mitochondrial or plasma membrane damage to circuit hyperactivity and Aβ-induced Ca^{2+} influx across the plasma membrane can increase cytosolic Ca^{2+}, which may in turn trigger Ca^{2+} release from the ER. Interestingly, PS1 has been shown to be a key regulator of

ER Ca^{2+} release[111]. Furthermore, the AD risk gene *Slc24A4* encodes a potassium-dependent, Na^{+}/Ca^{2+} exchanger. While its impacts on cellular function remains unknown, *Slc24A4* mutations could alter cellular Ca^{2+} handling, thereby increasing LOAD risk[38]. Ca^{2+} can also induce pathologic signaling cascades; for example, Ca^{2+} mediated calpain cleavage of Cdk5 activator p35 to p25 regulates physiologic synaptic depression in neurons[149]. However, under pathologic conditions, enhanced p25-Cdk5 signaling results in HDAC2 increases, synaptic depression, spine loss, neurodegeneration, inflammation, and aberrant tau phosphorylation, which in mouse models also correlates with NFT-like pathology.[132,149,150] Elevated Ca^{2+} abundance in the cell can also produce ionic imbalance, facilitate aberrant presynaptic neurotransmitter release, and dysregulate postsynaptic signal transduction that ultimately alters gene regulation, cellular dynamics, and activity[73,127,149].

In the brain, cells span large distances and distal processes require transport of signaling molecules, nutrients, and organelles to and from the soma for proper functioning[126]. Dystrophic neurites and aggregated cytoskeletal proteins are hallmarks of AD and indicate that abnormalities arise in the maintenance of cellular structure[28]. One possible cause is the molecular insults that destabilize assemblies responsible for structural organization and subcellular traffic. In neurons, microtubules are the primary cytoskeletal protein, and the tubulin filaments serve as tracks on which molecular motors run. While the pathophysiological processes underlying neurite collapse remain uncertain, numerous studies demonstrate axonal transport deficits in AD[126]. These may result from destabilization of either the motor-vesicle associations or microtubule assemblies; it is likely both play a role in deficits and dystrophy[151,152].

The stability of microtubule assemblies depends on microtubule-associated proteins (MAP), and the tau protein found in NFT pathology in AD is an important MAP that dynamically binds within the microtubule network[153,154]. NFT pathology is requisite for AD diagnosis and the levels of NFT correlate well with AD progression and cognitive symptoms[28]. NFT result from assembly of hyperphosphorylated tau into paired helical filaments, which further combine inside neurites and soma to form mature pathology. tau binds microtubules in its unphosphorylated state, and site-specific phosphorylation weakens its microtubule binding capacity, making tau cytosolic and less soluble[153,154]. Dephosphorylation by PP2A phosphatases maintains appropriate tau dynamics, allowing it to actively bind to and release from the cytoskeletal network[155,156]. However, in AD, pathological processes like circuit hyperactivity and Ca^{2+} influx trigger aberrant tau phosphorylation by kinases like GSK3β, Cdk5, and (cAMP dependent protein kinase A (PKA), and induce concomitant dysfunction of PP2A that leads to tau hyperphosphorylation, insolubility, and aggregation[150,152,157]. tau may also regulate microtubule motor

activity and direction, and loss of tau may disrupt transport kinetics[158]. The demise of axonal transport impairs bidirectional signaling, reduces mitochondrial number at the synapse, and destabilizes actin--another cytoskeletal protein-- in distal, highly dynamic processes[158,159]. For many years, the assumed pathogenicity of tau related to disassembly of the microtubule network, induction of axonal transport deficits, and mislocalization to dendrites[154,160,161], however recent studies suggest tau plays an important role at the synapse, where it coordinates postsynaptic density proteins and may be released in an activity-dependent manner[162,163]. Additional observations of aberrant acetylation of tau and accumulation of tau-rich autophagosomes in AD brains indicate tau acts in complex cellular systems, the dysfunction of which is only beginning to be understood[164–167].

Endocytosis and endocytic/lysosomal sorting and degradation are also critical processes that regulate intra- and extracellular milieus to affect cellular and circuit homeostasis[168]. Intracellular proteostasis requires that large cytosolic protein assemblies and aged organelles undergo lysosomal degradation via macroautophagic processes that utilize clathrin-mediated endocytosis (CME) of donor membrane to engulf particles into autophagosomes[164]. These organelles mediate protein degradation, and alterations in risk loci associated with endocytosis (e.g. *BIN1*) may impair this ability[117]. A recent study shows that bidirectional modulation of levels of another AD risk product, PICALM, slows autophagosome formation and hinders tau engulfment, leading to increased cytosolic presence, aggregation, and NFT formation. The same manipulations also impaired autolysosome formation[164]. Cumulatively, the effects of arrested autophagosome progression and slowed intracellular tau clearance potentially reconcile the presence of tau pathology despite an apparent increase in degradative autophagosome number in AD brain[164,169].

Synaptic activity and plasticity also critically depend on CME in both pre- and postsynaptic terminals. At the presynapse, it regulates recycling of neurotransmitter vesicles, which is essential to maintain the readily releasable synaptic vesicle pool that enables fast signaling[170]. At the postsynapse, CME mediates plasticity via receptor trafficking and signal transduction cascades[79]. Importantly, synaptic APP and BACE1 undergo internalization from the plasma membrane via CME, and one recent study suggests that despite separate secretory pathways, rapid fusion of APP/BACE1 containing vesicles into recycling endosomes regulates activity dependent cleavage to Aβ[70]. There is also evidence that activity-dependent trafficking of late-endosomes mediates γ-secretase proximity to APP.[67] Interestingly, landmark studies in yeast looking at Aβ-induced dysfunction identified several genetic toxicity modifiers in the endocytic pathway.[128] Thus, in addition to genetic risk in the CME pathway that can confer deficits that impair synaptic plasticity and enhance Aβ production, Aβ itself can also disrupt CME. The yeast studies suggest

Aβ may alter the pattern of clathrin aggregation at the plasma membrane, exemplifying the complex feedback processes that regulate this cellular function[128].

As with intracellular degradation and clearance pathways, maintenance of the extracellular milieu also requires the removal of debris to protect connectivity and signaling capacities. The primary cells responsible for this elimination in the brain are microglia, which survey their environments for unwanted and potentially pathogenic debris[58,61]. Microglia can remove such waste from the parenchyma via specialized endocytic processes called phagocytosis and pinocytosis. Phagocytosis of Aβ seems to be a primary means of Aβ aggregate degradation, and recent studies showed that loss of *TREM2*, a LOAD risk gene, reduced phagocytic cell migration toward plaques and exacerbated Aβ pathology[59,60]. Another recent study showed down-regulation of phagocytic genes in microglia following Aβ accumulation[171]. Thus there may be pathogenic feed-forward processes at play, where genetic- or Aβ-induced deficits in phagocytosis lead to increased Aβ, and further dysfunction. Microglia have also been shown to uptake Aβ oligomers via pinocytosis, a related endocytic process[61]. Because these oligomers induce LTD and have other deleterious effects on the synapse[79], loss of phagocytic functioning may contribute to inefficient communication and circuit dysfunction even before overt plaque pathology.

Interestingly, emerging functions of microglia at synapses suggest they also directly participate in synaptic remodelling.[58,125] While considerable data implicate microglia in AD pathogenesis, their exact role in disease progression remains contentious. Two ground-breaking studies suggest that activated microglia can be both protective and damaging to circuits, further complicating the understanding of their role in AD[125,172]. In one study, Chen and colleagues demonstrate that lipopolysaccharide-activated microglia shear inhibitory presynaptic terminals from the soma of excitatory neurons to enhance coherent firing and up-regulate protective pathways.[172] However, a more recent study in an AD-specific model shows that in response to oAβ, microglia pathologically phagocytose synapses via a complement-mediated pathway.[125] Though both studies indicate that microglia play a significant role in shaping synaptic communication and circuit firing properties, whether they initiate neurodegeneration, confer protection, or affect both outcomes remains unclear. It is possible these contrasting findings may reflect distinct responses of microglia during different phases of disease progression. Although microglia may augment circuit dysfunction through aberrant synaptic pruning, how their responses to increasing pathological burden impact cellular and circuit dysfunction as AD progresses remains unknown. More generally, microglial-mediated immune responses and inflammation are also likely to impact AD progression, however these responses also remain poorly understood in AD. Future studies utilizing -

omics screening and live imaging will be necessary to disentangle the complex functions of microglia in AD.

Microglia are not the only non-neuronal cells to affect circuits; astrocytes, oligodendrocytes, and endothelial cells play critical roles in maintaining circuit function. In AD, each cell type undergoes pathophysiological changes that undoubtedly affect neuronal activity, a topic thoroughly covered in a recent review by De Strooper and Karran[14]. Building on their conclusion that mapping cellular alterations can provide insight to incipient changes that underlie memory loss, it is also critical to understand *how* these changes alter circuit dynamics to change cognition. For example, one striking finding in both Aβ and tau models of AD is that pathology increases the size and decreases the stability of hippocampal place fields[173–175]. The ensemble firing of these cells generates a map to promote spatial navigation and location recognition, and alterations may explain the spatial deficits seen in AD patients[176,177]. Place fields emerge from circuit-level interactions of neuronal subpopulations and long-range inputs from the medial septum and entorhinal cortex[178], but whether these deficits are due to intrinsic inability of place cells to encode information or altered network dynamics during encoding or retrieval remains to be seen. Because the consistent deficits in place fields arise from different circuit dysfunction in the AD and tau models, better understanding of the pathological circuit states, and how different cell types and processes affect them, will be necessary to characterize dysfunction in AD. Also because AD affects multiple brain regions and each contributes to distinct cognitive functions, complete spatiotemporal characterization of the circuit- and network- level alterations will provide insight to the deterioration of successive functions.

Network dysfunction predicts cognitive symptoms.
Circuit activity within local cell groups affects long-range networks, and because cognitive function relies on the concerted efforts of multiple brain areas, investigating this dysfunction can connect aberrant cellular and circuit activity to memory loss in AD. Furthermore, identifying brain regions with vulnerable circuits that are dysfunctional early in the disease can reveal critical locations to probe for circuit-disrupting pathological processes. Additionally, discovering how the disease systematically propagates through connected brain regions can suggest critical locations where aberrant activity directly impacts cognition.

The earliest evidence for network dysfunction in AD was the observation of cholinergic cell loss in postmortem cases[179]. Cholinergic cells are located in a few distinct subcortical brain regions and primarily use acetylcholine as their neurotransmitter. The regions connect to each other, and have diffuse processes throughout the brain, which allow them to modulate the excitatory tone of circuits and enable different

states like sleep, wakefulness, and attentiveness[180]. Identification of NFT formation in, and degeneration of, these specific cells[181] supported the cholinergic hypothesis: that the loss of cholinergic neurons is a causative event in AD pathogenesis[182]. Though these cells do strongly affect cognitive processing through modulation of circuit activity and coherent firing[183], and drugs targeting this signaling pathway account for 75% of US FDA approved AD treatments, the efficacy of pro-cholinergic therapies is short, and they can only slow, not reverse, memory decline[184]. Though enhancement of cholinergic signaling is not sufficient to reverse AD, the slight efficacy suggests that loss of the important regulatory tone contributes to escalating dyshomeostasis, which accelerates memory loss. Accumulating evidence indicates that the long-range network structure and use of metabolic substrates for neurotransmitter function may make these types of cells particularly susceptible to axonal transport deficits and metabolic insults, which can induce NFT and other AD pathology[185]. The recent identification of additional subcortical neuromodulatory systems that show early tau pathology indicate that studying these networks may pinpoint specific vulnerabilities in cellular processes that change early in AD[186]. However, because cholinergic drugs do not have long-term cognitive efficacy, other strategies are needed to treat AD.

The first clinical symptoms AD patients report are difficulty remembering new information and episodic memory loss[5]. Neuropathological examinations show early accumulation of NFT pathology occurs in the entorhinal cortex (EC), and spreads through the hippocampal (HPC) formation-regions associated with learning and memory[187]. Recent advances in PET tracers have allowed tau-PET imaging with ^{18}F-T807, which shows similar patterns to those determined by neuropathological analyses, suggesting these may be good tools for early diagnosis[188]. Supporting this, alterations in the EC-HPC regions in cognitively healthy individuals impair learning and retrieving episodic memories, thus these anatomical findings agree with the first clinical symptoms.[189,190] Furthermore, AD pathophysiological processes that alter circuits in these regions may impair learning and memory, and because subsequent accumulation develops in connected brain regions that control planning, emotion, and navigation; the temporal sequence of increasing burden may explain the progressive deterioration of cognitive and emotional function with AD advancement[191,192].

Importantly, pathological NFT and Aβ both propagate into and through the limbic system, a network of distinct brain regions that specifically control memory and emotional behaviors[193,194]. The serial involvement of successive limbic brain regions, and loss of their proper function, may explain the clinical symptom progression, and MRI studies in AD patients demonstrate that specific atrophy within nodes of the network correlates with cognitive complaints.[195] These regions receive massive regulatory inputs from

subcortical structures, especially those afflicted with tau burden, the development of which may contribute to the dysregulation of their targeted limbic regions[196]. Additionally, PET imaging for glucose metabolism shows significantly reduced glucose utilization in HPC and other limbic temporal regions[197]. Furthermore, disruption of limbic white matter correlates with cognitive decline in aMCI patients.[198] Reecent human trials support limbic network dysfunction as an underlying cause of memory loss because preliminary data from a small cohort of AD patients suggests that electrical stimulation of the fornix, a major white matter bundle connecting limbic regions, leads to enhanced cognition.[199]. Stimulation also induces DMN activation, indicating the DMN may be downstream of many limbic nodes[199]. This observation may also reconcile the temporal sequence of cognitive symptoms, and point to the earliest hubs of pathological generation. In the future, more longitudinal, high-resolution fMRI and PET investigations should specifically examine the subcortical limbic nodes to ascertain whether Aβ and functional disconnection may be detected in these regions prior to the deficits seen in DMN. If so, novel methods for assessing limbic function may be useful in identifying earliest stage AD patients.

In addition to uncertainty of the core networks affected by AD, the mechanisms of NFT and Aβ spread remain unknown. Aβ and tau released at the synapse may propagate pathology in a prion-like manner, but the biological pathways underlying this travel are unclear and a direct demonstration of seed propagation remains technically difficult.[200] An alternative explanation for pathological spread is that circuit dysfunction causes alterations in network activity which affects circuit function at downstream targets, and that the abnormal activity within local circuits drives Aβ elevation and tau aggregation. Thus, regional vulnerability can propagate circuit-susceptibility to pathophysiological cascades, which unchecked over time develop into AD hallmark pathologies. Though increasing evidence suggests that Aβ and tau spread within network connections, regional vulnerability to experiential factors like aging, diet, emotional stress, and mental health may also explain the distribution of pathology[185,201]. The limbic system is especially responsive to stress and diet, and many major regions, like the HPC, express high levels of hormone receptors for signals like stress-related glucocorticoid release and diet-related gut hormone signaling.[202,203]Indeed, high fat diets and chronic stress can cause HPC damage, and these environmentally responsive limbic structures may be key points of convergence between experience, genetic risk, and AD onset.[185,204] In a direct test of this, emotional stressors exacerbate spine loss in the HPC of AD mice, and repeated exposure to a stressor in normal mice led to a neurodegenerative-like phenotype in the HPC, along with cognitive impairment.[205,206]

Network treatments may restore memory and cells.

Aβ-targeted therapeutics have been largely unsuccessful at restoring cognition, and although some hope remains, most of the cognitively effective AD treatments target networks to improve or protect circuit activity.[12,199] (Figure 3) The primary drugs prescribed to patients with early-stage memory loss- donepezil, rivastigmine, and galantamine- promote cholinergic signaling by inhibiting degradation to maintain its levels in the extracellular space[184]. This is thought to promote neuronal activity and improve cholinergic tone, and it is likely these compounds also affect microglia and astrocytes, which both express acetylcholine receptors and are responsive to cholinergic signaling[207,208]. Another therapeutic approved for AD treatment is memantine, an NMDA glutamate receptor antagonist[184]. It is the only compound approved for use in late-stage AD, and may promote circuit connectivity by preserving synapse integrity. Memantine likely counteracts the effects of hyperactive excitatory circuits and prevents high levels of glutamate from weakening synapse strength.[208] These network-level treatments are effective at slowing disease progression, but like Aβ-targeted strategies, have yet to stop cognitive deterioration or restore memory function.

Additional molecular treatments to restore cellular health and repair circuit and network function are under development. Alongside Aβ, antibody-based treatments targeting tau aggregation and ApoE have also emerged, though the nascency of the trails precludes judgement on their efficacy[209]. These antibody-based strategies likely influence immune function, however the increasing evidence for non-inflammatory roles of microglia in circuit maintenance suggests directly affecting these functions may better mitigate cognitive impairment. Consistent with this, known anti-inflammatories do not seem to have cognitive efficacy, so perhaps directly targeting the circuit-maintenance functions of these cells may protect neurons, promote normal circuit activity, and preserve network connectivity[210,211].

Interestingly, directly targeting activity of brain networks may also work to restore memory. Phase I clinical trials that used deep brain stimulation techniques to directly manipulate network activity in individuals with AD reported positive memory outcomes in the majority of the patients.[199,212] This intervention also changed protein expression at the cellular level in preclinical models, suggesting that the development of non-invasive brain stimulation paradigms may be a scalable and safe model for restoring cellular health and network function.[213] Furthermore, optically exciting cells in the hippocampus to increase spine number restored learning and memory,[214] and because previous studies found similar effects using HDAC inhibitors,[215] it is likely that diverse treatment strategies can leverage these effects to repair circuits. Together, the efficacy of these experiments also provides promise for using network- and circuit-based intervention to restore cellular health in AD.

Prospective

Ultimately, a growing understanding of cognitive impairment in Alzheimer's disease suggests that pathological alterations at the genetic and cellular levels contribute to circuit dysfunction, which impacts long-range network connectivity. By restoring these connections and the circuit- and cellular-level processes that support them, it may be possible to reverse memory loss. Because no single strategy or target has been fully efficacious in promoting cognition, it is likely a multi-tiered approach to treating AD will be necessary. Treatments to reduce Aβ levels should stop the pathological cascade that triggers cellular dyshomeostasis, and these will be especially important for FAD patients, whose genetic mutations directly induce overproduction of Aβ. Alongside amyloid reduction to halt disease progression, restoring cognition and brain health will likely require therapeutics that regulate circuit activity and stimulate neuronal communication to improve long-range network function. The traditional path to these treatments lies in identifying the pathophysiological processes that go awry in LOAD patients, and thus understanding which dysfunctions contribute to Aβ accumulation and circuit disruption is key. However, because circuit activity also affects cellular processes, it may be possible to circumvent this pipeline by restoring network- and circuit-level function in AD patients. This type of treatment may be able to directly improve memory function and feedback to re-establish cellular health, re-paving the road to a healthy aging brain.

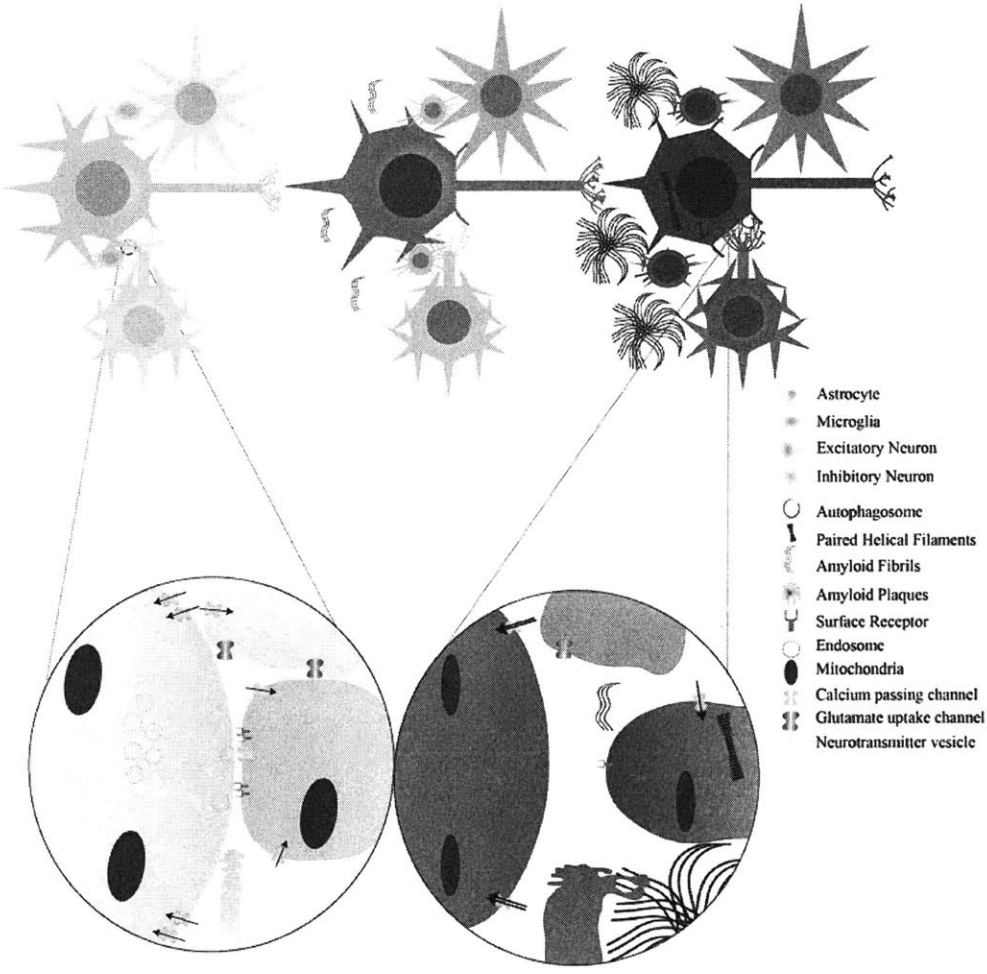

Figure 1: Circuits and synapses through AD progression. Top: Circuits are synaptically connected subpopulations of neurons and the glia that modulate them. They control brain activity in local domains, and the sequential activation of circuits gives rise to long-range network communication. As AD progresses, intrinsic changes in cellular physiology concurrent with the accumulation of Aβ and tau contribute to weakened cellular connections and loss of normal homeostatic functioning, which impedes signal transduction and compounds AD pathology.[14,39] Bottom: At the synapse, two neurons meet to transmit signals. Through AD, a host of intrinsic changes that result from and lead to Aβ and tau accumulation function to weaken connectivity and prevent communication. Because astrocytes and microglia modulate the communication through uptake/release of their own chemical signaling molecules and through structural modification of synaptic components, dyshomeostatic responses in these cells also fundamentally change transmission of information through the brain.[14] (Artwork: Rebecca Canter)

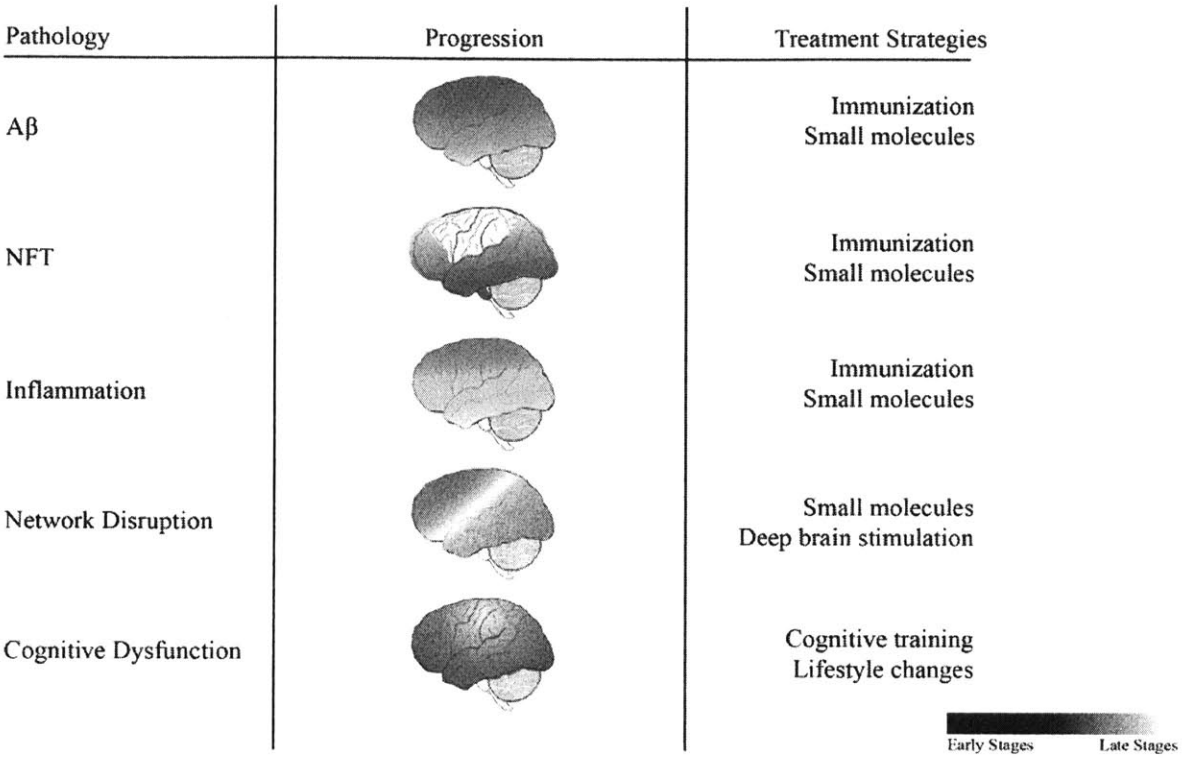

Figure 2: Pathology and its molecular therapeutic targets. Hallmark pathological features of AD include Aβ plaques, NFT, and cognitive impairment.[10] Recent studies suggest network disruption and inflammation are also critical mediators of AD pathophysiology.[87,216] Each observed alteration seems to start in specific functional subregions, and spreads through networks to encompass most of the brain during late-stage AD. Therapeutics aimed at molecular pathologies show minimal cognitive efficacy and rely on traditional drug and immunization strategies. Alternatively, treatments to directly restore network disruption and cognitive dysfunction have better efficacy and can make use of emerging technologies to provide different types of cures. (Figure: Rebecca Canter)

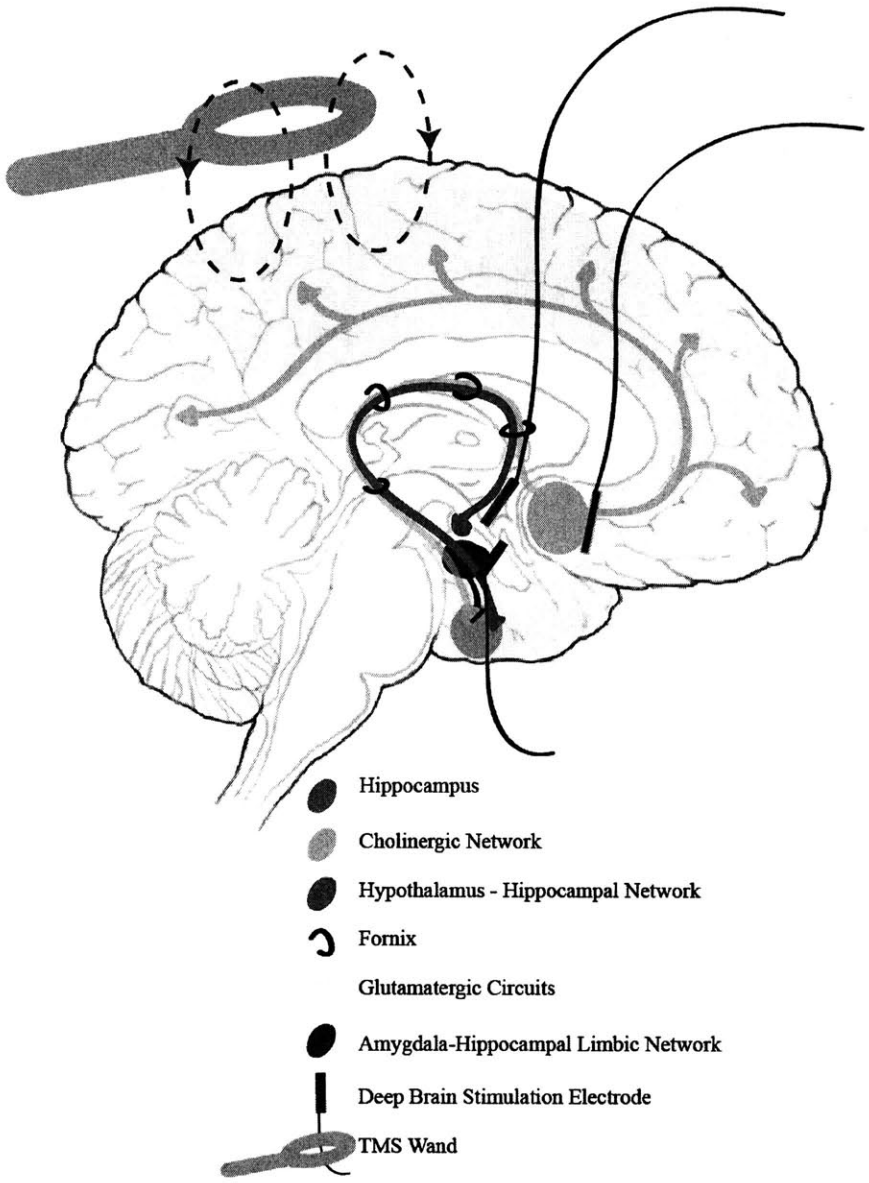

Figure 3: Network level treatments with efficacy in AD. Drugs targeting cholinergic and glutamatergic circuits have minimal efficacy, but remain the only approved treatments for Alzheimer's disease.[184] Preliminary human studies using deep brain stimulation electrodes within the basal forebrain cholinergic system and hypothalamic regions have shown efficacy in slowing disease progression.[199,212] Pilot studies in preclinical models also show that these treatments improve cellular physiology.[213] Together, the human data suggest that targeting networks involved in cognition and memory should be a primary therapeutic strategy that can slow the course of AD while also potentially restoring physiological health. (Brain outline: Christine Yao; Additional art: Rebecca Canter)

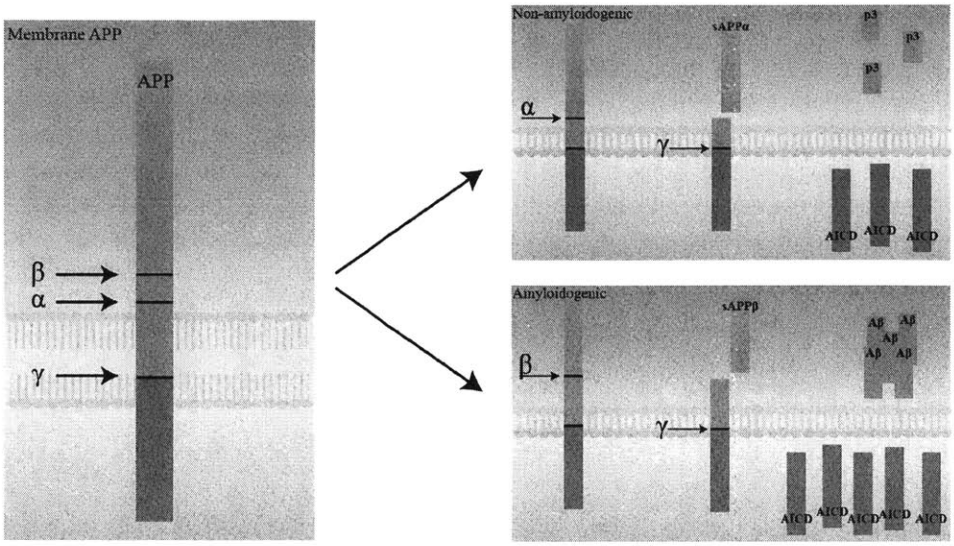

Box 1: Amyloid Processing

At the center of AD pathophysiology is the amyloid β (Aβ) peptide and its aberrant accumulation in AD patients' brains. Aβ results from the sequential cleavage of β-amyloid precursor protein (APP), a type I integral membrane glycoprotein. Two well-studied pathways compete for APP substrate, leading either to amyloidogenic or non-amyloidogenic processing of the protein. [217]

The non-amyloidogenic pathway starts with APP cleavage at the α-secretase site within the Aβ domain by a complex containing ADAM metalloproteases. This cleavage releases the soluble APP ectodomain (sAPPα) and the shorter c-terminal fragment (CTFα) fragment. CTFα undergoes secondary cleavage by γ-secretase, resulting in the soluble p3 extracellular peptide and the APP intracellular domain (AICD). The exact functions of these non-amyloidogenic fragments remain elusive though they may have neuroprotective roles and may also negatively regulate gene transcription. [218]

Alternatively, amyloidogenic fate begins with APP cleavage by β-secretase, (β-site APP Cleaving Enzyme, BACE1), into sAPPβ and the CTFβ fragment. CTFβ is in turn cleaved by γ-secretase (of which PS1 and PS2 are components) to yield Aβ peptides of varying lengths, alongside the AICD fragment. The pathogenic impact of Aβ peptides varies with length: while shorter $A\beta_{1\text{-}x...40}$ species are generally unstructured, longer $A\beta_{1\text{-}42}$ and $A\beta_{1\text{-}43}$ have regular beta-sheet structure that make them prone to aggregation and prion-like seeding. Because the longer structures seem to be more toxic, the ratio of $A\beta_{42}$/ $A\beta_{40}$ may predict AD severity. [42]

Novel pathways for APP processing continue to emerge. The recently identified η-secretase pathway yields Aη fragments that inhibit neuronal function. Furthermore, N-APP, a mediator of axonal degeneration, arises from sAPPβ following β-secretase cleavage. Finally, caspase-mediated cleavage of the AICD may result in transcriptionally active products.[217,219]
(Artwork: Rebecca Canter)

Acknowledgements

We would like to thank the support from NIH grants RO1-NS051874, RO1-NS078839, RF1-AG042978, and RF1-AG047661 to L-HT for this work. We would also like to thank the Barbara Weedon Fellowship and Norman B. Leventhal Fellowship for support of RGC, and the Human Frontier Science Program for support of JP. Additionally, we thank the JPB Foundation, Belfer Neurogdegeneration Constortium, and Glenn Foundation for Aging research for their support of LHT and for their continued championship of aging and neurodegenerative disease research. We would like to thank Christine Yao for the beautiful brain outline on which we could build Figure 3. Finally, we express profound gratitude to Ashley Watson, Hiruy Meharena, Waseem Raja, and Nina Dedic for their insightful comments on the manuscript.

Chapter 2:

iSWITCH labeling for *in situ* proteomic investigation of large volume tissue specimens.[b]

Abstract

The structure and spatial organization of the brain are key to its function. Throughout development, distinct groups of cells assemble into regional circuits that can work together to produce coordinated activity and connect to other ensembles, sometimes over long distances. Molecular investigation of the proteins that underlie brain activity has long required segmenting the tissue into smaller pieces to enable biochemical or imaging analyses, however significant information is lost in the process. In molecular experiments, the high cost of unbiased –omics studies necessitates hypothesis-driven dissection into anatomically ambiguous brain regions from which relevant samples can be extracted, but this segmentation is error prone and biases investigation to areas for which some function or involvement is already known. In traditional imaging experiments, molecular information is derived from slices of the whole organ, however this practice limits the type of information that can be gained about 3D cellular structure and arborization and also restricts the type of analyses that can be performed on physically and functionally connected long-range circuits. Though emerging technologies enable the investigation of intact tissue structures, their widespread adoption by biologists has been slow, likely due to nuanced and tricky protocols and the high cost of troubleshooting individual experiments. This chapter describes updated methods for large-volume tissue analyses, termed iSWITCH, based on the SWITCH technique that are 1) easy and inexpensive for biologists to troubleshoot, 2) rely on traditional chemicals found in most laboratories, and 3) compatible with commercially available microscope systems for imaging.

Contributions:

R.G.C., K.C., L.H.-T. conceptualized the ideas for the chapter.
R.G.C. designed all of the experiments in the chapter, wrote the chapter, and performed the experiments and analyses under the supervision of L.H.-T.. R.G.C. also trained and oversaw the work by: C.Y., T.A., F.A., and S.B.
I.D. provided human brain specimens.
H.C. performed SPIM image acquisition and file stitching of all whole brains.
C.Y. performed experiments in Figures 1H, S1C, S2 and contributed the artwork for Figure 1A.
T.A. performed experiments in Figure S2
F.A. sectioned the brain featured in Figures 4C, 4D, 4E and brains that contributed to data in Figure 5.
S.B. sectioned brains for the data in Figure 5.

---

[b] The data in Chapters 2 and 3 are in preparation for submission of the manuscript: 4D Mapping of Amyloid-beta pathology reveals subcortical susceptibility in Alzheimer's Disease. Authors contributing to this work include: Rebecca Gail Canter, Kwanghun Chung, Li-Huei Tsai, Ivana Delalle, Heejin Choi, Chrinstine Yao, Tajwar Ahad, Fatema Abdurrob, and Stephanie Bousleiman..

Introduction

The biological architecture of the brain is intricate.[220] From genetic expression through behavioral output, the rich diversity that enables the brain to perform its many tasks also presents significant challenges to understanding its function. As investigations into the mechanisms of brain function intensify, improving and increasingly accessible technologies for high-throughput biochemical screening are providing unprecedented advancement and insight to the diverse molecular landscapes of the brain with single cell resolution.[221] Yet, progress to understand how these biological differences influence cognitive function remains limited. The study of brain circuitry has the potential to functionally link abstract cognitive capacity to measurable cellular function. But, as illuminating studies continue to demonstrate the importance of long-range connectivity to cellular activity and circuit function,[222] it is becoming increasingly less clear how to meaningfully map region-specific molecular data to cellular- and network-level functions. To bridge this gap and definitively connect alterations to behavioral output, it will be necessary to extend observations across multiple investigational levels. However, the tools to probe molecular changes at the brain-wide scale are lacking.

Traditional molecular experiments use targeted *ex vivo* biochemical assays or thin-section *in situ* imaging techniques to gain brain-region specific mechanistic insight.[132,223] Biochemical studies lose critical spatial information at both the whole-brain and subcellular levels because examining molecular alterations typically requires extracting quantifiable substrate from bluntly dissected tissue specimens. Although techniques exist to finely remove specific brain regions,[224] the choice of which area to take is usually hypothesis-driven and thus biases research towards areas for which information is already known. Furthermore, by destroying the tissue structure to separate the molecules of interest, these approaches can only provide correlational evidence about the subcellular localization of the target molecules. This loss can influence functional interpretations of the data, especially in highly polarized cells of the brain like neurons, where directionally regulated RNA and protein trafficking occurs throughout the distal processes.[225] Conversely, popular imaging techniques permit whole-brain analyses and subcellular localization, however because they require slicing the specimens into very thin sections through which light can travel for imaging purposes, the segmentation loses critical information about long-range connectivity and three-dimensional cellular structure.[193] Additionally, the largest specimens have mostly been limited to proteomic interrogation because techniques for detecting other biological molecules remain difficult to scale. Excitingly, recently developed technologies enable imaging of large, intact tissue samples.[226] Because they permit imaging of fluorescently tagged probes in whole brain *in situ,* they have the potential to revolutionize neuroscience research by providing the capability for multiplexed

molecular, circuit, and network investigation in intact, post-mortem brain specimens.[227] Towards this goal, protocols for proteomic investigation in the intact samples have emerged.[228–230] Though proof-of-concept investigations have been lauded, the first generation technologies have been difficult to implement and researchers have been slow to adopt them. This is largely due to multi-stage technological and financial obstacles that range from troubleshooting the labeling and clearing techniques, through sample imaging and quantification of the data.

Second generation clearing and labeling techniques, like system-wide control of interaction time and kinetics of chemicals (SWITCH), improve accessibility, however many of the technical challenges in implementing the protocols remain.[229] SWITCH, which uses sodium dodecylsulfate (SDS) to clear samples at high temperatures and then also to facilitate homogenous large-sample labeling, works well for a small number of dyes and antibodies.[229] The harsh heat treatment and repeated SDS exposure, however, may denature many proteins and may not be suitable for all labeling interactions, limiting its wide-scale applicability. Additionally, because SDS forms micelles that diffuse ~20X slower[c] than the ionic content of the solvent solution,[231] the protocol will work differently in large samples than smaller ones, magnifying the effects of poor labeling efficiency in larger samples. This makes the protocol difficult to troubleshoot because its efficacy must be tested empirically for each antigen/antibody pairing and it requires the use of large samples, which makes it time consuming and cost ineffective. Thus, we present modified SWITCH labeling protocols termed 'iSWITCH', which capitalize on the isoelectric point of the target protein and/or ionic concentration of the labeling solution to permit homogenous, large sample labeling. These techniques can be easily tested in smaller samples to apply to larger specimens and, importantly, the specific buffers needed to optimize any antigen/antibody pairing can be predicted based on the isoelectric point of the target protein. Furthermore, though imaging of large samples has grown easier with SPIM microscopy,[232] the burden of analyzing such large datasets remains. We also present methods for hand-segmenting whole-brain data for region-specific analyses, and demonstrate differential amyloid burden across brain regions in a mouse model of Alzheimer's disease as proof-of-concept. Finally, we present data to suggest that this technique is similarly generalizable across sample types, and show significant amyloid burden in human post-mortem AD patient specimens. With more accessible techniques and cost-effective protocol optimization, these technologies can become more widely available to researchers who can begin to address increasingly difficult questions.

---

[c] Equation(1) [309]: $t = x^2/(2*D_{coeff})$. 't': time; 'x' = distance; 'D_{coeff}' = diffusion coefficient; $D_{SDS} \cong 0.8e\text{-}6$ (ref. [310]); $D_{Na} \cong 1.628e\text{-}5$.

Results

Perfusion-mediated fixation and subsequent clearing maintain tissue integrity similarly to SWITCH-processed samples.

Original SWITCH fixation protocols were designed to enable scalable fixation to use across sample types, including post-mortem human autopsy specimens.[229] Though the methods make them broadly applicable, for preclinical research purposes in which animal models can undergo transcardial perfusion,[233] the latter method is preferred. Perfusion serves the dual purpose of quickly fixing the entire brain, eliminating time-dependent degradation and reorganization of unfixed proteins,[233] and also clears blood from the vasculature, which when left intact, can interfere with immunolabeling techniques.[234] Because the advantages of clearing and sample re-labeleing depend on the resistant tissue properties, which were initially verified using SWITCH fixation, we first sought to test whether fixation with paraformaldehyde (PFA) and glutaraldehyde (GA) via perfusion (Paradigm Overview, Figure 1A) would preserve tissue structure similarly to passive SWITCH methods. To test this process, we transcardially perfused mice with ice cold phosphate buffered saline (PBS), followed by either 4% PFA or the SWITCH-tested fixative solution of 1% GA and 4% PFA. Immediately following perfusion, we extracted the brains and incubated them in their respective fixative for three days post-perfusion to ensure thorough fixation. Next, we bisected the brains into the two hemispheres and stored one randomly chosen half uncleared at room temperature while the other proceeded through the optimized clearing process. After perfusion and extraction, the brain was intact, and side-by-side comparison (Figure 1B, Figure S1A) as well as length, width, and height measurements (Figure 1D, 1E, 1F; Figure S1B) demonstrated that, as expected, the two hemispheres were equally sized (Figure 1B, 'Pre-Clearing'; Pre-clearing vs. Not Cleared, Figure 1C, Dunnett's multiple comparisons test, $q = 0.8821$, $p = 0.7903$). This finding enabled us to perform side-by-side comparisons across clearing stages.

After fixation and bisection, we proceeded through lipid elution (clearing) taking measurements of the tissue at each step. First, in the hemispheres slated for clearing, we inactivated the fixative in a solution containing 1% acrylamide and 1M glycine in PBS. The inactivation step is critical for successful clearing because it binds exposed fixative moieties to prevent over-fixation upon heat exposure and eliminates non-specific antibody fixation during immunolabeling of cleared tissue. Without an inactivation step, we find the tissue clearing time is greatly extended and, in some cases, the specimens never fully clear (data not shown). Inactivation did not alter the size or shape of the tissue (Figure 1B, 'Post-Inactivation'; Figure 1C, Dunnett's multiple comparisons test, Pre-clearing vs. Post-Inactivation, $q = 0$, $p = 0.9999$).

Next, hemispheres were cleared with gentle shaking at 55C in CLARITY clearing solution.[235] Though this heat treatment is less harsh than the protocol used in the original SWITCH paper,[229] tests in 1mm thick sections suggest there are not significant differences in opacity following short clearing in 37C, 55C, and 80C (Figure S2A, Figure S2C, Two-way ANOVA, $F_{(2,12)}$=1.433, p=0.2767). Although longer time-course experiments demonstrate that higher temperatures lead to increased translucency, and at a faster rate (Figure S2B, Non-linear regression, $F_{(6,75)}$ = 21.77, p < 0.0001), these differences become insignificant after immersion in refractive index matching solution (RIMS) which is necessary prior to imaging (Figure S2D; S2E, One-way ANOVA, $F_{(2,9)}$ = .2092, p = 0.8151). Though we note that previous reports indicate significant antigen retention at 70C,[229] which may spare significant protein compared to our 80C condition, our qualitative experiments at the highest temperatures suggest a loss of antigenicity for certain proteins (data not shown). To be safe, we chose 55C to balance the benefits of high thermal energy-mediated clearing with certain antigen retention.

Immediately after removal from clearing solution, samples demonstrated swelling (Figure 1B, 'Post-Clearing'; Figure 1C, Dunnett's multiple comparisons test, Pre-clearing vs. Post-clearing q = 9.041, p < .0001). However, after washing in primary iSWITCH buffers at room temperature, the tissue returns to its original size (Figure 1B 'iSWITCH'; Figure 1C, Dunnett's multiple comparisons test, q = .2205, p = .9982) Despite the restoration, we wanted to ensure the temporary size increase did not alter tissue structure. Because PFA/GA fixed samples can withstand multiple rounds of immunolabeling,[229] we performed repeated experiments to visualize the effects of tissue swelling in 100um sections. For the first round of labeling, PFA- or PFA/GA-fixed 100um sections from transgenic 5XFAD transgenic Alzheimer's model mice were labeled with Alexa-488 conjugated isolectin to visualize vascular structure using normal immunofluorescent (IF) protocols. Images were taken from anterior, middle, and posterior sections, and representative images are shown (Figure 1H). Following imaging, sections were cleared at 55C, which not only removes lipids from the sample, but also strips antibodies from the tissue.[229] For the second round, IF was repeated with the identical protocol to round 1. Qualitative analyses suggest antibody removal and structural preservation of both extra- and intra-cellular proteins (Figure 1H). Finally, to ensure the refractive index matching solution (RIMS) that we used also does not change the tissue structure, samples from IF round 2 were un-mounted from slides after imaging, incubated in RIMS overnight, and re-mounted on the slides for re-imaging. Analyses of this third round of imaging suggest that RIMS does not change the labeling patterns samples (Figure 1H). Because each size measure returns to its normal size (Figure 1G, Pre-clearing vs. iSWITCH, Dunnett's multiple comparisons test, q = .2712, p = .9962) and the imaging appears structurally intact, we concluded that none of the manipulations alter

the cellular-level structural integrity of the PFA/GA sections. Importantly, the same processes repeated in PFA sections causes significant tissue deformation (Figure S1C), suggesting the addition of GA is critical to preserving tissue integrity through clearing. Together this data indicates that the perfusion-based fixation protocols work similarly to SWITCH fixation in mouse brain samples.

iSWITCH techniques are simple and predictable immunofluorescent protocols for large-volume tissue specimens.

Once we achieved satisfactory tissue clearing and ensured the samples maintained resilience properties similar to SWITCH-fixed specimens, we wanted to label intact mouse brain for spatially unbiased proteomic analyses. In sample testing we noticed that seemingly low-affinity antibodies which usually require longer incubation times for detectable labelingled to homogenous IF signal throughout the tissue (Figure S3). Unfortunately, due to the kinetics of these antibodies, they did not label strongly with the original SWITCH OFF/ON buffer system (data not shown), so we set out to use SWITCH principles to design novel buffer systems that might be compatible with the wide range of available antibodies (Protocol Overview, Figure 2A). Because most antibody companies seek to produce high affinity antibodies, we wondered if there was a way to make these commercially available reagents act like lower affinity counterparts during sample preparation. To achieve this, we needed to weaken antibody/antigen interactions just enough to prevent fast interactions at the surface, which would allow antibodies to diffuse through the tissue and bind more homogenously. Typical IF protocols use neutral buffered saline solutions that sometimes contain non-ionic detergents. These conditions are ideal for antibody-antigen reactions regardless of the proteins' biochemical properties, and the non-ionic detergents enhance tissue penetration by enhancing cell membrane permeability and reducing surface tension to increase diffusivity without affecting the antibody-antigen interactions[236]. For large samples, the detergent is helpful to enhance antibody penetration throughout the volume, however the ionic conditions that are permissive for interaction are not ideal for weakened reaction kinetics. Because antibody-antigen interactions largely depend on non-covalent hydrogen and electrostatic bonds, we hypothesized that by manipulating the ion concentration and electronegativity of the labeling solutions, we could alter reaction timing[237].

We decided to test the hypothesis using high-abundance antigens for which significant surface effects are typically seen in IF labeling, and settled on GFAP and myelin basic protein (MBP). Because the system depends on the non-covalent interactions between the antibodies and antigens, we can use the isoelectric point (pH_i) of the target proteins to predict the buffer solutions that will minimize interactions. Importantly, by manipulating the charge and ionic concentration we will not completely eliminate

antibody binding because there are additional intermolecular forces that govern the interactions,[237] thus allowing slowed kinetics without completely disrupting interactions. To decide on the buffers we had two options: 1) bring the pH towards the pH_i of each of the proteins to reduce the charge and thus interaction or 2) alter the pH to charge the proteins and provide increased ionic substrate to saturate electrostatic interactions, thereby reducing the probability of antibody-antigen interactions. We started with buffer system 1, hoping that a low net charge would provide appropriate reaction kinetics for large-sample labeling, and tested a 'weak binding solution' near the isoelectric point of MBP (predicted 9.58, ExPASy) with 2X NaCl concentration to provide slightly extra substrate to boost the effects. Secondary antibody labeling was performed in PBST in both conditions. The novel iSWITCH system did work to improve homogeneity of the labeling in the sample over standard IF buffer of PBS plus triton-x (PBST) (representative images, Figure 2B). Although at first glance, the signal between the first and last optical sections appeared consistently bright across buffer conditions (Figure 2C, 'First-Last', Student's t-test, $t_{(22)}$=.7988, p = .4329), the signal intensity retention of the middle sections compared to the edges was significantly enhanced in iSWITCH (Figure 2C, 'First-Middle', Student's t-test, $t_{(22)}$=2.793, p = .0106; 'Middle-Last', Student's t-test, $t_{(22)}$=2.93, p = .0077) compared to PBST. Furthermore, depth-wise analyses (quantification Figure 2D, Non-linear regression, $F_{(3,858)}$ = 55.1, p <.0001) demonstrate that IF signal in iSWITCH labeled tissue decreases through the sample with laser attenuation (Figure 2D, Non-linear regression, First-order decay, R^2 = .5685), whereas the PBST labeling demonstrates edge effects of the labeling (Figure 2D, Non-linear regression, Second order polynomial, R^2 = .5795). Although the bright signal in the PBST condition seems like it would be advantageous for identifying structures during analyses, we hypothesized that the effects would magnify in larger tissue samples, leaving targets near the center of large specimens poorly labeled.

To test this system in larger samples in which kinetic alteration can be more effective at increasing homogeneity, we took aged Alzheimer's model mice (13 months, 5XFAD), which have been reported to show significant amyloid plaque burden throughout the brain,[223] and used iSWITCH techniques to label for amyloid plaques. To ensure consistency of the plaque burden between samples, we used paired hemispheres to test the differences in protocols. APP has a pH_i of 4.73, suggesting that the pH10.5 buffer plus additional salt should create weakened binding conditions. We labeled one of two hemispheres with iSWITCH primary solution and the other with PBST. Similarly to the thinner sections, iSWITCH does not alter the total number of identified plaques (Figure 2F), and the signal intensity significantly differs between the two conditions (Figure 2G, F-test of variance $F_{(9,9)}$ = 65.65, p < .0001, Mann-Whitney U Test, U = 0, p <.0001). Confirming our hypotheses, however, PBST labeled samples have a dark center

compared to iSWITCH samples(Figure 2E), and regression analyses show that the iSWITCH labeling significantly improves homogeneity of signal throughout the sample (Figure 2H, linear regression, $F_{64.44,21332} = 64.44$, $p < .00011$; slope 'iSWITCH' = 5.601, slope 'PBST' = 24.94).

Labeling human autopsy specimens with iSWITCH techniques reveal unprecedented amyloid load in temporal cortex.

Finally, to test whether our iSWITCH protocols work in tissue preserved using SWITCH fixation and across species, we obtained a formalin-fixed, paraffin-embedded human brain autopsy specimen. After deparaffinization, the sample was fixed in 1% GA to impart structural resilience, then cleared at 55C. Following clearing, the sample was labeled with the same iSWITCH buffers as the mouse hemispheres. 3D reconstruction suggests the antibodies labeled the samples well, and fully penetrated the sample (Figure 3A). Higher magnification and reconstruction also suggests that the microstructure of the sample remains intact after thermal clearing and iSWITCH labeling (Figure 3B). Because the tissue cleared well, we wanted to see if the clearing and iSWITCH labeling could enhance our ability to see the interaction of multiple proteins in human brain. Most individuals with dementia have multiple pathological insults relating to different dementias,[19] thus being able to label for each of the hallmark pathologies in a single brain specimen may be advantageous for both preclinical and diagnostic purposes. To test this, we labeled a piece of the specimen with six different dyes and antibodies (Figure 3C). To our surprise, using a white-light laser and confocal imaging we were able to see specific labeling across the wavelength spectra. This signal could be enhanced using Imaris reconstruction tools (data not shown), and thus we conclude that this is a robust tool for looking at the interactions of multiple proteins or cells in human samples. When considered alongside the possibility for fine morphological reconstruction and the robust tissue properties of SWITCH samples that make them resilient across multiple rounds of investigation, iSWITCH labeling of human post-mortem samples has the potential to greatly enhance pathological detection and understanding, and may advance pathological diagnostic tools.

White-matter guided hand segmentation of 3D data is easy and reliable.

With successful whole-brain and large sample labeling, the next challenge was to segment the data for meaningful spatial analysis. Because 3D molecular reconstruction at the brain-wide scale is relatively novel, we were unaware of any publically available software that could perform automatic regional segmentation and unbiased molecular structural identification.[238 (source code coming soon)] Using information from human imaging literature, another viable option in the absence of reliable atlases is manual parsing based on structural landmarks in the images.[239] Because the PFA/GA fixation prevents full lipid elution

from the tissue,[229] white matter remains mildly autofluorescent under SPIM imaging conditions (Figure 4A). To use this for segmentation, we imported the datasets into to commercially available 3D reconstruction software that would allow slice-wise visualization of the data in each axis (Figure 4B).

Using the white matter patterns as structural guidelines, we hypothesized that we could trace individual regions as delineated by 2D mouse brain atlases. We chose the Allan Brain Atlas (coronal), for its ease of digital navigation and widespread availability. Using slice-wise viewing of surface rendering tools, we segmented each region using salient white-matter tracts within and around the area, and also using overall structural orientation as a guide (Figure 4C). Outlines were drawn approximately every 200um through the anterior-posterior axis of each brain, for a total of ~80 slices per brain (Figure 4D). After regions were drawn, software-specific rendering tools created volume objects in the size and shape of each region (Figure 4E). Within the software package, the volume-rendered regions can be used to localize independent identification of molecular signal.

Overall, we determined that each brain takes at least 48 working hours to hand segment, and thus the task is laborious. However, hand segmentation precludes the need for custom algorithms and computationally difficult software packages. Additionally, unlike many automated algorithms which stretch data to fit a pre-determined atlas or must make assumptions about structural relationships across all brains, manual parsing is robust to gross alterations of brain morphology and can account for differences between brains that occur during processing or imaging.

iSWITCH-enabled mapping of β-amyloid protein in Alzheimer's model mouse brain demonstrates significant amyloid burden in human-identified disease-related brain regions.

Alzheimer's disease (AD) is on track to be the leading cause of death in developed countries.[7] Despite decades of research, a full understanding of the basic neuroanatomical spread of the characteristic extracellular beta-amyloid (Aβ) aggregates that may underlie the disease remains elusive.[8,9] The lack of consensus is largely due to discrepancies between post-mortem pathological analyses, which indicate widespread pathological burden, and *in vivo* patient imaging techniques that emphasize cortical amyloid. To demonstrate the power of iSWITCH methods and whole-brain molecular identification, we set out to map the anatomical distribution of Aβ aggregates (plaques) in mouse models of AD. Because the ph_i of APP is 4.73, we hypothesized that an iSWITCH primary buffer at pH 10.5 with .275M NaCl concentration would sufficiently slow reaction kinetics to allow whole-brain labeling. Homogenous

labeling is especially important in the significantly aged animals, where widespread cortical plaque could prevent antibody penetration to the deeper structures.

Because there is minimal lateralization in rodent brains,[240] we bisected the brains of aged AD-model mice and used iSWITCH to label one randomly chosen hemisphere for β-amyloid (D54D2). Overview of the whole brain reconstruction depicts widespread plaque deposition (Figure 5.1A), showing significant burden as reported in the literature.[223] Importantly, optical slice-wise analyses showed that the labeling was successful throughout the sample (Figure 5.1B). Although the brains used for this experiment were hemispheres, labeling of whole, intact brain demonstrates that the technique also works in the larger specimens (Figure S4). Overall, the aged brains show significant numbers of Aβ plaques (Figure 5.1C) and heavy burden, as determined by the density of plaques across the entire brain (Figure 5.1D). Despite the seemingly high brain-wide Aβ labeling, regional analyses from hand-segmented data shows that Aβ plaques are not evenly distributed throughout the tissue, and neocortical regions like the motor, entorhinal, and somatosensory corticies (Figure 5.2E, Repeated-measures one-way ANOVA, $F_{(44,88)} = 5.457$, $p < .0001$) have the highest number of aggregates. k-means clustering of regions by plaque count reveal five specific groups (Figure 5.2F, Euclidean distance, cluster number = 5), and remarkably, the regions associated with Group 2 reflect nodes of the rodent default mode network (DMN),[241,242] which has been shown to display early functional alterations in human AD patients.[87,88] Additionally, regions clustered in Group 4 are cortical nodes of the limbic system, suggesting similar plaque counts emerge within connected brain regions.[243,244] Together, these findings recapitulate observations of Aβ in both post mortem analyses and patient imaging studies,[82,88] suggesting that the mouse model accurately reflects human amyloidosis.

Although this data is intriguing, one potential confound of using raw plaque count to measure Aβ load is that brain areas vary greatly in size. Because differing Aβ concentrations have dissociable effects on activity and cellular health, it is important to understand which regions have the highest load to begin to form hypotheses about the consequences of this network-level spread. Thus we looked at amyloid aggregate density to see which regions may have the most significant amyloid-induced alterations. Using a density measure demonstrates that subcortical regions – specifically the mammillary body and the septum -- have the highest regional load (Figure 5.2G, Repeated-measures One-way ANOVA, $F_{(44,88)} = 1.808$, $p = .0094$), which differs from the cortical observations by plaque count. Interestingly, despite the appearance of novel burdened regions in the density measure, k-means clustering of this data again shows that the DMN and olfactory regions show similar plaque load, and limbic structures still cluster together

(Figure 5.2H, Euclidean distance, cluster number = 5). Because measures of both raw count and density show similar levels of Aβ load within functionally connected networks, our data indicate that amyloid burden is not random, and instead may relate to functional connectivity of circuits that have been shown to become disrupted in AD.

Discussion

Alzheimer's pathological specificity.

Aβ is a major hallmark of AD, and its presence within the brain is an early predictor of a long-term dementia diagnosis.[245] The clinical diagnosis, however, often comes years after the onset of pathophysiological processes in the brain, once Aβ levels have plateaued in many cortical regions.[24] Understanding how these peptides slowly ravage the brain is key to treating the disease, yet to date complete investigation of brain-wide molecular pathological affliction has been lacking. Using Alzheimer's model mice and optimized tools for whole-brain observation of molecular phenotypes, we show that Aβ deposition occurs in specific areas across the brain, which strengthen human post-mortem and patient imaging data that show preferential affliction of cortical and limbic networks. Furthermore, the specificity of the observations suggests that functionally connected brain regions show similar levels of pathology, indicating that interregional connectivity may play a role in the development of AD. Studies using a targeted approach to circuit-specific pathological affliction have begun to show that connectivity plays a role in Aβ propagation,[246] and have led to the suggestion that misfolded proteins spread in a prion-like manner in AD.[97] However, the current investigational tools for following the progression of pathology impede observation and interpretation of critical information about connectivity, and may preclude direct observation of this phenomenon. These shortcomings in the current literature can be rectified by spatially-unbiased, 3D phenotyping using novel intact specimen approaches.

Molecular imaging joins the era of big data.

Large sample imaging techniques are in their infancy, however big data science has paved the way for thinking about these types of screen-like datasets. Sequencing of the human genome[247] ushered in an era of big-data that has brought about high-throughput genomic[38], epigenomic[132], transcriptomic[248], and proteomic[249] analyses to identify broad intracellular changes and molecular systems interactions. With these technologies, untargeted and less-biased subcellular phenotyping is generating an abundance of new hypotheses about fundamental cellular biology, and making major advances in realizing the biological complexity that drives its diverse functionality. In the brain, differences in the molecular milieu drive the regional specialization that underlies cognitive and behavioral functions at the circuit and network

levels.[134] However, until recently, unbiased spatial pheontyping of these molecular environments across the brain to provide systems-level insights on par with big-data –omics studies was largely impossible. With mounting evidence that suggests that alterations in molecular systems are key to brain disorders, neuroscientists cannot afford to continue the biased research towards a few, well-studied brain regions, using tools that preclude investigation of molecular interactions with neural connectivity.

Fortunately, the advancement of tissue processing techniques to allow for intact sample imaging has, for the first time, enabled observation of molecular and cellular structures in intact specimens. Alongside these technologies, new tools for -omics style interrogation *in situ* are beginning to emerge. With the possibility of molecular phenotyping across the whole brain, we are now able to perform spatially unbiased investigations that can help us understand how molecular- and cellular- level effects interact with alterations at the circuit and network levels. While tools for circuit and network manipulation have also become widespread,[250] the protocols for integrating molecular and brain-wide phenotyping remain in their infancy. As the principles of large-volume tissue processing become more widely understood, new ideas and new challenges have also emerged, all the while encouraging a full-throttle push toward whole-brain investigation.

Accessible, predictable, and safe technologies enable better research.

As researchers across the biological spectra adopt systems-level tools to better understand health and physiology, widespread dissemination of protocols must cater to a diversely experienced audience. First generation tissue clearing technologies use a wide range of buffers, solvents, polymers, and systems to achieve intact investigation,[235,251,252] however the complexity of the systems and nascency of the technology made them unsuitable for general adoption. The second generation techniques stem from many of the same principles, yet are generally easier to implement and more reliable.[228–230] These techniques enable molecular mapping in the clarified specimens, making the technologies increasingly useful for broad investigation.

Despite the quickly advancing field, many of the protocols remain too specialized for the general biology community because they still require special equipment, solvents, and large amounts of financial resources for optimization and troubleshooting in each new application. In this paper, we present an optimized SWITCH-principle immunolabeling protocol that takes advantage of the predictability of the isoelectric point of biological proteins to enhance antibody penetration and improve post-image acquisition analyses. This system, termed 'iSWITCH' 1) has predictable success in any given set of

buffers, 2) is useful for enhancing labeling in relatively thin and very large samples, 3) can be easily optimized in small tissue specimens with parameters that generalize to larger volumes, 4) describes buffers that are safe for researchers and the expensive equipment on which the samples must be imaged, and 5) integrates efficiently and is compatible with SWITCH fixation techniques for repeated use of precious samples, like from human autopsy.

Insights from imaging datasets can drive mechanistic discovery.

Using the spatially-unbiased whole-brain imaging approach is both laborious and enlightening. While the computational tools for handling the large datasets have yet to arrive, clearing and immunolabeling technologies have significantly advanced our capacity for novel discovery at the systems level of neuroscience. We took advantage of these protocols to relate rodent models of AD to the human disease, and have shown connectivity-biased accumulation of hallmark AD pathology. Future experiments can utilize whole-brain labeling to elaborate the mechanisms underlying the specificity of Aβ accumulation within these circuits. Of particular interest would to know why the two most densely burdened regions, the mammillary body and septum, show such significant pathology, and how their burden relates to the other functional circuits identified in this work. Because these regions have not been characterized in the human literature, understanding whether they show burden in human AD patients is also key to the relevance of this work. Furthermore, because we show these technologies can provide unprecedented information in smaller samples, they may yield critical insight to the microstructural differences in amyloid burden and cellular reaction across different brain regions. Discovering which cell types and molecular environments are most conducive to Aβ accumulation is extremely important, as it will likely reveal mechanisms of susceptibility at the brain-wide scale. Finally, using these tools to temporally map hallmark AD pathologies in mouse models may uncover better, earlier biomarkers for AD dementia. Applying the information to human imaging may also enhance patient screening, pharmaceutical testing, and guide longitudinal outcome studies that can bring us closer to cure.

Methods

Animals

5XFAD (Tg 6799) breeding pairs were acquired from the Mutant Mouse Resource and Research Center (MMRRC) (Stock No. 034848-JAX) and maintained as hemizygous on the BL6 background. Animals were group housed on a 12h light/dark cycle without enrichment and sacrificed at the ages noted in the text.

Mouse Tissue Fixation

Mice were anesthetized with isoflurane (Isoflurane, USP, Piramal Healthcare, Andhra Pradesh, India) and underwent transcardial perfusion with ice cold 1X PBS (10X stock, Gibco, #70011-044) followed by ice-cold fixative made of 4% paraformaldehyde (32% stock, Electron Microscopy Sciences (EMS), Hatfield, PA, #15714) and 1% glutaraldehyde (10% stock, EMS #16110) in 1X PBS or just 4% paraformaldehyde in 1X PBS. Brains were removed from the skull and post-fixed in the same fixative for 3 days shaking at 4C.

Mouse Brain Section Processing

Brains were sliced to 100um – 999um (as noted in the text) on a vibratome (Leica VT100S) and stored at 4C in 1X PBS + 0.02% sodium azide (Sigma-ALdrich, #S2002). For 100um sections, individual sections incubated in clearing solution shaking at 55C for 2 hours, and were washed in 1X PBS. Sections were immunolabeled with the 'Mouse Brain Section iSWITCH' protocol attached (Appendix A).

Clearing Temperature Testing

999um mouse brain sections were put into 50mL clearing solution. Slices were incubated at the temperatures noted in the text for 48 hours, with pictures taken prior to clearing then at hours 0, 2, 4, 6, 30, 32, 34, 48. After clearing, slices were washed in 1XPBS and incubated in RIMS. Clearing solution for this experiment contained from 0.0 – 0.5% thioglycerol, but the solution had no effect on clearing (data not shown) so the data were grouped by temperature.

Whole Mouse Brain Processing

After washing in 1X PBS, brains incubated in inactivation solution of 1% acrylamide (40% stock, Biorad #161-0140), 1M glycine (Sigma-Aldrich, St. Louis, MO, #G7126) in 1X PBS. After washing in 1X PBS, brains were put into clearing solution of 200mM sodium dodecyl sulfate (SDS) (Sigma-Aldrich, #L3771), 20mM lithium hydroxide monohydrate (Sigma, #254274), 40mM boric acid (Sigma-Aldrich, #7901), pH 8.5-9.0 and left shaking at 55C for 4 weeks until white matter tracts were translucent to the eye in SDS. Brains were washed in 1X PBS or Weak Binding Solution (WBS) for up to 1 week and immunolabeled with the 'Whole Brain iSWITCH' protocol attached (Appendix B).

Human Tissue Processing

Human tissue blocks were deparaffinized by sequential immersion in xylene, ethanol, and water (Protocol for Human iSWITCH processing in Appendix C). Then, blocks were incubated in 1% GA in 1X PBS for 10 days at 4C. Brains were incubated in clearing solution shaking at 55C until the tissue appeared translucent (4-8 weeks). Following clearing, tissue was labeled using the Human iSWITCH protocol (Appendix C) with sequential rounds of 1) D54D2 and 2) 4G8.

Antibodies & Dyes

The primary antibodies used are as follows:

Target	Host	Company	Product #	Dilution
Aβ (D54D2)	Rabbit	Cell Signaling Technologies	8243	1:100 –1000
APP/ Aβ (4G8)	Mouse	BioLegend	800701	1:100 –1000
GFAP (GA5)	Mouse	Cell Signaling Technologies	3670	1:100 –1000
Iba1	Rabbit	Wako Chemicals	019-19741	1:100 –1000
Myelin Basic Protein* SMI-99	Mouse	BioLegend	808401	1:50 –500
Myelin Basic Protein* SMI-94	Mouse	BioLegend	836502	1:50 –500

*These antibodies were used concurrently as per the manufacturer's recommendation.

Additional labeling reagents:

Lectin dye was acquired from Vector Laboratories (#DL-1174).

Hoechst 33528 was used for nuclear labeling (Sigma #14530).

All secondary antibodies were Pre-adsorbed F(ab)2' AlexaFluor-conjugated from AbCam.

Section Image Acquisition

For section and human tissue imaging, tissue was mounted onto microscope slides (VWR VistaVision, VWR International, LLC, Radnor, PA) with either Fluromount G Mounting Medium (Electron Microscopy Sciences, Hatfield, PA, USA) or RIMS solution (See Appendix C: 'iSWITCH Solutions).

With the exception of Figure 1H and S2, all slice images were acquired on a Zeiss LSM Inverted 710 microscope using Zen 2012 software (Carl Zeiss Microscopy, Jena, Germany). Images with cellular resolution were taken using a C-apochromat 40X, water immersion objective, NA 1.20. Section overview images used a Plan-apochromat 5X, air objective, NA 0.16. Pinhole, optical sectioning, and laser settings varied between individual experiments in separate figures, but were kept consistent between images that were included in single quantification graphs.

Images in Figure 1H were taken on a Leica SP8 Upright Confocal Microscope using Leica LASAF software (Leica Microsystems, Wetzlar, Germany). Images were taken using a 25X 0.95NA objective, and the pinhole, optical sectioning, and laser settings remained constant across conditions.

Images in Figure S2 were taken with a DSLR camera (Nikon, Japan).

Whole Brain Image Acquisition

Whole brain images were acquired on a custom SPIM microscope built by H.C. Images were acquired using 10X 0.6NA CLARITY optimized objective (XLPLN10XSVMP; 8.0mmWD) from Olympus. Laser settings were determined for each brain such that 5% of the images are saturated to the maximum gray level to enhance signal to noise in each individual brain.

Clarified Brain Measurements (Figure 1)

Length, width, and height measurements in millimeters were taken immediately after removing hemispheres from the respective solutions.

3D Image Quantification

Images were analyzed using Imaris (Bitplane, Zurich, Switzerland). Each whole brain file was segmented by hand using white matter tract boundaries and regional guidelines from the Allen Brain Atlas (Allen Mouse Brain Atlas, Coronal) to bound each major brain region. For whole hemisphere SWITCH test

analyses (Figure 2), each hemisphere was digitally sliced into 5 – 100um coronal sections and 6 – 100um sagittal sections. An Imaris Spots object was created to identify plaques in a single digital section. Identical parameters were used to create spots objects on the remaining sections from both conditions, so that the same analyses parameters were used across all testing groups. Data was exported into a CSV analyzed in Matlab (Matlab, The Mathworks Inc, Natick, MA, USA) and GraphPad Prism 7.0a for Mac (GraphPad Software, La Jolla, CA, USA). All quantification steps were performed on raw images. For whole brain analyses (Figure 5), spots object was created on a 12 month brain. The parameters were fixed over the entire brain, and spots were separated into the bounded brain regions using the Spots into Surfaces tool in Imaris Xtensions. The identical Spots object with the same parameters was created on each brain. These objects were similarly split into brain regions using the Xtension. Data was exported into CSV and analyzed in Matlab and GraphPad Prism 7.0a for Mac. All quantification steps were performed on raw images.

2D Image Quantification

For Figure S2 Clearing Temperature Testing, TIFF images were imported into FIJI[253] and quantified for signal intensity. Mean values were exported to GraphPad for analyses. For Figure 2 SWITCH Test, Zstack images were imported into FIJI as TIFF stacks. Images were split, merged, and collapsed to RGB. The z-axis profile of each image was taken and the list of X/Y coordinates was exported into Microsoft Excel. The first section with a mean intensity of '1' or greater was taken as the first image, then the first 10 sections were thrown away to account for images taken in focal planes outside of the tissue. This left each stack with the brightest slice first, which was set to 'Section 1', and the rest of the images were normalized to this one as 100% signal intensity. Data were exported to GraphPad for analyses.

Representative Images from Whole Brain Data

Representative images from the whole-brain datasets are either 2D images of the 3D rendered whole dataset or digitally sectioned at 5-100um in Imaris using the Orthoslicer tool. For SWITCH test (Figure 2), images have reduced maximum brightness to 5000 to enhance signal for viewing. The parameters were set and fixed to be applied equally across experimental groups. For whole brain images in Figures 4,5, and S4 the maximum brightness was also reduced to enhance signal for viewing. These parameters were chosen per brain and differe between figures because there are no direct comparisons made between those figures.

Statistics

All statistics were performed in MatLab or GraphPad Prism. Individual statistical tests are indicated in the text and figure legends for the appropriate experiments. Graphs were created in the respective analytical software packages and exported as .TIFF or .JPEG for inclusion in the document.

Experiments to Add

Below is a list of on-going experiments that will be included in the final manuscript, but were not complete at the time of initial thesis submission:

1. *iSWITCH buffer tests with 'method 2', which use different buffer schemes to manipulate the binding properties of the antibody-antigen interaction to determine the limiting conditions of the protocol (Figure 2)*
2. *measurements of inter-rater reliability to quantify consistency across analysts (Figure 4)*
3. *within-rater reliability tests to gauge repeatability of measurements by a single rater (Figure 4)*

Acknowledgements and Contributions:

In this chapter, I would like to thank:

Dr. Li-Huei Tsai: for her mentorship and encouragement to pursue such a risky technology implementation project, and for supporting it through the ups and downs.

Dr. Kwanghun Chung: for his teaching and guidance in all things chemical engineering, tissue clearing, and large-volume imaging.

Dr. Ivana Delalle: for her belief in our mission, providing human tissue specimens, and the time she took to help us identify important facets of human neuropathology.

Dr. Heejin Choi: for SPIM imaging of the whole-brain datasets.

Dr. Hiruy Meharena: for enlightening me to the biochemical and biophysical interactions that enable the protocols to work and suggesting tools to predict our the buffer systems.

Christine Yao: for her meticulous work fine-tuning and performing the tissue fixation, clearing, and labeling experiments to ensure that our protocols are effective. Also for her fantastic artwork featured throughout the chapter, and especially in: Figure 1a.

Tajwar Ahad: for helping Christine to optimize the protocols and painstakingly photographing slices for days on end. His photographs are featured in Figure S2.

Fatema Abdurrob: for beautifully segmenting whole brains despite the dark, cold microscopy room.

Stephanie Bousleiman: for manually segmenting brains day in, and day out, and having the most consistent tracing and labeling scheme on the entire team.

Naveed Bakh: for explaining diffusion to me enough times that it finally sank in.

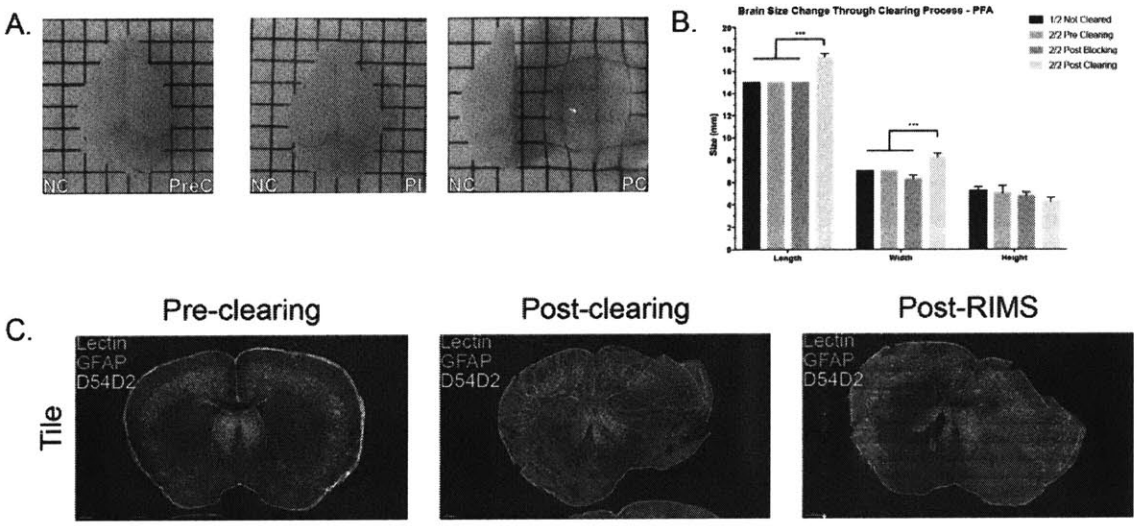

Figure S1: PFA tissue is not resistant to thermal clearing. A) Representative side-by-side images of PFA-fixed brains through the clearing protocol in Figure 1A. B) Quantification of tissue deformation. Statistics noted in the text. C) Qualitative analyses of PFA sections suggest loss of structural integrity after heat-clearing. *NC: non-cleared; PreC: PreClearing; PI: PostInactivation; PC: PostClearing *p<.05 **p<.01 ***p<.001 ****p<.0001 ns: not significant*

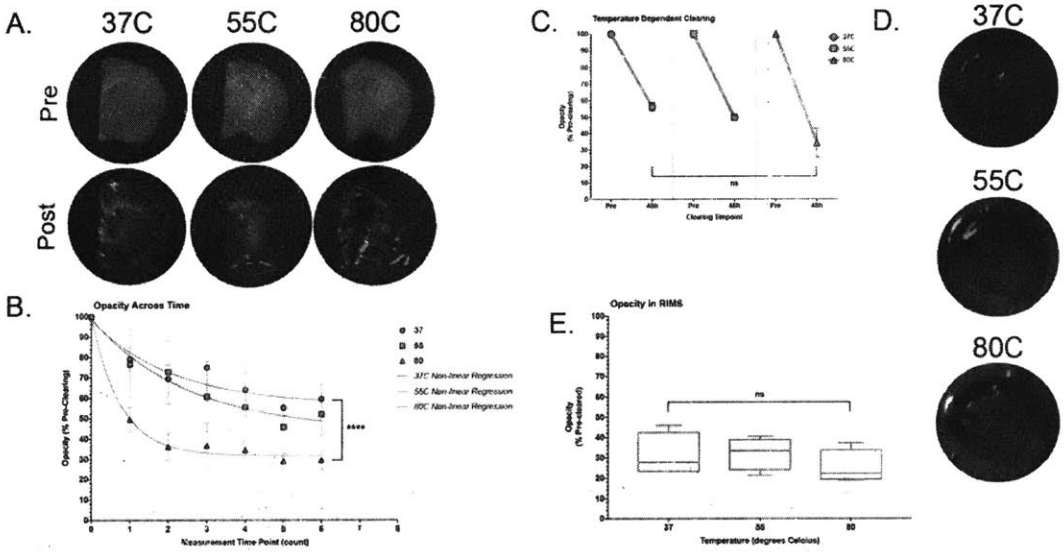

Figure S2: Increasing temperature provides minimal clearing benefits. A) Representative images of slices before (top) and after (bottom) clearing at three different temperatures. B) After three days clearing, significant differences in final opacity emerge. Statistics noted in the text. C) No differences between pre and post-clearing opacity at 48h. D) Represetnative images of slices cleared at three different temperatures in pre-imaging RIMS. E) Incubation in refractive index matching solution (RIMS) mitigates temperature-dependent differences in opacity. *Pre: PreClearing; Post: PostClearing;*p<.05 **p<.01 ***p<.001 ****p<.0001 ns: not significant*

Figure 1

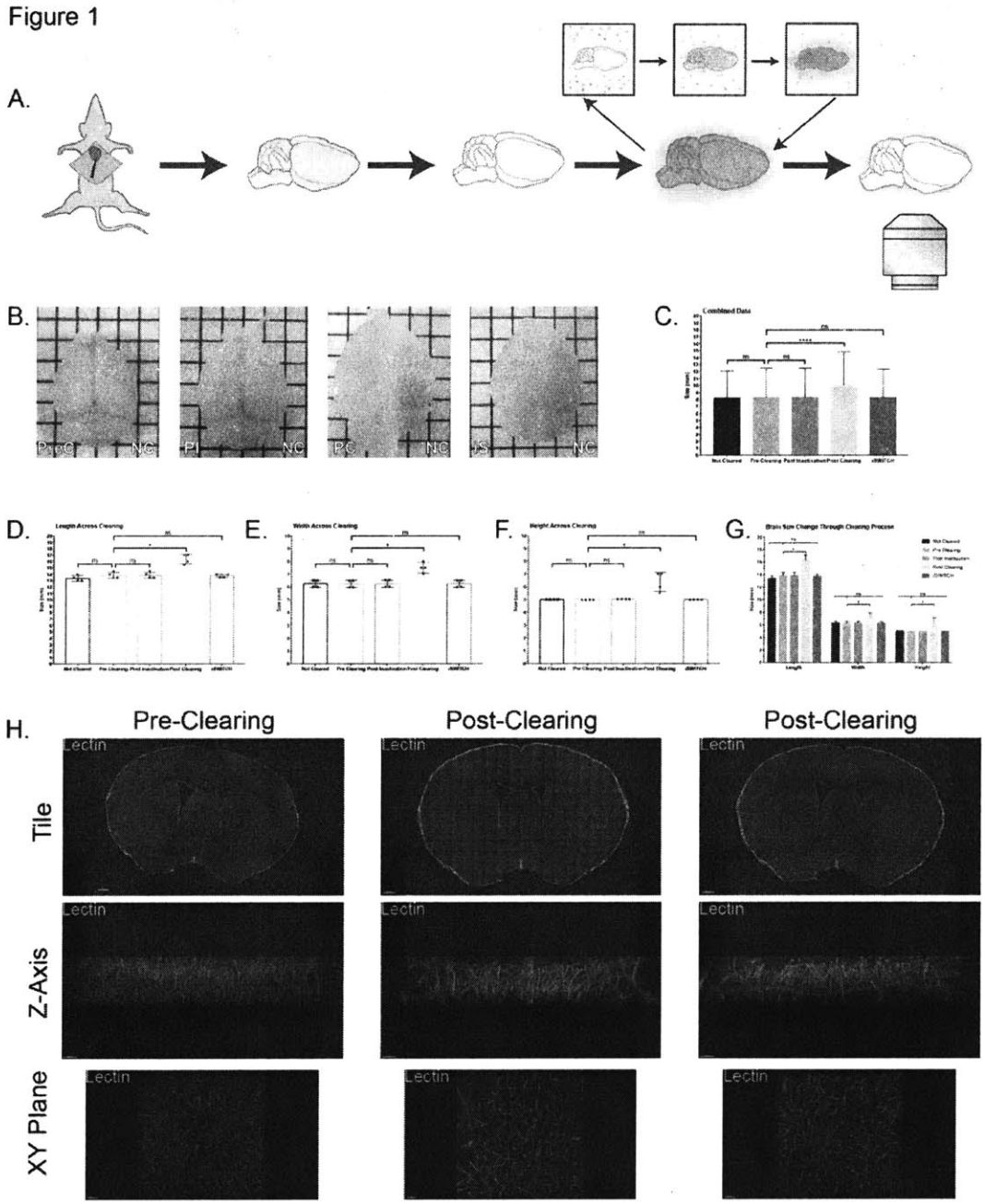

Figure 1: Perfusion-mediated PFA/GA fixation yields robust tissue. A) Overview of sequential steps: the protocol starts with perfusion, is followed by inactivation, then clearing, iSWITCH labeling, and finally SPIM imaging. B) Representative images of brains through the clearing process. The non-cleared brain is on the right, while the processed brain appears on the left. (C-G) Quantification of tissue deformation across clearing stages. Statistics noted in the text. H) Qualitative analyses of structural labeling suggests specimens remain intact despite temporary tissue expansion. *NC: non-cleared; PreC: PreClearing; PI: PostInactivation; PC: PostClearing; iS:after incubation in iSWITCH primary buffer. *p<.05 **p<.01 ***p<.001 ****p<.0001 ns: not significant*

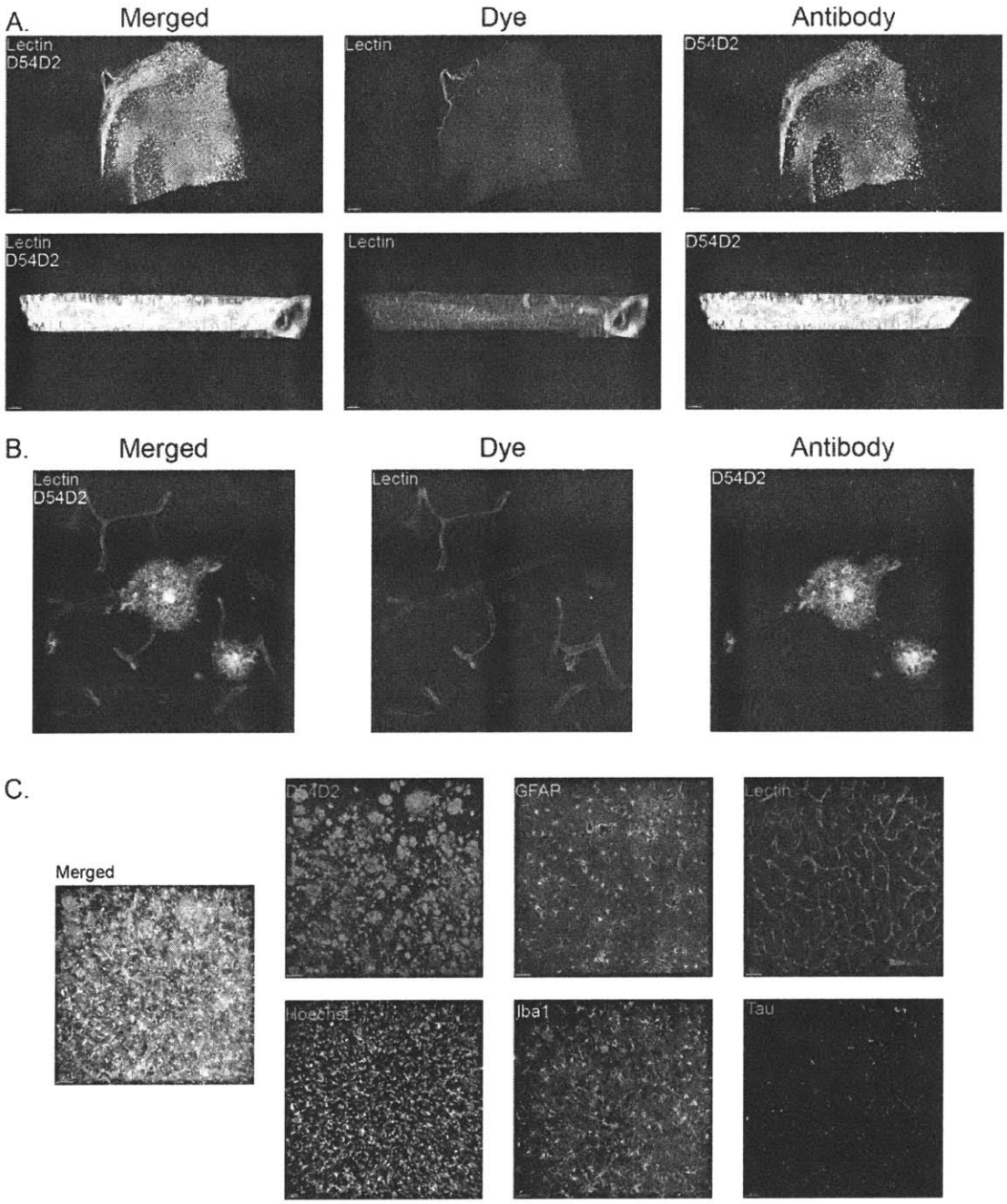

Figure 3: SWITCH fixation and iSWITCH labeling preserve the integrity of human post-mortem samples. A) Top: Representative images of a human autopsy specimen labeled to visualize amyloid-beta (D54D2) and vasculature (lectin) Bottom: Images showing full penetration of both the antibody and dye using iSWITCH methods. B) Confirmation of microstructural preservation. C) Multiplexing of up to six taget structures is possible in SWITCH tissues.

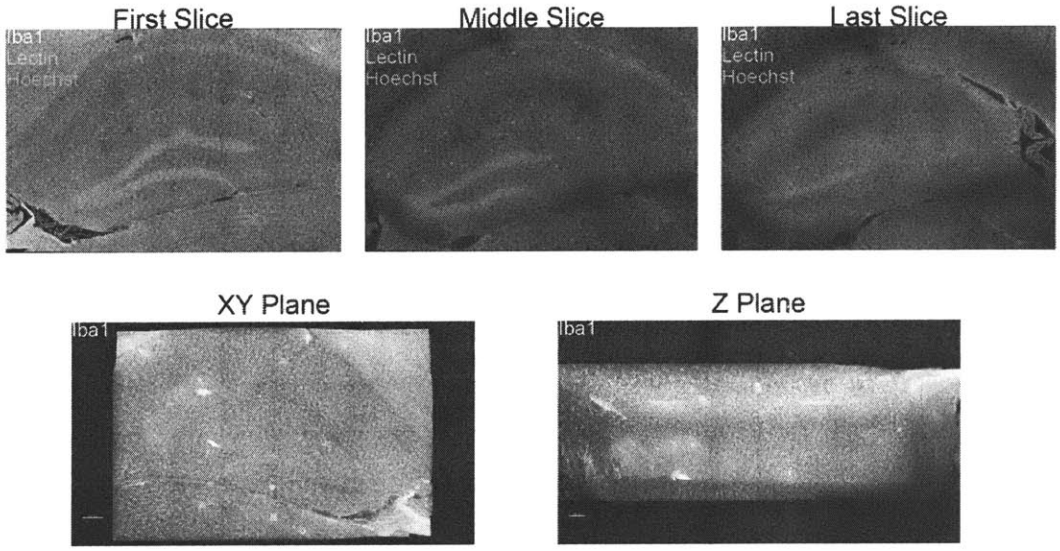

Figure S3: Antibodies that label better with longer incubation times do not require SWITCH methods. A) Representative images to show full penetration of Wako Iba1 antibody through a 1mm sample. B) Iba1 specific signal to show significant labeling across the tissue and through the entire depth of the specimen.

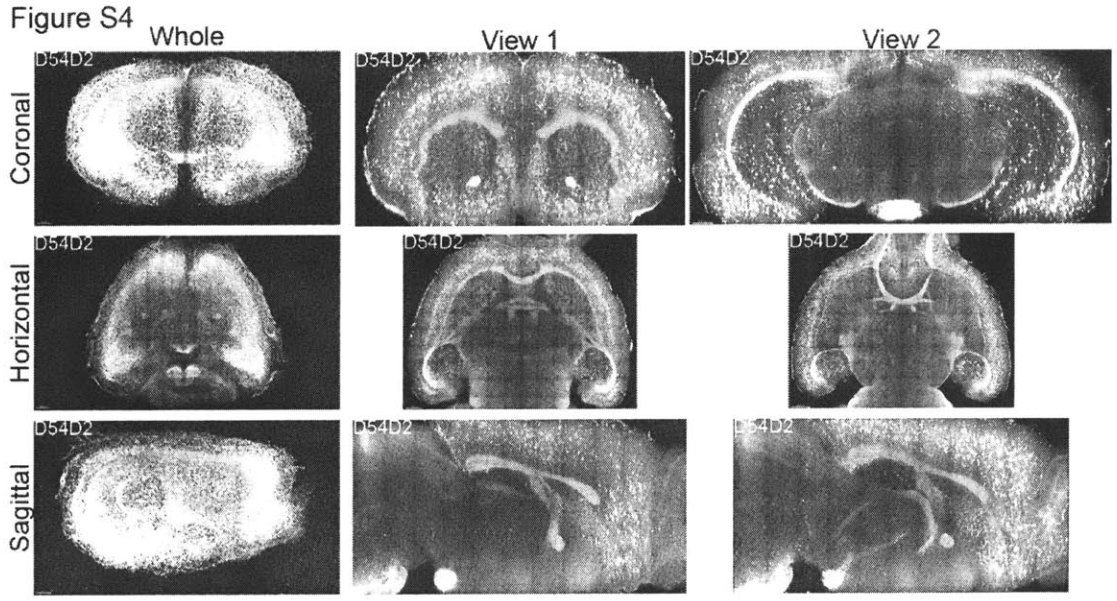

Figure S4: Amyloid-beta iSWITCH immunolabeling works in whole brain as well as hemisphere samples.

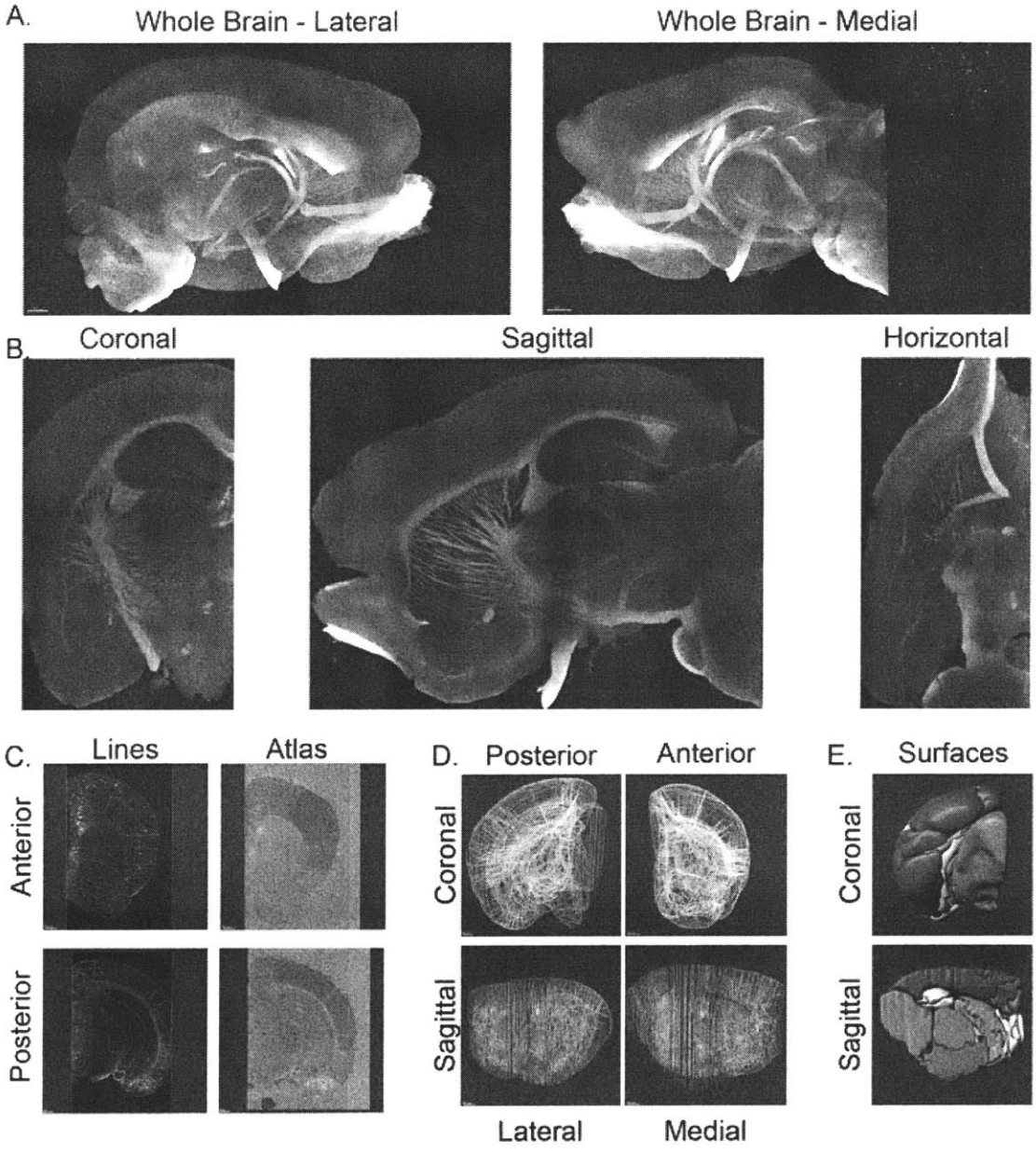

Figure 4: White-matter based hand segmentation of brain areas provides robust identification of specific regions. A) White matter tracts in the whole mouse brain. B) Optical slice-wise visualization of white matter tracts. C) Representative examples of hand-drawn segmentation (left) next to the Allen Mouse Brain Atlas section (right, anterior section #43, posterior section #85) from which they were drawn. Website: © 2015 Allen Institute for Brain Science. Allen Mouse Brain Atlas [Internet]. Available from: http://mouse.brain-map.org[311] D) Representative images showing the whole-brain segementation. E) Representative images of the volume-rendered segmentation.

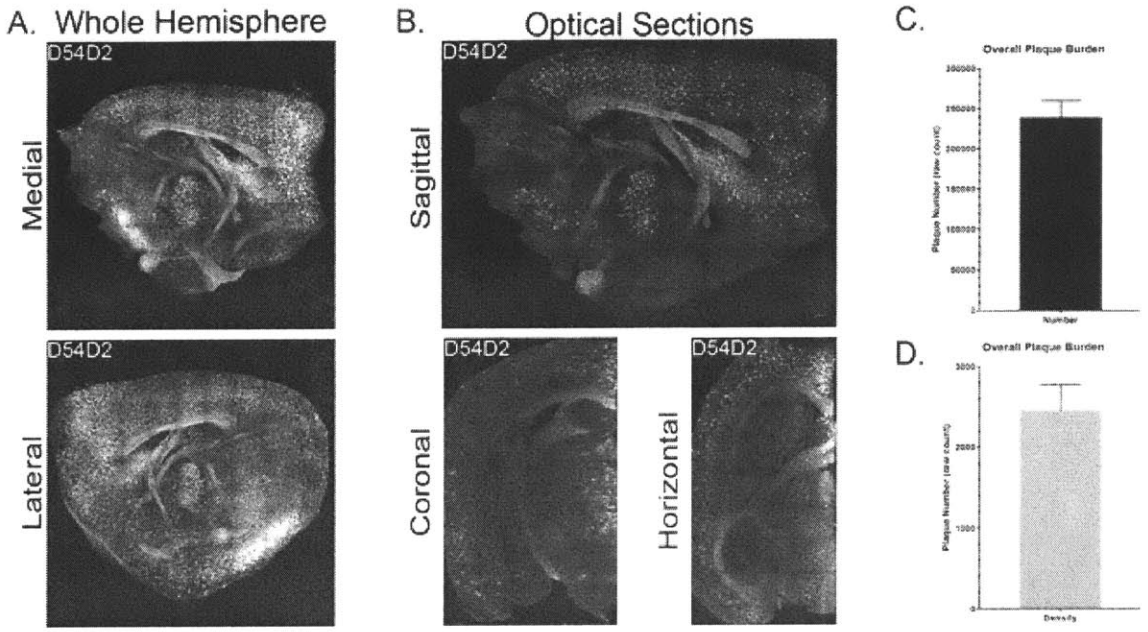

Figure 5.1: Whole-brain mapping reveals network-level correlations in amyloid burden. A) Images of the amyloid burden in whole hemispheres from the brain of a representative 12-month old 5XFAD mouse. B) Optical slice confirmation iSWITCH mediated homogenous labeling. C) High plaque counts in the aged 5XFAD mice. D) Density better reflects the overall burden and can account for differences in brain size. *;*p<.05 **p<.01 ***p<.001 ****p<.0001 ns: not significant*

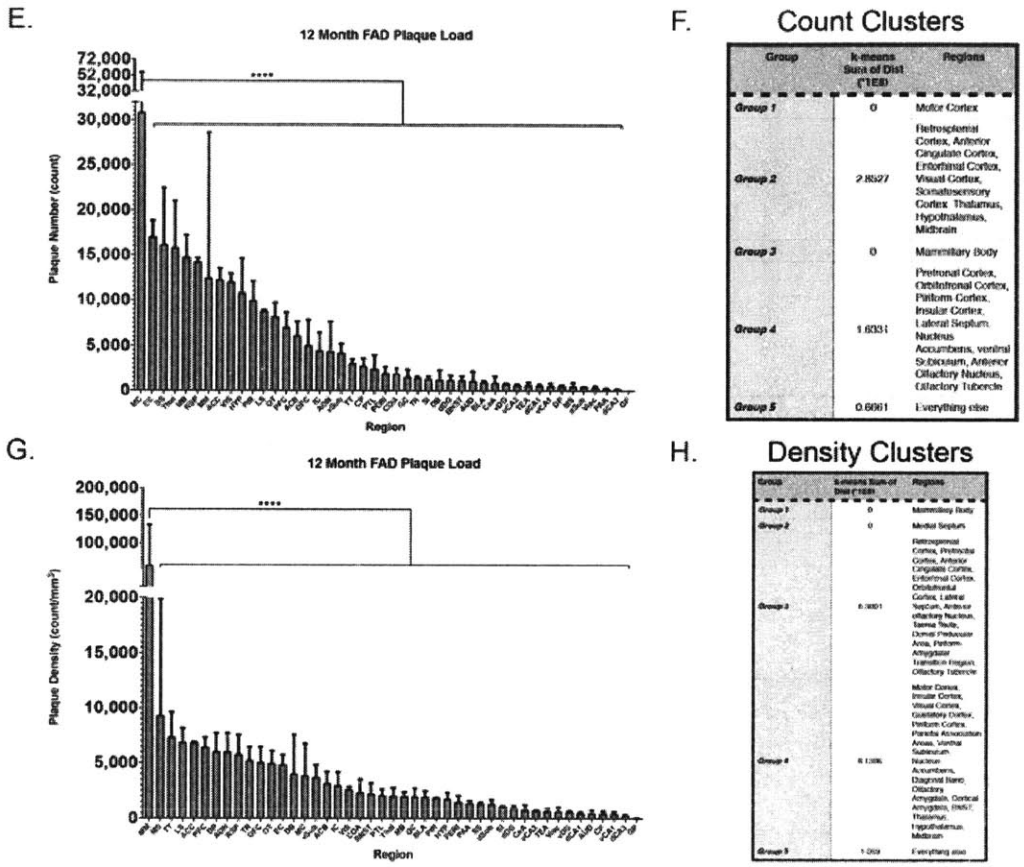

Figure 5.2: Whole-brain mapping reveals network-level correlations in amyloid burden. E) Ranking brain region by raw plaque count suggests cortical regions are most severely affected. F) Brain regions clustered by raw plaque count reveal functional networks have similar numbers. G) Ranking brain region by density shows that subcortical regions are likely the most severely affected by accumulating amyloid. H) Functional networks also cluster by density, although the pattern appears more obscure. *ACB: nucleus ccumbens; ACC: anterior cingulate cortex; AON: accessory olfactory nucleus; AUD: auditory cortex; BLA: cortical-like amygdalar regions; BNST: bed nucleus of the stria terminalis; CeA: striatial-like amygdalar regions; COA: olfactory-life amygdalar regions; CP: caudoputamen; DB: diagonal band; dCA1: dorsal CA1; dCA3: dorsal CA3; dDG: dorsal dentate gyrus; DP: dorsal peduncular area; dSub: dorsal subiculum; EC: entorhinal cortex; GC: gustatory cortex; GP: globus pallidus; HYP: hypothalamus; IC: insular cortex; LS: lateral septum; MC: motor cortex; MB: mid-brain; MM: mammillary body; MOB: main olfactory bulb; MS: medial septum; OFC: orbitofrontal cortex; OT: olfactory tubercle; PAA: piriform-amygdala area; PERI: perirhinal and ectorhinal corticies; PFC: prefrontal cortex; PIR: piriform cortex; PTL: parietal association areas; RSP: retrosplenial cortex; SI: substantia innominate; SS: somatosensory cortex; TEA: temporal association areas; Thal: thalamus; TR: piriform-amyloid transition region; TT: taenia tecta; vCA1: ventral CA1; vCA3: ventral CA3; vDG: ventral dentate gyrus; VIS: visual cortex; Visc: visceral cortex; vSub: ventral subiculum. ;*p<.05 **p<.01 ***p<.001 ****p<.0001 ns: not significant*

Chapter 3:

4D mapping of circuit-specific Alzheimer's pathology reveals early subcortical vulnerability to Aβ deposition.[d]

Abstract

Predominant hypotheses posit that the accumulation of amyloid peptides in the brain is the proximal cause of Alzheimer's disease (AD). While amyloid does demonstrate severe cellular toxicity, its levels in the parenchyma plateau long before the onset of cognitive symptoms. For years the temporal lag between prodromal disease initiation and clinical symptom onset has impeded investigations into the origin and spread of pathology, and thus its earliest consequences. However, new methods that allow us to unbiasedly survey the spatial and temporal pattern of protein expression can help us to reveal the precipitating patterns of AD inception. In the previous chapter, I presented optimized iSWITCH protocols for intact specimen immunolabeling, and used them to reveal network-level correlations in amyloid-beta (Aβ) burden. Here I use the novel methods to create a spatially-unbiased, temporally precise map of amyloid accumulation in AD-model mice. The resulting 4D map identifies subcortical nodes and white matter tracts of the Papez memory circuit as regions that are particularly vulnerable to significant, early pathological aggregation. Alongside functional impairments and neuroinflammation, I also demonstrate unique white matter pathology that may resolve both the mechanisms of Aβ propagation and the temporal lag between cerebral amyloidosis and AD-related memory loss. Because similarly processed human samples from Papez circuit regions also have significant Aβ burden, I conclude that this core memory network is particularly vulnerable to Aβ deposition, and may act as a seed region to drive progressive alterations in long-range memory circuits. For the first time, these observations raise the possibility that network-specific Aβ accumulation -- rather than whole-brain or cortical burden -- may underlie AD-related progressive memory loss.

Contributions

R.G.C., L.H.-T. conceptualized the ideas for the chapter.
R.G.C. designed all of the experiments in the chapter, wrote the chapter, and performed the experiments and the analyses under the supervision of L.-H.T. R.G.C. also oversaw the work by: N.D., F.A., and S.B.
I.D. provided human brain for Figure 7, and immunohistochemical labeling for Figures 7B &7C
H.C. performed SPIM image acquisition and file stitching of all whole-brains.
N.D. performed experiments in Figure 4A '4G8' and 4J 'GFAP(rb)'.
A.L.W. performed the ISH/IHC in Figure S1.
J.W. performed the electrophysiology experiments and initial analyses in Figure 5.
F.A. & S.B. sectioned brains for Figure 3A.

---

[d] The data in Chapters 2 and 3 are in preparation for submission of the manuscript: 4D Mapping of Amyloid-beta pathology reveals subcortical susceptibility in Alzheimer's Disease. Author's involved in the work in this chapter: Rebecca Gail Canter, Li-Huei Tsai, Ivana Delalle, Heejin Choi, Ashley Watson, Jun Wang, Nina Dedic, Fatema Abdurrob, and Stephanie Bousleiman..

Introduction

Alzheimer's disease (AD) presents as a progressive memory impairment that impacts patients' abilities to recall specific events.[15] This type of 'episodic' memory relies on the hippocampus (HPC),[254] indicating that in AD, memory loss may result from dysfunction in this region. Supporting this idea, the HPC and related entorhinal cortical (EC) regions show marked cellular loss that predicts cognitive decline.[255,256] However, linking HPC dysfunction to the hallmark aggregates that are thought to be the root of AD -- extracellular aggregates of the amyloid-beta (Aβ) peptide and intracellular neurofibrillary tau inclusions (NFT) -- remains difficult because these pathologies only affect the HPC late in disease progression.[82,187] Recent patient imaging experiments corroborate the temporal discrepancy between observations of high Aβ (which is thought to be the initiator of AD) and HPC-dependent impairment because cortical levels of Aβ appear to plateau years before overt signs of memory loss.[257] Despite the inconsistency between the clinical symptoms and the neuropathological observations, epigenomic sequencing and electroencephalogram (EEG) studies also demonstrate significant cellular- and network- level alterations in the hippocampus during AD progression.[21,132] Thus, while increasing evidence suggests HPC dysfunction underlies memory loss, the cause of these changes in the absence of pathological biomarkers remains uncertain.

Although the hippocampus shows late AD-related protein aggregation, other brain regions which project to and modulate the HPC do demonstrate significant pathological burden early in the disease.[187,194,258] In particular, Aβ is widespread in patients' brains,[82,84] and has been correlated with early alterations in networks involving the HPC.[87,259] However, these networks show significant Aβ burden in study populations, thus they cannot determine in which exact regions pathological accumulation initiates and are unable to observe how it progresses to affect increasing neural area and cognitive function. Additionally, controversy remains about the role of these proteins in memory imapriment,[260] largely due to the promiscuity of Aβ across brain regions and different dementias and the poor temporal resolution of human studies. Yet abundant experimental evidence links Aβ with pathophysiological processes regularly observed in AD.[66,78,261,262] This has led to the 'cellular phase' hypothesis of cognitive decline which postulates that biochemical insults, like Aβ accumulation, lead to dyshomeostatic responses in cells, and these alterations are acutely responsible for memory loss.[14] Though this explanation unites diverging ideas about the etiology of cognitive decline, it still cannot explain the origins of AD, how it spreads, and why the memory loss is consistent and specific.

Recent investigations into the sequential progression of Aβ deposition in mouse models suggest that the aggregates spread between connected brain regions in a prion-like manner.[96,193] Our previous data (Chapter 2) also indicates network-level correlations in Aβ burden, however none of the studies addressed which regions show endogenous susceptibility to Aβ plaques or whether functional disruption of circuit activity or physical prion-like propagation contributes to Aβ spread. Here, we capitalize on the temporal reproducibility of mouse models and utilize our novel iSWITCH labeling methods to create a spatially unbiased, temporally precise map of AD-like pathology. Our results demonstrate for the first time that structures of the Papez circuit, specifically the mammillary bodies (MM) and subiculum, are particularly vulnerable to Aβ deposition and undergo early functional alterations that may destabilize memory circuits. Furthermore, we reveal circuit-specific white matter tract Aβ deposition and aggregates within axonal projections traveling within them. Together these data suggest that both physical propagation and functional disruption may contribute to disease progression. Because we confirm AD-related Aβ within patient fornix and MM, this data indicates that subcortical Papez regions that connect to and modulate HPC function may be early susceptibility hubs from which AD pathology can spread.

Results

A 4D map of Aβ pathology reveals subcortical susceptibility hubs within the Papez memory circuit.

Because our previous data suggested functional network-level correlations of Aβ load, we wanted to ascertain whether the pattern emerges randomly, or if the correlations persist across time suggesting that connectivity between the regions may contribute to the spread. To describe the sequential involvement of molecularly identified regions, we decided to use iSWITCH labeling methods to produce a spatially unbiased map of immunologically identified endogenous Aβ accumulation. Because mouse models afford temporal precision and control over lifetime experiential factors that often confound human staging studies,[14] we decided to use the 5XFAD model of AD-like amyloidosis for our initial insights.[223] These mice show age-dependent increases in extracellular Aβ aggregates,[223] however the full brain-wide pattern of deposition has not been reported. Our previous data suggested that 12-month aged animals have significant burden throughout the forebrain, thus we decided to start our time course in 6-month mice, expecting that we might observe region-specific burden. To our surprise, these animals show plaques throughout the brain (Figures 1 1A and 1.1B) with high overall aggregate number (Figure 1.1C), and a relatively high plaque density (Figure 1.1C). When ranked by count, however, we noticed that some regions showed significantly higher number than the rest of the brain (Figure 1.2D, Repeated Measures One-way ANOVA, $F_{(46,46)} = 1.946$, $p = 0.0130$), suggesting that despite high overall levels of Aβ at 6 months, there is specific aggregation within certain brain regions. The motor cortex has significantly more

plaques than the rest of the brain, may be due to its significant size. Performing further clustering analyses to better understand the pattern of aggregation in our data (Figure 1.2E, k-means, Euclidean distance, Cluster Number = 5), we see that regions of the olfactory and cortical-limbic systems (e.g. basolateral amygdalar complex (BLA), piriform cortex (PIR), entorhinal cortex (EC)) also have high numbers of Aβ aggregates. Interestingly, these networks segregate into separate clusters from the primary hippocampal (e.g. dCA1) and striatal (e.g. caudoputamen (CP)) regions. However, as we noted with the motor cortex, raw count measures are not sensitive to regional volume and may purely reflect differences in size. To overcome this, we also looked at which areas have the densest Aβ to make a more direct comparison and infer levels of cellular stress from the peptide accumulation. When the data is normalized by volume to create a measure of aggregate density, regional specificity becomes more significant (Figure 1.2F, Repeated-measures One-way ANOVA, $F_{(46,46)} = 3.881$, $p < .0001$) and distinct subcortical structures – the MM and pontine gray (PG) -- now show the highest burden. Clustering by density (Figure 1.2G, k-means, Euclidean distance, Cluster Number = 5) reveals that distinct functional networks have similar burden, further supporting our previous results. For example, the extended cortico-limbic system cluster together (cluster 4), as do the subiculum and septum (cluster 3). These observations suggest that the amyloid burden within a given network is evenly distributed, however, across different functional networks, the burden varies. Additionally, this data shows that by molecularly identifying total Aβ correlations in amyloid load can be seen even in advanced AD, a finding which pathological samples cannot predict. Considering the networks involved at this stage behaviorally, the literature suggest that they relate to emotional processing[243] and episodic memory.[263] This revelation is particularly interesting because it suggests that network-level distribution of Aβ accumulation matches circuits that underlie known behavioral alterations in early AD.[264]

Although the data already reveal interesting network correlations, it was unable to show whether the consistent circuit clustering pattern results from sequential spread, or arises randomly. We extended our map to earlier ages when the Aβ burden should be less dense, and whole-brain imaging could reveal some of the earliest affected regions. At 4 months, the burden is noticeably less than older animals (Figures 2.1A and 2.1B), and the mice show much lower overall plaque count and density (Figure 2.1C). Ranking by plaque count demonstrates that distinct regions have significant Aβ load (Figure 2.2D), and cluster analysis (Figure 2.2E, k-means, Euclidean distance, Cluster Number = 5), shows that regions homologous to those that function as nodes of the default mode network (DMN) segregate into specific groups (1,2,3), while hippocampal-projecting regions also cluster together (4). This finding is striking because in humans, DMN alterations occur in cognitively healthy individuals with Aβ burden, and in AD, Aβ seems

to preferentially deposit in nodes of the DMN.[88,259,265] The DMN engages during passive mentation like daydreaming, and is highly interconnected to the hippocampus and temporal lobe.[266] Alterations in DMN function range drive varied cognitive responses that range from undetectable to mild impairment (MCI). To understand how the normalized burden may affect the circuit interpretation, we ranked by regional plaque density (Figure 2.2F, 2.2G), and similarly to the aged mice, the PG and MM show the highest overall density. Followed by these regions, the DMN nodes of the anterior cingulate cortex (ACC) and retrosplenial cortex (RSP) show significant burden, indicating that the despite raw counts that suggest brain-wide paucity of Aβ at this age, the aggregates that develop are highly specific and spatially restricted. This indicates that there are likely dissociable patterns of accumulation between brain regions, which may have differential functional consequences. Remarkably, regions in the two most affected clusters (the MM in cluster 1 and the subiculum, RSP, ACC in cluster 2) not only correlate with DMN activity, but are also specifically connected to each other and form the Papez long-term memory circuit.[267] Because the Papez circuit also includes the HPC, underlies episodic memory, and projects to the DMN, this finding predicts that the earliest Aβ-induced network dysfunction should result in episodic memory difficulties, which is consistent with patient observations.[197] Furthermore, because this occurs at the earliest stages of AD-related pathological change, this finding may suggest that the temporal lag between first signs of Aβ accumulation within a network and detectable consequences on cognitive symptoms is longer than expected. This is consistent with predictions from a recent meta-analysis,[245] and also complicates interpretations of the functional consequences of the cortical amyloid seen later in disease progression.

Connected subcortical hubs within the Papez circuit precipiatate Aβ aggregation

With a narrowed focus on the Papez circuit due to its exceptional burden and interesting connectivity, the next question was whether we could pinpoint the source of Aβ within that circuit. We extended our temporal map to analyze 2-month aged mouse brains, and saw extremely specific nodes containing Aβ aggregates (Figures 3.1A and 3.1B). At this age, we observe only the MM, septum, and subiculum with significant regional accumulation (Figure 3.1C, Repeated-measures One-way ANOVA, $F_{(46,46)} = 9.259$, $p < .0001$). The MM and septum (Figure 3D.1, k-means, Euclidean distance, Cluster Number = 5, clusters 1 and 2, respectively) separate from the rest of the Papez and DMN-related regions, and these other areas groups together at this time point (cluster 3). This suggests that those three regions may be key to Papez circuit vulnerability, and may act as hubs in its spread through the extended DMN and limbic systems. One notable observation is that despite very low levels of Aβ at this time, the medial septum (MS) and nucleus of the diagonal band (DB) cluster together, away from the rest of the unaffected regions (cluster

4). This suggests that although these regions do not stand out for having particularly high plaque density at any point in the progression, their Aβ burden increases early and plateaus. This is significant because these regions are core parts of the basal forebrain cholinergic system,[268] which is known to degenerate early in AD.[269] Cholinergic dysfunction is one of the longest-standing hypothesis for the etiology of AD,[179] and 75% of the drugs currently approved by the United States Federal Drug Administration for the treatment of AD act on the cholinergic system.[269] Though this hypothesis has been largely discarded, the drugs do show mild efficacy at the earliest stages of AD, and these findings may suggest that they plan an early, but fleeting, role in Aβ propagation.[184]

Finally, with increasing evidence to suggest that the pattern of network spread is hierarchical and not random, we wanted to determine if one of these dense regions may be a 'seed' region from which pathology spreads to the rest of the brain. We analyzed one final 1.5-month time point and at this earliest stage, only the MM and subiculum show amyloid burden (Figure 3.2E), suggesting these key regions of the Papez circuit act as the earliest hubs from which dysfunction and Aβ can spread. Qualitative analyses suggested that there were no amyloid deposits in the brain at 1 month of age (data not shown), indicating the pathology in these regions is not a developmental phenotype. The summary data (Figure 3.2F) suggest that from the MM and subiculum, cholinergic regions (septum, DB) are next affected, followed by the DMN, from which it spreads to the extended limbic system, and eventually the rest of the brain (Figure 3.2G, top). Importantly, the sequence cannot be explained by the pattern of transgenic mRNA expression in the mouse line (Figure S1), suggesting that aggregation patterns result from biologically relevant vulnerabilities in each brain area. This mapping not only correlates well with the human clinical imaging literature,[87,198,270] but also suggests a behavioral-cognitive progression that can be determined by the functional roles of the circuits. Ranking the network-level correlations of Aβ by age predicts a progressive pattern of cognitive impairment that begins with episodic memory loss (Papez) followed by dysfunctional executive processing (DMN) that expands into emotional dysregulation (Limbic), followed by generalized cognitive impairment (Figure 3.2G, bottom). This model provides a framework to unite disparate observations of affected networks throughout the literature, and may be used to correlate clinical assessments of behavioral change with investigative and/or predictive imaging biomarkers.

Mammillary body dysfunction begins at the earliest stages of amyloidosis.

While the subiculum is known to show early atrophy and dendritic loss that correlates with memory impairment in AD patients,[271–273] the MM is poorly understood in the context of memory except for its role in transmitting hippocampal signals.[274,275] Its involvement in AD progression is not known.

Interestingly, the MM are implicated in Korsakoff's syndrome (KS) and Wernicke's encephalopathy (WE) which show similar amnesia to AD, but are otherwise unrelated memory impairments.[276,277] Because of these observations, we wanted to investigate what contributions the MM might make towards the progression of AD. We hypothesized that it may act as a seed region for physical propagation[96,278] or, if it shows significant functional dysregulation, it might feed network instability that could lead to brain-wide vulerability in the AD model.

Although Aβ is typically thought to be acutely toxic,[279] it is also believed that deposits may be protective against certain pathological changes.[59,280] To investigate the influence of Aβ on the MM, we first wanted to ensure that the whole-brain mapping data revealed the true Aβ burden in the region, and did not result from imaging or analyses artifacts. To test this, we labeled 100um, cleared sections with the same Aβ antibody used for the whole-brain timeline (D54D2) and a second well-verified amyloid antibody (4G8). With both antibodies, sections show significant amyloid load in the MM of 2 months aged FAD mice (Figure 4A). Next, because Aβ closely associates with the vasculature in AD brains[281] and has been suggested to be a primary cause of cognitive impairment in the disease,[282] we wanted to see whether Aβ in the MM at the earliest stages affects the neurovasculature. In the MM we see vessel-associated plaques (Figure 4B), and qualitatively observe a subtle change in vascular integrity (Figure 4B), suggesting some AD-typical amyloid angiopathy in this region. Aβ in the vasculature and parenchyma also fundamentally alters glial functioning and typically induces a neuroinflammatory response, especially in the regions around aggregates[283,284]. These reactions may critically mediate some of the physiological alterations in AD, but it is debated whether they are largely protective or harmful.[125,285] To determine whether the MM has a typical neuroinflammatory phenotype, we labeled 100um thick sections for Iba1, a macrophage specific protein that, in the brain, is expressed primarily by microglia, and also for glial fibriallary acidic protein (GFAP) which levels increase in immune-reactive astrocytes. To our surprise, microglial morphology does not change in the MM in response to the significant Aβ burden (Figure 4C, Quantification: Figures 4D- 4I, Welch's T Tests, all $p > .10$). This suggests that microglia in the MM are either just at at the onset of mounting an immune response, or that there are different or fewer reactive microglial cells in the MM in response to Aβ deposition. Similarly, there seems to be no astrocytic response in the MM in response to Aβ (Figure 4J) using two different antibodies towards GFAP. This lack of immune response is potentially interesting, and likely relevant to the regional susceptibility because microglia and astrocytes are thought to be key mediators of inflammation -- and Aβ clearance -- in AD.[61,171,286] Importantly, in other brain regions without obvious Aβ accumulation, there are also not differences in Iba1+ or GFAP+ cells, however all the regions observed with plaques, we did not observe

others that significantly lacked an immune response (data not shown). Together, this suggests that increased Aβ deposits in the MM may lead to slight vascular alterations, however they do not induce morphologically detectable microglial or astrocytic responses. This quiescence may drive the early vulnerability of the region.

Because there was no immune response, we wanted to know if there are Aβ-induced alterations in neuronal activity. Previous work conflicts as to whether immune responses are protective or damaging to neurons,[125,171,172] but the literature does indicate that Aβ induces hyperexcitability in cells.[20,39] To test whether MM neurons show disrupted firing properties, we used whole-cell patch recordings to observe action potential output in response to increasing current injection. Interestingly, MM neurons in FAD mice show enhanced action potential firing compared to littermate controls (Figure 5A, Two-way ANOVA, 'Genotype' $F_{(1,503)} = 90.15$, $p < 0.0001$; 'Interaction' $F_{(10,503)} = 1.807$, $p = .0568$), and this is not due to altered action potential threshold (Figure 5B, Welch's t test, $t_{46} = 1.146$, $p = .2577$) or kinetics (Figure 5C, Welch's t test, $t_{32} = 0.7107$, $p = 0.4824$). The neurons in 5XFAD MM do show an increased resting membrane potential (Figure 5D, Welch's t test, $t_{40} = 4.807$, $p = 0.0001$) and smaller action potential amplitude (Figure 5E, Mann-Whitney U Test, $U = 87.5$, $p = 0.0497$) which may drive the hyperexcitability phenotype we observe. Recent studies of this phenotype in AD models suggest that the phenotype may emerge from dendritic shrinkage and spine loss.[66] Thus, we wanted to observe whether loss of synaptic input and alterations in spine number might account for the phenotype in the MM. We ran a proof of concept experiment in 6 month aged tissue to test our antibody and protocol (Figure 5F), and to our surprise, at 6 months there is a 35% reduction in synaptophysin labeling (Figure 5G). Further experiments in the septum of 2 month aged mice, which also have significant plaque load, also show reduced synaptophysin labeling, indicating a loss of synaptic connectivity at this young age (data not shown). We are currently performing follow-up experiments in the 2 month aged mammillary body samples. Furthermore, work from our group has previously shown that alterations in histone deacetylases (HDAC),[215] and specifically increases in HDAC2,[134] correlate with reduced spine density and worse synaptic plasticity in AD-related regions. Thus we will test whether the MM shows alterations in HDAC2 that may underlie the observed synaptic loss. Understanding how this alteration in excitability and synaptic connectivity affects circuit and network function is the next major step in this project. Parsing the role of the MM in basic learning paradigms, and in understanding how its functional demise impacts AD progression, are two important and as yet unanswerable questions. Overall, the data we present here shows that the MM has an atypical neuroinflammatory response to increasing Aβ and, rather than

quiescent glial cells protecting regional function, the MM shows functional deficits and a profound loss of connectivity that is likely to impact memory from the earliest stages of AD.

The fornix and related white matter tracts show unique vulnerability to Aβ deposition.

One remaining question to understand Aβ initiation and propagation in the brain was whether the aggregates in the MM are due to local APP proteolysis or result from Aβ trafficked from afferent fibers. We noted that the mammillary body and subiculum are not only the earliest hubs to show amyloid in our model, but are also functionally connected via the fornix white matter tract. Interestingly, in aged animals we noticed that the fornix develops Aβ deposits along its length (Figure 6A), and that this aggregation is specific to the fornix (Figure 6A, green arrows). Though other investigators have noted white matter amyloid,[287,288] to our knowledge this is the first description of tract-specific white matter deposition. Thus, we were interested in the nature of the aggregate, and wondered if plaques deposit along or within the tract. To investigate this, we took cross-sections of the fornix and labeled for Aβ and also myelin basic protein (MBP) to identify the location of the tract (Figure 6B). In these sections we saw that fornix and related white-matter structures showed significantly more aggregation than other white matter tracts (Figure 6C, Friedman Test, $W = 40.29$, $p < .0001$). Interestingly, however, the morphology of the Aβ within the fornix appeared different than the aggregates within the other tracts. To better observe the structure, we imaged the tracts at high resolution for 3D reconstruction. Remarkably, what looked like hazy amyloid labeling typical of non-aggregated Aβ in the XY plane (Figure 6D), actually resembles axonal tracts when observed in the YZ plane (Figure 6D). Because many other white matter tracts are present in the same coronal section (Figure 6B), we imaged additional structures to determine if the Aβ aggregation pattern was widespread, or unique to the fornix. To our surprise, while the fimbria, alveus, and cingulum all showed significant fibrous Aβ, the corpus callosum did not (Figure 6E). This was especially surprising because neurons in the cortex show equally high transgenic expression (Figure S1), and cortical regions have high Aβ burden (Figure 1A). Thus, the specificity suggests that Aβ aggregation along axonal projections is unique to fibers of the Papez circuit, and suggests circuit-specific trafficking patterns that may reflect the physiological function of the native peptides.[217,225,289,290]

Finally, because these observations are from aged mice with significant plaque burden throughout the brain, we wanted to test whether this may be a mechanism of Aβ propagation at the earliest stages. In cross sections of the fornix from 2m mice, we see similar fibril structures to those detected in aged brains (Figure 6F), however many fewer than in aged mice. Because the MM neurons show significant intracellular protein (Observations of 3D rendered data presented in Figure 4A), the primary source of Aβ

remains uncertain. Though future experiments will need to clarify the source for a full etiological understanding of the disease, observations of intra-axonal Aβ specific to Papez circuit white matter tracts suggest that projection neurons of memory-circuit hubs have specific vulnerability to Aβ and identifying the subiculum and MM as early susceptibility hubs can enable better testing of early interventions and screening paradigms.

Human mammillary body shows significant AD-related amyloid burden.

Together our observations suggest that subicular-fornix-mammillary body network may be vulnerable to Aβ aggregation, and that this burden may drive circuit dysfunction in AD. However, while the fornix and subiculum have been implicated in human AD-related memory loss, the neuropathological status of the MM in AD patients remains largely uncharacterized. Few papers exist on the MM in AD, and most suggest the presence of Aβ,[291,292] however this is strongly contested (personal communication). To determine whether our observations of MM Aβ are relevant to the human disease condition, we acquired 4 post-mortem human autopsy mammillary body specimens (Figure 7A). From these, we first took traditional pathological sections from the MM (Figure 7B) and labeled for diagnostic Aβ (6F/3D). As expected, these sections showed both dense-core and diffuse Aβ plaques (Figure 7C), confirming that AD patients have Aβ in the MM similar to the mice. These sections demonstrate consistent amounts of Aβ across the AD stages, which is inconsistent with our observations in mice.

To determine the density of Aβ plaques in the MM and ascertain whether the pathology is significant enough to potentially induce regional dysfunction, we used iSWITCH fixation and labeling methods to examine large-volume samples from this region. To our surprise, MM had significantly more pathological density than the thin-section labeling suggested (Figure 7D). Indeed, density measurements indicate that human MM has significant Aβ load, although the numbers suggest that the pure count may not be indicative of disease stage (Figure 7E). We hypothesized this may be to do a significant amount of small plaques in the earliest staged individual and examined the volume as a proxy for age of the plaque. In the the small cohort we examined, amyloid median volume (Figure 7F) and mean volume (Figure 7G) both increase with Braak and Braak stage. Interestingly, in each of the patients with Braak staging, we not only see deposits within the MM itself, but also accumulation along the white matter tracts within the structure. Importantly, a cognitively healthy individual did not have Aβ anywhere in the region. All together, this data provides proof-of-concept evidence that the MM is a site of AD-related Aβ accumulation in humans. Prospective imaging studies and large-volume analyses of a larger cohort of post-mortem brains will enable precise pathological staging. Overall, the presence of Aβ in the MM

suggests that the mouse model might be predictive of human disease spread, and indicates that pathophysiological alterations within the Papez circuit may be a common mechanism of AD-related memory loss.

Discussion

Until recently, limitations in tissue processing and imaging technologies have restricted investigations of pathological propagation in AD to either gross estimations across multiple brain regions, or targeted analyses of thin sections. Through these experimental approaches, a cursory understanding of the hierarchical spread of pathology led to in-depth characterization of the HPC and cortical regions, which have not yielded significant progress towards treatments, interventions, or understanding the etiology of AD. To overcome these hurdles, we have used novel intact-specimen tissue preparation techniques to create a spatially unbiased, temporally precise map of pathological susceptibility in whole mouse brain. Our data reveals that, contrary to the hierarchical regional staging; progressive network susceptibility is key to the progression of AD.

Network disconnection can explain the lag between gray matter Aβ deposition and memory loss.

We identify the Papez memory circuit as a critical early hub of Aβ pathology, which spreads to increasingly expansive, connected networks with advancing age. We show that within the Papez network, the subicular-fornix-mammillary body complex is particularly vulnerable. Despite previously uncharacterized molecular pathology in the fornix and MM, local Aβ burden within the MM causes functional impairments that may contribute to network instability in early AD. While this dysfunction likely does not directly drive the profound memory loss, we also describe progressive white matter pathology within the fornix tracts that may explain the lag between initial Aβ deposition and cognitive decline.[257] The mammillary body and subiculum show early accumulation, however the fornix-traversing projections connecting these regions are slower to develop pathological aggregates. Despite the delay, these tracts are the first we observe to have Aβ deposition, suggesting the axonal pathology may secondarily derive from worsening proteostatic imbalance. One intriguing idea is that the development of axonal Aβ leads to the neurofibrillary tau inclusions that correlate with cognitive impairment. This would explain why tau correlates more closely with cognitive decline,[260] but has few known pathological mechanisms in cellular degeneration. These findings indicate that while local Aβ burden may drive some aspects of AD-related decline, advancing disease results in profound long-range projection pathology. Thus, the deterioration of long-range projections may physically and functionally disconnect networks

and be acutely responsible for memory loss. Investigating the integrity of these pathways may better correlate Aβ accumulation to cognitive decline.

A changing role for the HPC in Alzheimer's disease?

Because the HPC is a core node in each of the affected networks, it is unsurprising that the clinical symptom of AD appears to be HPC-dependent memory loss. However, our results suggest that rather than local HPC dysfunction, key regions that rely on and support the HPC are altered in AD. From these observations, the possibility arises that the HPC undergoes pathophysiological compensation as the network adapts to changing physiological conditions, but is not a core seed of AD-related decline. Even more controversially, it is also possible that alterations in the HPC do not underlie the impairments seen in AD because the nascency of investigation into human memory, and subcortical circuits in general, precludes a complete understanding of how individual nodes in the networks contribute to specific facets of memory and cognition.[254,267] With this understanding, it will be increasingly important to investigate whole networks and multiregional circuit functions alongside molecular characterization of the cellularly and cytoarchitecturally diverse structures that compose most memory circuits.

The mammillary body in memory and cognition.

Contrary to supporting a critical role for the HPC in AD, our data suggest that the MM is a core mediator pathophysiological processes. This region is interesting for the study of AD on multiple levels, as it is situated at the crossroads of many molecular- and circuit-level observations. From a functional standpoint, the MM participates in recognition memory, and mediates spatial and association memories.[293–296] It also integrates visual information into head-direction processing.[297] Disruption of these functions are key deficits in AD,[5,15] and although there is little evidence for MM atrophy in the disease,[298] our data suggests functional alterations within this region due to pathological burden may be the earliest signs, thus our observations remain is consistent with the clinical progression of the disease and neuroimaging biomarkers. Interestingly, the MM are thought to be critically involved in Korsakoff's syndrome (KS), and to a lesser extent Wernicke's encephalopathy (WE), which have very similar memory impairments to those seen in AD,[276,277] including loss of cholinergic cells.[299] Although neither is a fundamentally progressive disorder, careful examination of the stages of WE and KS mental symptoms suggest a similar circuit-wise progression of dysfunction.[300] At the molecular level, these diseases result from thiamine deficiency, which leads to MM and thalamic hypometabolism and atrophy.[300] Thiamine deficiency leads to inflammation,[301] which is critically involved in AD pathophysiological processes,[302] thus it is interesting to postulate that the MM may be particularly vulnerable to neuroinflammatory

insults. This is especially intriguing given the dearth of reactive astrocytes in the MM, even alongside significant Aβ burden, and considering that astrocytes may be primary mediators of the neuroimmune response.[171] Furthermore, the MM is known to be hormonally responsive, and has a major population of cocaine- and amphetamine- regulated transcript (CART)+ cells (Allen Brain connectivity atlas experiment #168364580-MM) that project widely through the memory circuit, including to the DG of the HPC. This suggests is one piece of evidence that suggests the MM may be a key point of convergence between memory systems, experiences, lifestyle factors, diet, and oxidative stress that contribute to AD risk.[303–305]

Clinically targeting the Papez circuit for AD intervention.

There are currently no cures or treatments that significantly alter the course of AD.[184] Compounded by a multitude of clinical drug failures,[36,100,306] industry has turned to immunization strategies, however the efficacy of these trails appears mixed.[12,13] Our data suggest that Aβ becomes critically involved in network deterioration long after widespread amyloidosis. This suggests that the window for treatment with Aβ-modifying treatments may be large, but likely closes at the onset of clinical symptoms. Thus the idea of network-level intervention is gaining popularity as it may be the only way to truly influence cognitive decline. Evidence that MM and fornix intervention may provide strong therapeutic potential is emerging, and clinical trials of network-activating deep brain stimulation of the fornix near its junction with the MM are showing significant efficacy in both slowing and reversing the course of AD in the initial trial population. [199] The cognitive reversal accompanies cellular-level remodeling, and brain structure in AD.[213,307] Because this stimulation also affects the DMN and limbic regions,[199] it strongly supports our findings that the MM-fornix-subiculum complex is at the core of the memory connectome. Long-term follow-up studies in these patients and others will reveal the true efficacy of this treatment, but in the meantime, preclinical experiments to understand the nature of this system in memory and how it is selectively vulnerable to pathology may reveal additional mechanisms of disease propagation and shed light on the multifaceted etiology of AD.

Methods

Animals

5XFAD (Tg 6799) breeding pairs were acquired from the Mutant Mouse Resource and Research Center (MMRRC) (Stock No. 034848-JAX) and maintained as hemizygous on the BL6 background. Animals were group housed on a 12h light/dark cycle without enrichment and sacrificed at the ages noted in the text.

Mouse Tissue Fixation

Mice were anesthetized with isoflurane (Isoflurane, USP, Piramal Healthcare, Andhra Pradesh, India) and underwent transcardial perfusion with ice cold 1X PBS (10X stock, Gibco, #70011-044) followed by ice-cold fixative made of 4% paraformaldehyde (32% stock, Electron Microscopy Sciences (EMS), Hatfield, PA, #15714) and 1% glutaraldehyde (10% stock, EMS #16110) in 1X PBS or just 4% paraformaldehyde in 1X PBS. Brains were removed from the skull and post-fixed in the same fixative for 3 days shaking at 4C.

Mouse Brain Section Processing

Brains were sliced to 100um on a vibratome (Leica VT100S) and stored at 4C in 1X PBS + 0.02% sodium azide (Sigma-ALdrich, #S2002). For 100um sections, individual sections incubated in clearing solution shaking at 55C for 2 hours, and were washed in 1X PBS. Sections were immunolabeled with the 'Mouse Brain Section iSWITCH' protocol attached (Appendix A).

Whole Mouse Brain Processing

After washing in 1X PBS, brains incubated in inactivation solution of 1% acrylamide (40% stock, Biorad #161-0140), 1M glycine (Sigma-Aldrich, St. Louis, MO, #G7126) in 1X PBS. After washing in 1X PBS, brains were put into clearing solution of 200mM sodium dodecyl sulfate (SDS) (Sigma-Aldrich, #L3771), 20mM lithium hydroxide monohydrate (Sigma, #254274), 40mM boric acid (Sigma-Aldrich, #7901), pH 8.5-9.0 and left shaking at 55C for 4 weeks or until white matter tracts were translucent to the eye in SDS. Brains were washed in 1X PBS or Weak Binding Solution (WBS) for up to 1 week and immunolabeled with the 'Whole Brain iSWITCH' protocol attached (Appendix B).

Human Tissue Processing - Blocks

Human tissue blocks were obtained from the Boston University School of Medicine and the Nethlands Brain Bank. They were deparaffinized by sequential immersion in xylene, ethanol, and water (Protocol for Human iSWITCH processing in Appendix C). Then, blocks were incubated in 1% GA in 1X PBS for 10 days at 4C. Brains were incubated in clearing solution shaking at 55C until the tissue appeared translucent (4-8 weeks). Following clearing, tissue was labeled using the Human iSWITCH protocol (Appendix C) with D54D2 for Aβ and lectin for positional mapping.

Human Pathology Sections

Formalin-fixed paraffin embedded human postmortem tissue blocks were sectioned at 5 μm thickness, dried at room temperature for 24 hours and heated at 80°C for 24 hours before IHC processing. Deparaffinization, antigen retrieval, and subsequent staining was performed with Boston Medical Center Pathology Department's *Ventana Benchmark Ultra* automated IHC instrument using commercially available primary antibodies specific for tau (rabbit anti-human tau [A0024] polyclonal antibody, 1:3200, *Dako*, Glostrup, Denmark) and Aβ (mouse anti-human beta-amyloid [6F/3D] monoclonal antibody, 1:50, *Dako,* Glostrup, Denmark), visualized by HRP-conjugated secondary antibody with diaminobenzidine (DAB) chromogen.

In situ hybridization probe design

RNA antisense probes were generated by PCR-amplifying human cDNA with human-specific *APP* primers with a T7 RNA polymerase recognition sequence (TAATACGACTCACTATAGGG) fused to the reverse primer (Table 1). The resulting PCR product was gel extracted and *in vitro* transcribed using a DIG-RNA labeling kit (Roche).

Immuno-*in situ* hybridization (Immuno-ISH)

Mice were anesthetized by isoflurane in an open system and perfused with RNase-free PBS followed by RNase-free 4% formaldehyde. Brains were dissected, drop fixed in RNase-free 4% formaldehyde for 12 hours, equilibrated in 30% sucrose-PBS, and frozen in O.C.T. (TissueTek). Cryosections (10μm) were incubated with a DIG-labeled RNA antisense probe (1:1000 in hybridization buffer) overnight at 65°C, washed in 1X SSC/50% formamide/0.1% Tween-20 3X 30 minutes at 65°C followed by 1X MABT for 30 minutes at room temperature. Sections were blocked with 20% heat-inactivated sheep serum/2% blocking reagent (Roche)/1X MABT for 1 hour and then incubated with mouse anti-DIG antibody (Roche; 1:2000) and rabbit anti-amyloid β (Cell Signaling; 1:500) diluted in blocking solution overnight. Sections were washed with 1XMABT 2X 20 minutes, incubated with donkey anti-rabbit Alexa-488 (Invitrogen; 1:1000) diluted in blocking solution for 1 hour, and washed with 1XMABT 5X 20 minutes. Sections were then prestained with 100mM NaCl/50mM $MgCl_2$/100mM Tris pH 9.5/0.1% Tween-20 2X 10 minutes, followed by staining with NBT/BCIP (Roche; 4.5 μl/ml and 3.5 μl/ml, respectively, in prestaining buffer) for 2 hours. Sections were washed with 1X PBS 3X 15 minutes, incubated in xylene 3X 5 minutes, and mounted with VectaMount (Vector Laboratories).

Gene	Forward Primer	Reverse Primer
h*APP*	GAGACACCTGGGGAT GAGAA	TAATACGACTCACTATAGGGACAGAGTCAGCCC CAAAAGA

Table 1. Primer sequences (5'-3') for *in situ* probe preparation.

Antibodies & Dyes

The primary antibodies used are as follows:

Target	Host	Company	Product #	Dilution
Aβ (D54D2)	Rabbit	Cell Signaling Technologies	8243	1:100 –1000
APP/ Aβ (4G8)	Mouse	BioLegend	800701	1:100 –1000
GFAP (GA5)	Mouse	Cell Signaling Technologies	3670	1:100 –1000
GFAP	Chicken	AbCam	Ab4674	1:100 - 1000
Iba1	Rabbit	Wako Chemicals	019-19741	1:100 –1000
Myelin Basic Protein* SMI-99	Mouse	BioLegend	808401	1:50 –500
Myelin Basic Protein* SMI-94	Mouse	BioLegend	836502	1:50 – 1:500
Synpatophysin	Mouse	Sigma-Aldrich	S5768	1:50 – 1:100
HDAC2	Rabbit	Bethyl Laboratories, Inc	A300-705A	1:100 – 1:500

*These antibodies were used concurrently as per the manufacturer's recommendation.

Additional labeling reagents:
Lectin dye was acquired from Vector Laboratories (#DL-1174).
Hoechst 33528 was used for nuclear labeling (Sigma #14530).
All secondary antibodies were Pre-adsorbed F(ab)2' AlexaFluor-conjugated from AbCam.

Section Image Acquisition
For section imaging, tissue was mounted onto microscope slides (VWR VistaVision, VWR International, LLC, Radnor, PA) with either Fluromount G Mounting Medium (Electron Microscopy Sciences, Hatfield, PA, USA) or RIMS solution (See Appendix C: 'iSWITCH Solutions). All slice images were acquired on a Zeiss LSM Inverted 710 microscope using Zen 2012 software (Carl Zeiss Microscopy, Jena, Germany). Images with cellular resolution were taken using a C-apochromat 40X, water immersion objective, NA 1.20. Section overview images used a Plan-apochromat 5X, air objective, NA 0.16. Pinhole, optical sectioning, and laser settings varied between individual experiments in separate figures, but were kept consistent between images that were included in single quantification graphs.

Whole Brain Image Acquisition
Whole brain images were acquired on a custom SPIM microscope built by H.C. Images were acquired using 10X 0.6NA CLARITY optimized objective (XLPLN10XSVMP; 8.0mmWD) from Olympus. Laser settings were determined for each brain such that 5% of the images are saturated to the maximum gray level to enhance signal to noise in each individual brain.

Human Brain Image Acquisition
Human brain images were acquired on a Leica TCS SP8 Confocal Microscope using LASAF software (Leica Microsystems, Wetzlar, Germany). Images were taken using a 20X 1.0NA CLARITY optimized objective with 12mm working distance. The pinhole, optical sectioning, and resolution and laser settings remained constant across conditions.

3D Image Quantification
Images were analyzed using Imaris (Bitplane, Zurich, Switzerland). Each whole brain file was segmented by hand using white matter tract boundaries and regional guidelines from the Allen Brain Atlas (Allen Mouse Brain Atlas, Coronal) to bound each major brain region. All data were exported into a CSV and analyzed in Matlab (Matlab, The Mathworks Inc, Natick, MA, USA) or GraphPad Prism 7.0a for Mac (GraphPad Software, La Jolla, CA, USA). All quantification steps were performed on raw images. *For whole brain analyses (Figures 1-3),* a Spots object was created on a 12 month FAD brain dataset. The parameters were fixed and spots were separated into the bounded brain regions using the Spots into Surfaces tool in Imaris Xtensions. The identical Spots object with the same parameters was created on each brain, with the exception of 2 month brains, which had significant artifacts in the Spots labeling. Separate Spots parameters were used for the 2 month cohort, however the parameters were fixed and kept constant for all 2 month brains. The spots objects were split into brain regions using the Xtension. Data was exported into CSV and analyzed in Matlab and GraphPad Prism 7.0a for Mac. All quantification steps were performed on raw images. For slice analyses (Figures 4, 5, 6), images were imported to Imaris for analyses. They were cropped in the Z-plane for size consistency. The first slice of the stack became the first optical section with the brightest average signal that also had full field-of-view signal. Then, the images were cropped to the size of the smallest z-stack. Surface objects for each channel were created on an FAD- dataset. *For microglia and GFAP signal:* the Surface objects were batch processed to analyze the entire 2 month cohort, then rebuilt within each file. The Surfaces were merged using XTensions tools, and then split using XTensions to identify individual cells. Group data was exported to a CSV. *For the vasculature:* a Surface object to identify the blood vessels and closely surrounding area was created. This was used to mask the lectin channel, which also had signal from glial cells and Aβ. Then, a second

vessels-based Surface object was created on the masked channel, and volume data were exported to CSV. *For Human brain analyses:* To account for differences in MM block size, regions of interest (ROI) $0.5um^3$ were sectioned randomly from the MM datasets. Within the ROI, a Surface object was created to identify Aβ signal. Number and size data were exported to CSV.

2D Image Quantification

For synaptophysin, Zstack images were imported into FIJI as TIFF stacks. Images were split, synaptophysin signal was collapsed to RGB. The z-axis profile of each image was taken and each stack was cropped to start at the brightest optical section, and end at the maximum stack size for the smallest acquired image stack. The stack was projected along the z-axis, and the mean signal intensity was recorded. Data were exported to GraphPad for analyses. For myelin and amyloid, images were kept in Z-stacks and a blinded rater outlined the tract for quantification in the myelin channel before moving to the thresholded amyloid channel to do a particle analyses. The threshold was kept constant within experiments, and the quantification was done bi-laterally.

Representative Images from Whole Brain Data

Representative images from the whole-brain datasets are either 2D images of the 3D rendered whole dataset or digitally sectioned at 5-100um in Imaris using the Orthoslicer tool. For whole brain images in Figures 1-3, the maximum brightness was reduced to enhance signal for viewing. These parameters were chosen per brain and different between figures because there are no direct intensity comparisons made between those figures.

Representative Images from Slices

If signal intensity was undetectable in any image of a representative dataset, the entire group was imported into Adobe Photoshop. The brightness was increased on each image a fixed amount that was the same for each image in any subfigure, but may have differed across subfigures.

Statistics

All statistics were performed in MatLab or GraphPad Prism. Individual statistical tests are indicated in the text and figure legends for the appropriate experiments. Graphs were created in the respective analytical software packages and exported as .TIFF or .JPEG for inclusion in the document. For clustering analyses, multiple cluster numbers were tested (cluster 5 – 10), and the clustering parameter with the fewest cluster distance sums = 0 and lowest total sum of distances.

Acknowledgements and Contributions:

In this chapter, I would especially like to thank:
Dr. Li-Huei Tsai: for her mentorship and encouragement to think outside the box and approach a traditionally molecular disease from my behavioral biology and systems neuroscience perspective.
Dr. Kwanghun Chung: for telling us that myelin basic protein looks really cool in 3D.
Dr. Ivana Delalle: for her belief in our mission and leading an amazing team that figured out how to hand-deparaffinize whole tissue blocks, and for processing the human immunosections in Figure 7B.
Dr. Heejin Choi: for SPIM imaging of the whole-brain datasets.
Dr. Ashley Lauren Watson: for performing the *in situ* hybridization experiments in Figure S1 and always being a fantastic listener when I needed to hash out ideas for the paper.
Dr. Nina Dedic for her time to label and image the 4G8 and GFAP(rb) in Figure 4 and for taking over the project and running with it.
Dr. Jun Wang: for performing all of the electrophysiology experiments in Figure 5.
Fatema Abdurrob: for her aesthetic talent that made teaching imaging fun, for segmenting whole-brain datasets, and for dealing with me being a creeper that regularly remotely logged in to the computer while she was trying to work.
Stephanie Bousleiman: for her persistence in brain segmentation, even when it was really un-fun.

Experiments to Add

Below is a list of on-going experiments that will be included in the final document, but were not complete at the time of initial thesis submission:

1. *Increase to N = 3 for each time point (2- 4m, in the process of segmenting). (Figures 2).*
2. *Increase N for electrophysiology experiments (data collection complete, Figure 5).*
3. *HDAC2 and synaptophysin quantification in 2m FAD mice (Figure 5).*
4. *Golgi impregnation for spine morphology analyses (Figure 5).*
5. *MAP processing for super resolution identification of synaptic connections (Figure 5).*
6. *Tau co-localization with Aβ (Figure 6)*
7. *Aβ-specific or APP-specific labeling (Figure 6).*

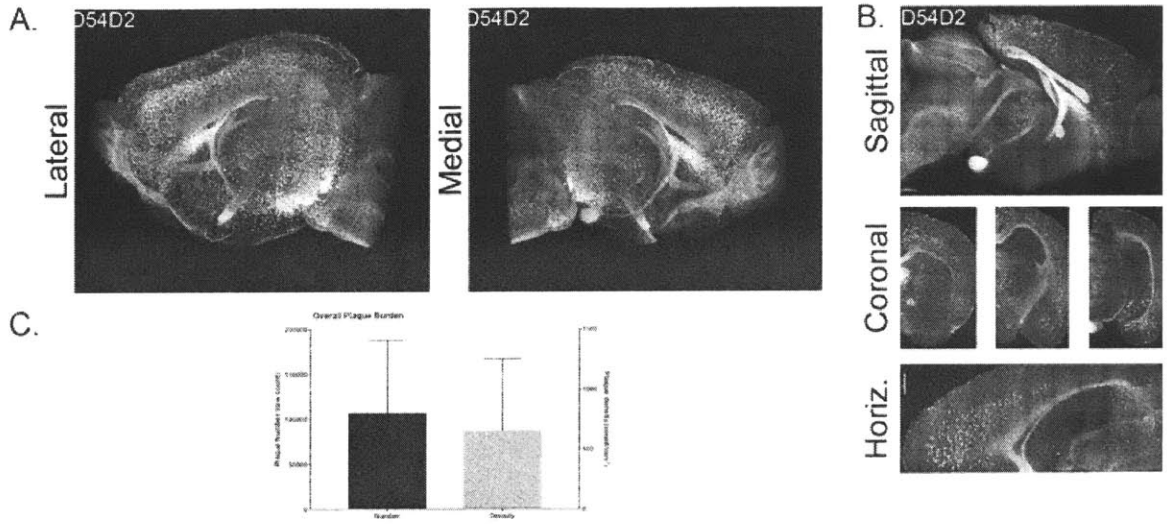

Figure 1.1: iSWITCH labeling of 6 month FAD mouse brain demonstrates network specificity. A) Images of the amyloid burden in whole hemispheres from the brain of a representative 6-month old 5XFAD mouse. B) Demonstration of the pathological burden in the sagittal (top), coronal (middle), and horizontal (bottom) planes. C) Aged FAD mice show significant plaque load. *;*p<.05 **p<.01 ***p<.001 ****p<.0001 ns: not significant*

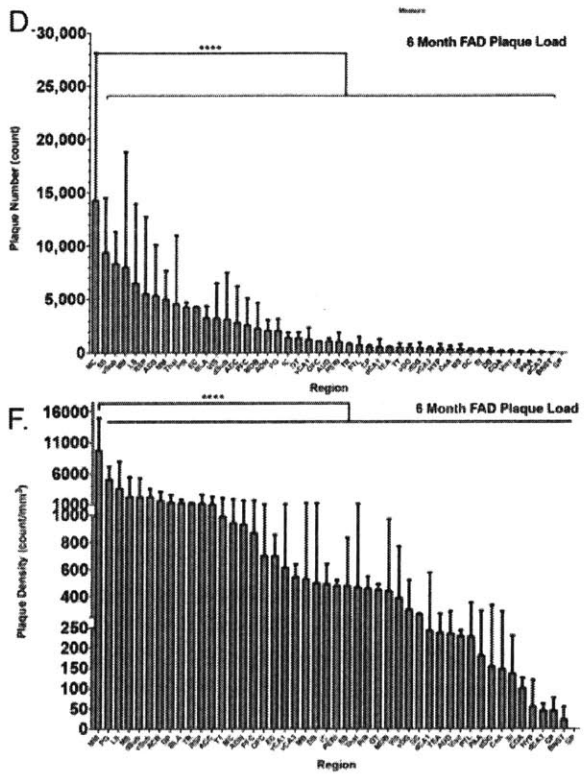

E.

Clusters by Count

Group	k-means Sum of Dist (*1E7)	Regions
1	0	MC
2	7.6072	RSP, vSub,Thal,ACB,LS,MB
3	0.7283	MM, PIR, EC, BLA
4	1.1701	ACC, PFC, dSub, Vis, MOB, AON, PG
5	1.3783	Everything Else

G.

Clusters by Density

Group	k-means Sum of Dist (*1E6)	Regions
1	0	MM
2	0	PG
3	3.5358	MS, LS, dSub
4	5.3253	RSP, ACC, PFC, MC, vSub, ACB, BLA, TR, DP, AON, TT
5	3.9743	Everything else

Figure 1.2: iSWITCH labeling of 6 month FAD mouse brain demonstrates network specificity. D&E) D: Ranking by plaque count and E: clustering by count demonstrate a few key regions of significant burden. F&G) F: Ranking by density changes the order of significance, but E: clustering reveals very specific nodes belonging to memory circuits. Statistics noted in text. *ACB: nucleus ccumbens; ACC: anterior cingulate cortex; AON: accessory olfactory nucleus; AUD: auditory cortex; BLA: cortical-like amygdalar regions; BNST: bed nucleus of the stria terminalis; CeA: striatial-like amygdalar regions; COA: olfactory-life amygdalar regions; CP: caudoputamen; DB: diagonal band; dCA1: dorsal CA1; dCA3: dorsal CA3; dDG: dorsal dentate gyrus; DP: dorsal peduncular area; dSub: dorsal subiculum; EC: entorhinal cortex; GC: gustatory cortex; GP: globus pallidus; HYP: hypothalamus; IC: insular cortex; LS: lateral septum; MC: motor cortex; MB: mid-brain; MM: mammillary body; MOB: main olfactory bulb; MS: medial septum; OFC: orbitofrontal cortex; OT: olfactory tubercle; PAA: piriform-amygdala area; PERI: perirhinal and ectorhinal corticies; PFC: prefrontal cortex; PIR: piriform cortex; PTL: parietal association areas; RSP: retrosplenial cortex; SI: substantia innominate; SS: somatosensory cortex; TEA: temporal association areas; Thal: thalamus; TR: piriform-amyloid transition region; TT: taenia tecta; vCA1: ventral CA1; vCA3: ventral CA3; vDG: ventral dentate gyrus; VIS: visual cortex; Visc: visceral cortex; vSub: ventral subiculum. ;*p<.05 **p<.01 ***p<.001 ****p<.0001 ns: not significant*

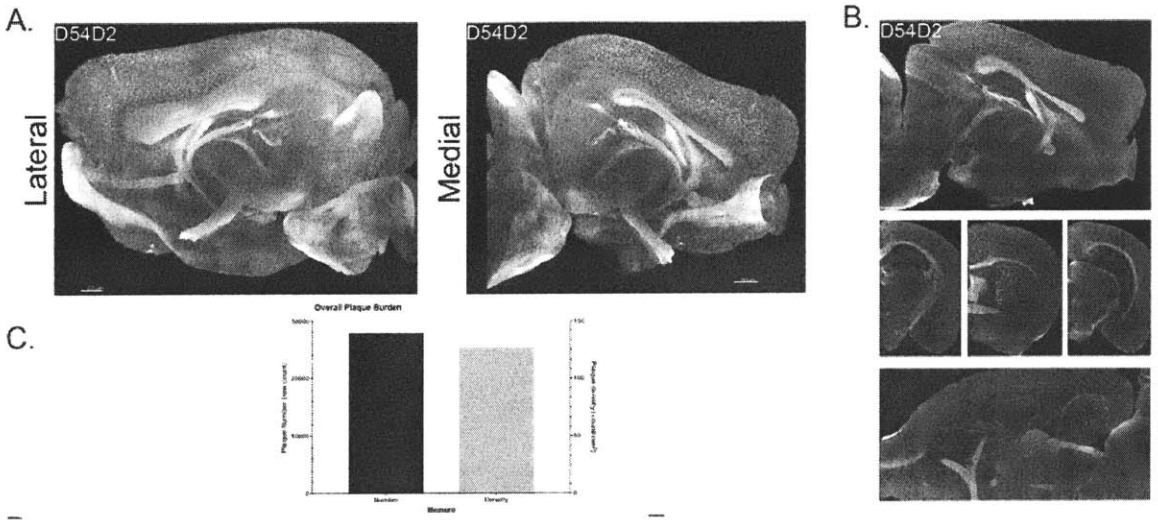

Figure 2.1: Younger animals reveal network-specific deposition patterns emerge early in the course of AD. A&B) Representative images of whole brain labeling in a 4 month old FAD mouse in the A: medial and lateral planes and B: in sagittal (top), coronal (middle), and horizontal (bottom) sections. C) Plaques by count and density are sparse. *$p<.05$ **$p<.01$ ***$p<.001$ ****$p<.0001$ *ns: not significant*

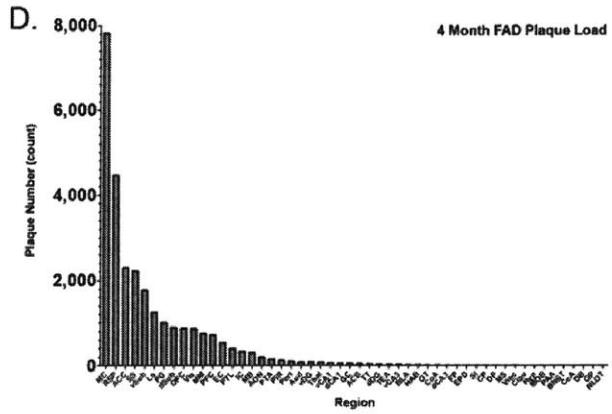

E.

Count Clusters

Group	k-means Sum of Dist (*1E5)	Regions
1	0	MC
2	0	RSP
3	1.6515	SS, vSub, ACC
4	3.0312	PFC, OFC, EC, VIS, dSub, LS, MM, PG
5	3.5409	Everything Else

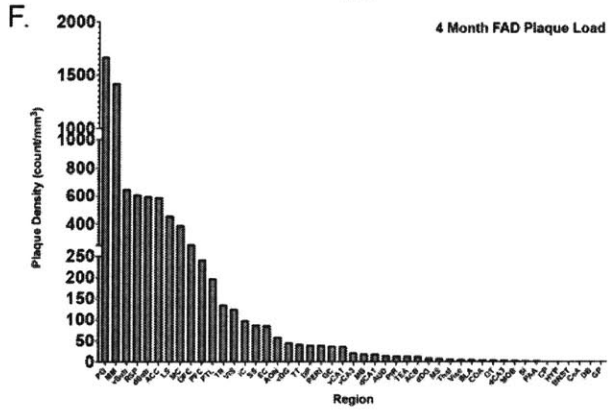

G.

Density Clusters

Group	k-means Sum of Dist (*1E3)	Regions
1	3.0544	MM, PG
2	0.1972	RSP, ACC, dSub, vSub
3	0.2284	LS, MC
4	1.3682	OFC, PFC, PTL, TR
5	2.3173	Everything Else

Figure 2.2: Younger animals reveal network-specific deposition patterns emerge early in the course of AD. D&E) Very few, specific regions have high plaque count by D: rank, and E: clustering reveals that regions of the limbic forebrain share similar levels of amyloid load. F&G) Density measures provide additional insight, showing DMN regions have particularly high burden early on. Statistics noted in text. *ACB: nucleus ccumbens; ACC: anterior cingulate cortex; AON: accessory olfactory nucleus; AUD: auditory cortex; BLA: cortical-like amygdalar regions; BNST: bed nucleus of the stria terminalis; CeA: striatial-like amygdalar regions; COA: olfactory-life amygdalar regions; CP: caudoputamen; DB: diagonal band; dCA1: dorsal CA1; dCA3: dorsal CA3; dDG: dorsal dentate gyrus; DP: dorsal peduncular area; dSub: dorsal subiculum; EC: entorhinal cortex; GC: gustatory cortex; GP: globus pallidus; HYP: hypothalamus; IC: insular cortex; LS: lateral septum; MC: motor cortex; MB: mid-brain; MM: mammillary body; MOB: main olfactory bulb; MS: medial septum; OFC: orbitofrontal cortex; OT: olfactory tubercle; PAA: piriform-amygdala area; PERI: perirhinal and ectorhinal corticies; PFC: prefrontal cortex; PIR: piriform cortex; PTL: parietal association areas; RSP: retrosplenial cortex; SI: substantia innominate; SS: somatosensory cortex; TEA: temporal association areas; Thal: thalamus; TR: piriform-amyloid transition region; TT: taenia tecta; vCA1: ventral CA1; vCA3: ventral CA3; vDG: ventral dentate gyrus; VIS: visual cortex; Visc: visceral cortex; vSub: ventral subiculum. ;*p<.05 **p<.01 ***p<.001 ****p<.0001 ns: not significant*

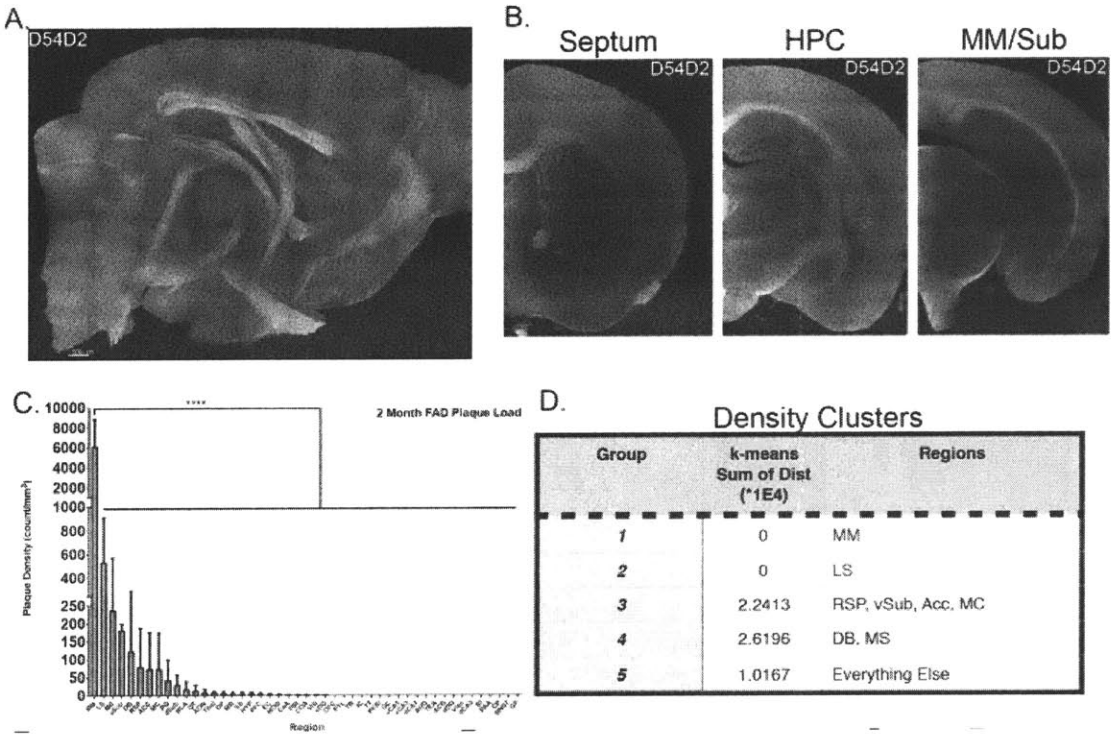

Group	k-means Sum of Dist (*1E4)	Regions
1	0	MM
2	0	LS
3	2.2413	RSP, vSub, Acc, MC
4	2.6196	DB, MS
5	1.0167	Everything Else

Figure 3.1: Early pathology begins in the subcortical nodes of the Papez memory circuit. A&B) Representative images of whole brain amyloid labeling in a 2 month old FAD mouse. A: medial plane showing MM and septum pathology and B: sagittal (top), coronal (middle), and horizontal (bottom) sections demonstrating the specificity. C&D) Density ranking demonstrates that the Papez circuit hubs are the most burdened and significant at the earliest stage while D: clustering reveals the rest of the circuit is similarly affected. Statistics noted in text. *ACB: nucleus ccumbens; ACC: anterior cingulate cortex; AON: accessory olfactory nucleus; AUD: auditory cortex; BLA: cortical-like amygdalar regions; BNST: bed nucleus of the stria terminalis; CeA: striatial-like amygdalar regions; COA: olfactory-life amygdalar regions; CP: caudoputamen; DB: diagonal band; dCA1: dorsal CA1; dCA3: dorsal CA3; dDG: dorsal dentate gyrus; DP: dorsal peduncular area; dSub: dorsal subiculum; EC: entorhinal cortex; GC: gustatory cortex; GP: globus pallidus; HYP: hypothalamus, IC: insular cortex; LS: lateral septum; MC: motor cortex; MB: mid-brain; MM: mammillary body; MOB: main olfactory bulb; MS: medial septum; OFC: orbitofrontal cortex; OT: olfactory tubercle; PAA: piriform-amygdala area; PERI: perirhinal and ectorhinal corticies; PFC: prefrontal cortex; PIR: piriform cortex; PTL: parietal association areas; RSP: retrosplenial cortex; SI: substantia innominate; SS: somatosensory cortex; TEA: temporal association areas; Thal: thalamus; TR: piriform-amyloid transition region; TT: taenia tecta; vCA1: ventral CA1, vCA3: ventral CA3; vDG: ventral dentate gyrus; VIS: visual cortex; Visc: visceral cortex; vSub: ventral subiculum. ;*p<.05 **p<.01 ***p<.001 ****p<.0001 ns: not significant*

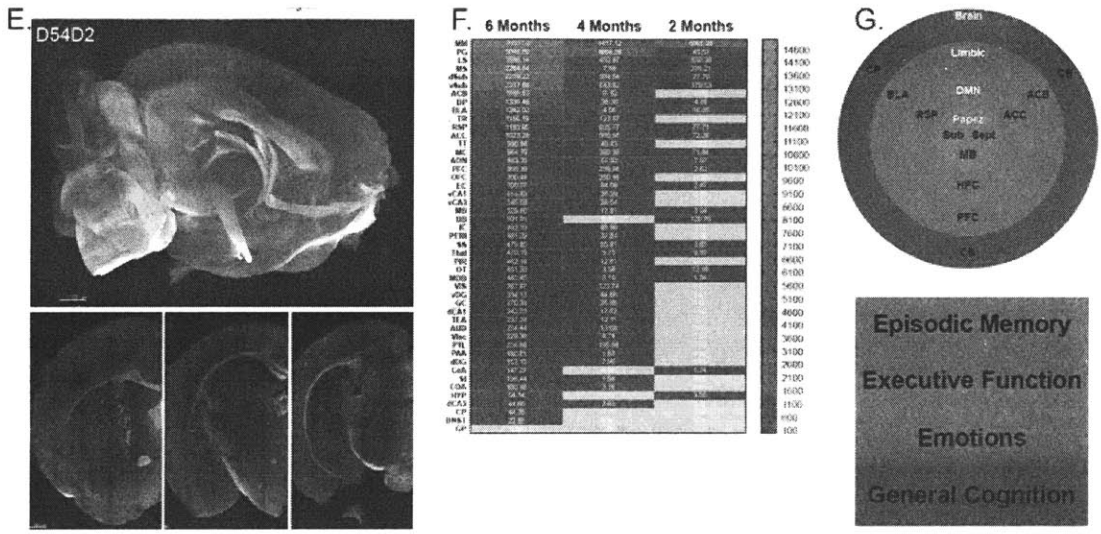

Figure 3.2: Early pathology begins in the subcortical nodes of the Papez memory circuit. E) Demonstration of pathology in a 1.5 month aged FAD mouse showing specificity in the MM and SUB. F) Summary data indicating the change across ages in all the brain regions identified. G) Model for network-level AB spread that suggest circuit susceptibility drives impairment. Statistics noted in text. *ACB: nucleus ccumbens; ACC: anterior cingulate cortex; AON: accessory olfactory nucleus; AUD: auditory cortex; BLA: cortical-like amygdalar regions; BNST: bed nucleus of the stria terminalis; CeA: striatial-like amygdalar regions; COA: olfactory-life amygdalar regions; CP: caudoputamen; DB: diagonal band; dCA1: dorsal CA1; dCA3: dorsal CA3; dDG: dorsal dentate gyrus; DP: dorsal peduncular area; dSub: dorsal subiculum; EC: entorhinal cortex; GC: gustatory cortex; GP: globus pallidus; HYP: hypothalamus; IC: insular cortex; LS: lateral septum; MC: motor cortex; MB: mid-brain; MM: mammillary body; MOB: main olfactory bulb; MS: medial septum; OFC: orbitofrontal cortex; OT: olfactory tubercle; PAA: piriform-amygdala area; PERI: perirhinal and ectorhinal corticies; PFC: prefrontal cortex; PIR: piriform cortex; PTL: parietal association areas; RSP: retrosplenial cortex; SI: substantia innominate; SS: somatosensory cortex; TEA: temporal association areas; Thal: thalamus; TR: piriform-amyloid transition region; TT: taenia tecta; vCA1: ventral CA1; vCA3: ventral CA3; vDG: ventral dentate gyrus; VIS: visual cortex; Visc: visceral cortex; vSub: ventral subiculum. ;*p<.05 **p<.01 ***p<.001 ****p<.0001 ns: not significant*

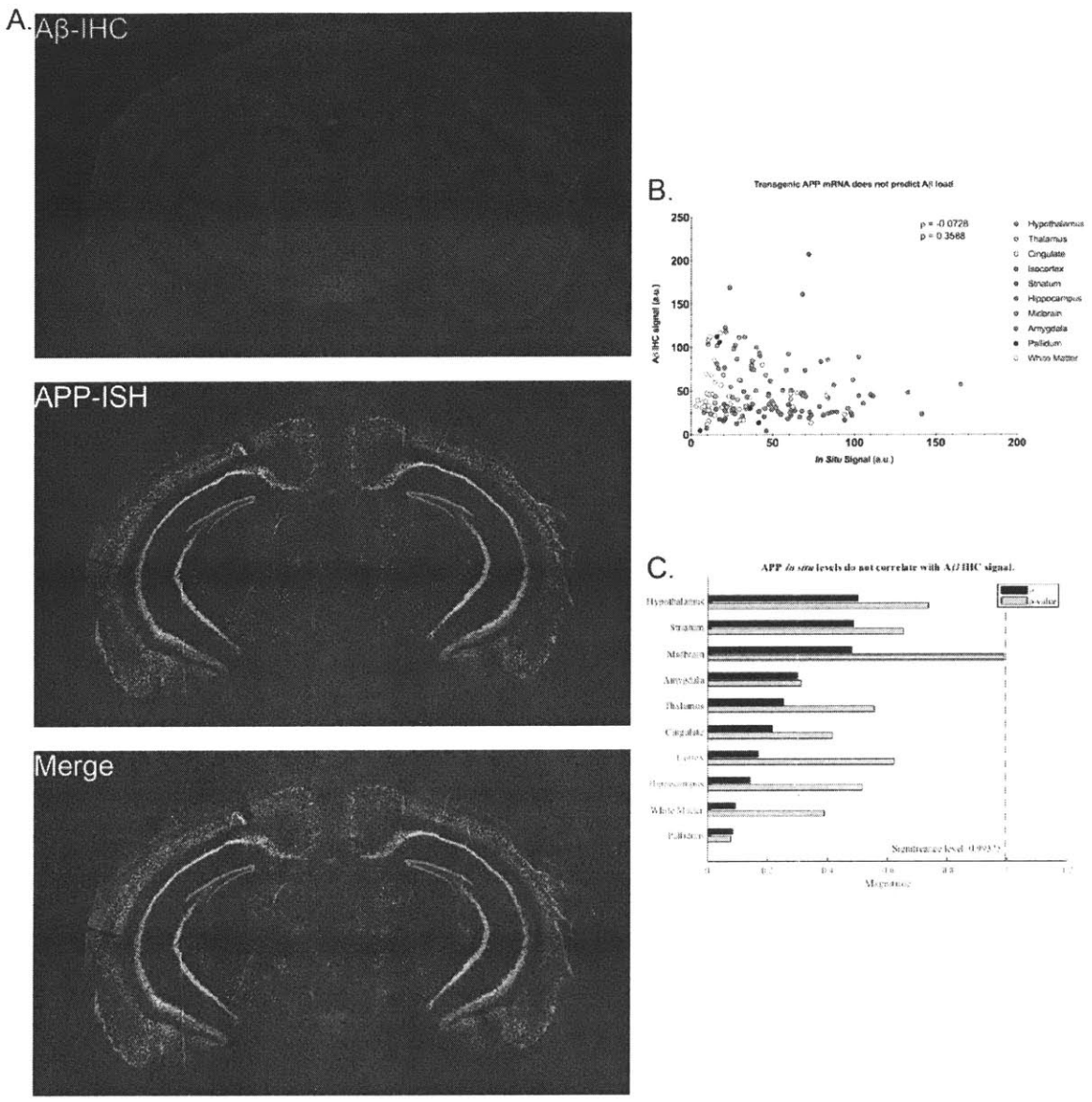

Figure S1: Amyloid burden does not correlate with RNA expression density measured by co-*in situ* hybridization- immnohistochimical methods. A) Representative images of a posterior section that shows the MM has relatively low levels of transgenic expression despite its early phenotype. B) Linear regression shows there is not a correlation between APP *in situ* signal and AB immunofluorescence. Beause data is skewed due to sparse signal in both channels, Spearman's Rank Corerlation Test was used to test the correlation in each graph. C) When split by brain region, some areas do show more correlation than others. Inverse p-value, with Spearman's rho statistic show the strength of the correlation.

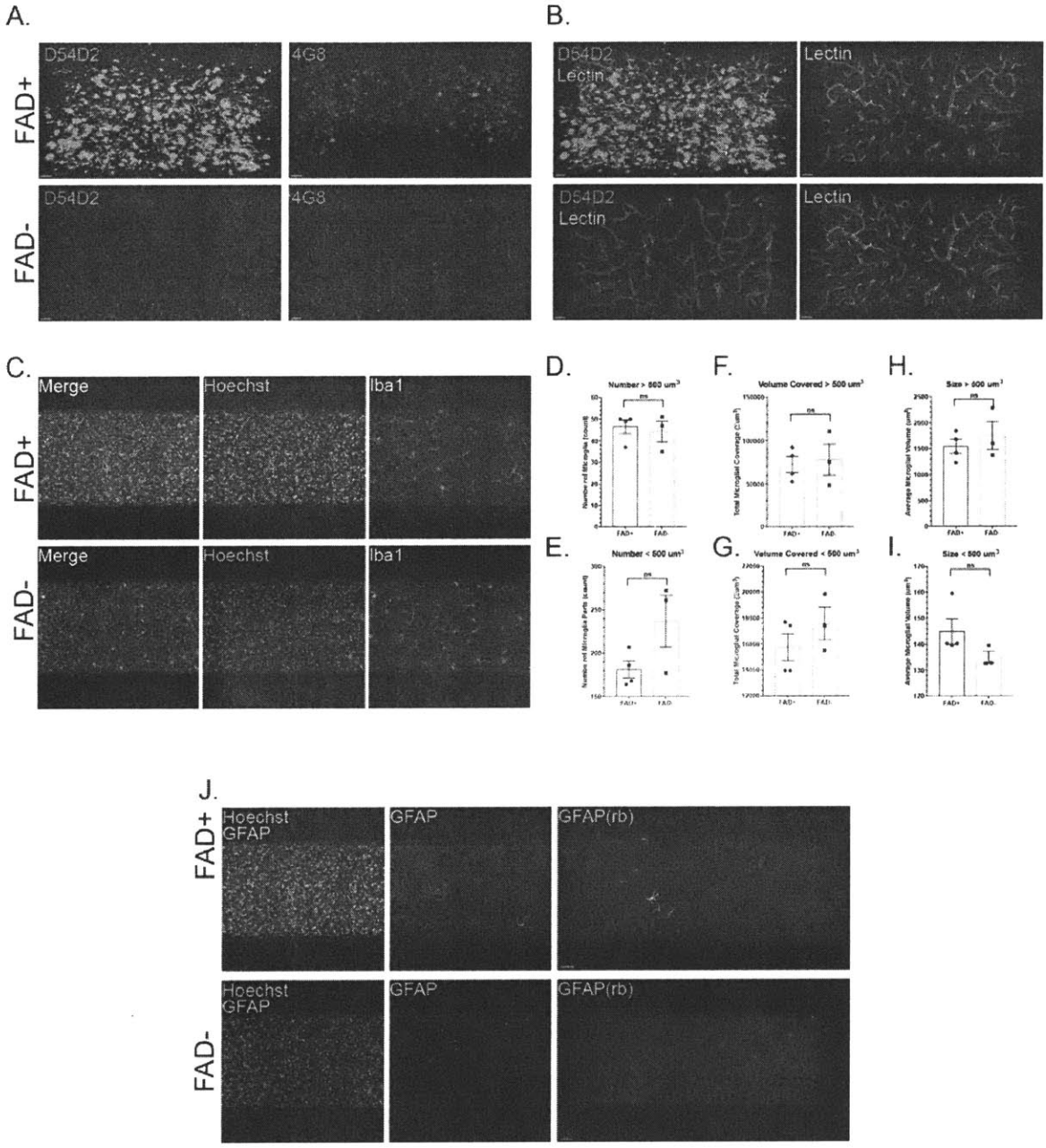

Figure 4: The mammillary body burden is robust, however does not trigger a typical Alzheimer's-like neuroimmune response. A) Images showing amyloid burden with both the D54D2 antibody used for whole brain labeling and the well-tested 4G8 antibody against amyloid/APP. B) Representative images qualitatively demonstrating the accumulation of amyloid around cerebral vasculature and its effects on the structure. C) Images of microglia in the MM of FAD+ and FAD – mice. D-I) Quantification shows no difference in response, despite the significant amyloid presence. J. Astrocytes in the MM do not show a GFAP-reactivity to amyloid using two antibodies against the epitope. Statistics noted in the text.

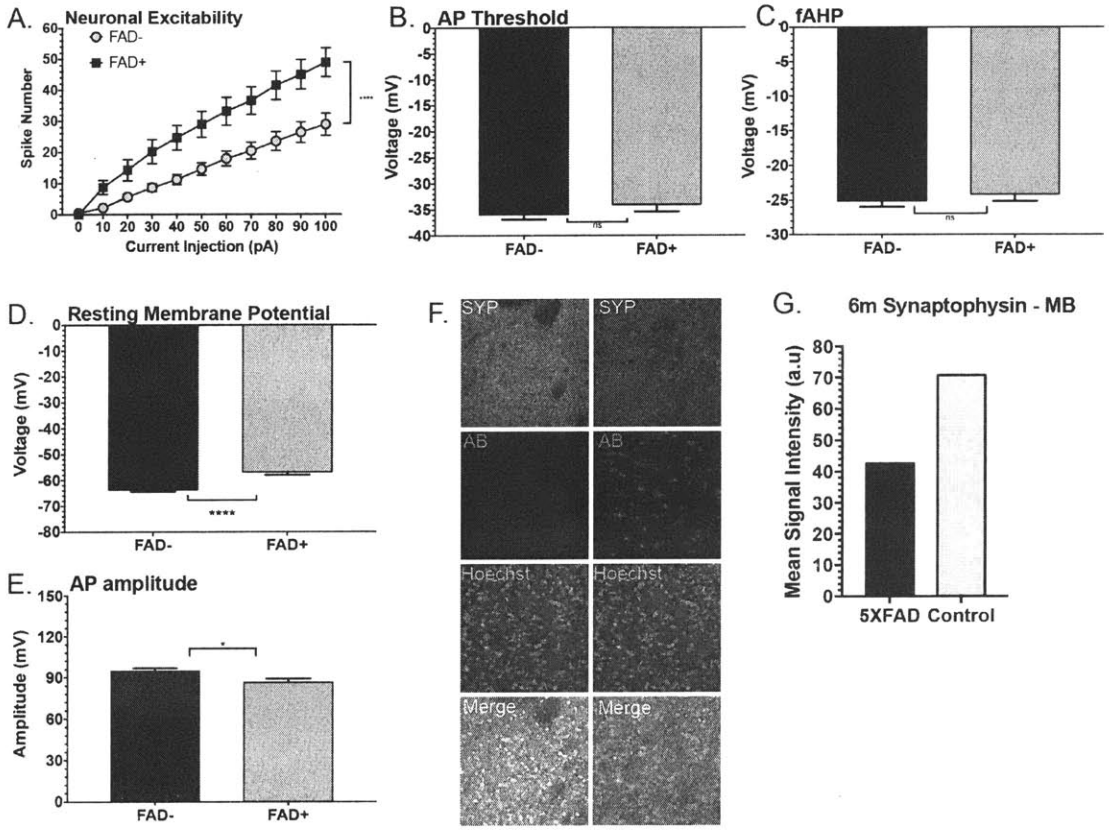

Figure 5: In the absence of an immune response, the MM shows significant functional impairments and loses its synaptic input. A) Action potential curves showing increased firing rate of FAD+ MM neurons compared to WT littermate controls. B) The action potential threshold of the cells does not change, neither does the C) afterhyperpolarization. D) The resting membrane potential is significantly decreased, which could underlie the excitability phenotype. E) The action potential amplitude is also significantly decreased in 5XFAD animals, which may represent further dysregulation and impairment. F) Representative images of test experiments checking for synaptic density in 6 month aged FAD animals. G) There is a reduction of synaptophysin. Statistics noted in the text.

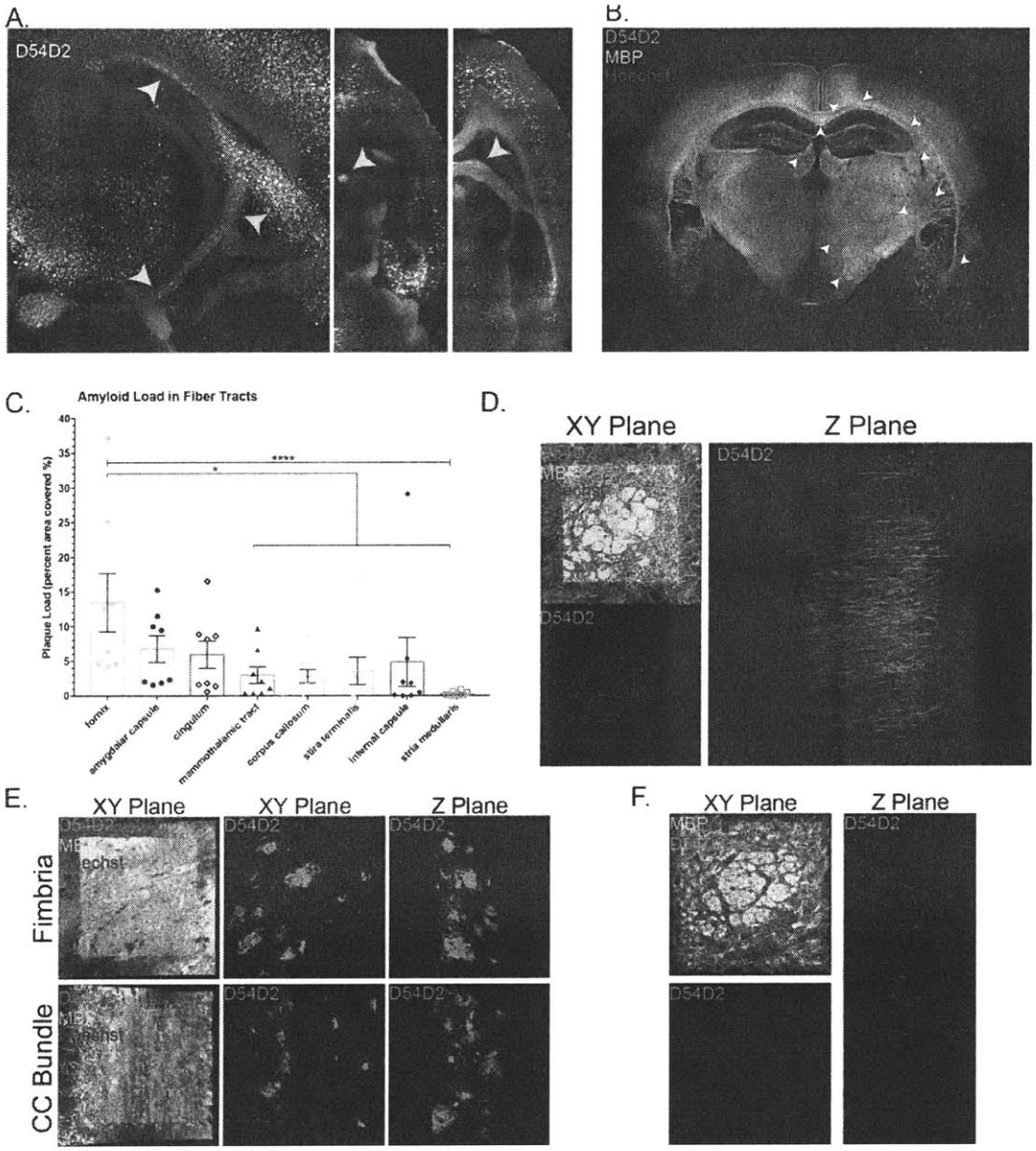

Figure 6: In addition to early gray matter susceptibility, the Papez circuit shows unique white matter pathology. A) Images showing the specificity of the fornix amyloid aggregates in a 6-month aged FAD mouse. Arrows point to the fornix tract itself. B) Representative image for the quantification of white matter amyloid. In clockwise order from the bottom left, arrows point to: fornix, mamillothalamic tract, stria medularis, dorsal fornix, corpus callosum, cingulum bundle, alveus, fimbria, stria terminalis, internal capsule, amygdalar capsule. Quantification was performed bilaterally. C) Quantification of white matter amyloid demonstrates susceptibility of the fornix. D) High-resolution image of a cross section through the fornix. In the XY plane (left, it looks like hazy amyloid deposition, however in the ZY plane (right), the fibrous nature of the amyloid becomes clear. E) The fimbria, alveus, and cingulum show similar pathology but there is a dearth in the corpus callosum. F) 2 month aged animals also show the tract-like labeling, however it is much more sparse. Statistics noted in the text.

A.

Patient Information Table

Patient	Gender	Age	Braak Score	CDR
1	male	70	0	0
2	male	80	2	0
3	female	91	3	0
4	male	74	5	AD

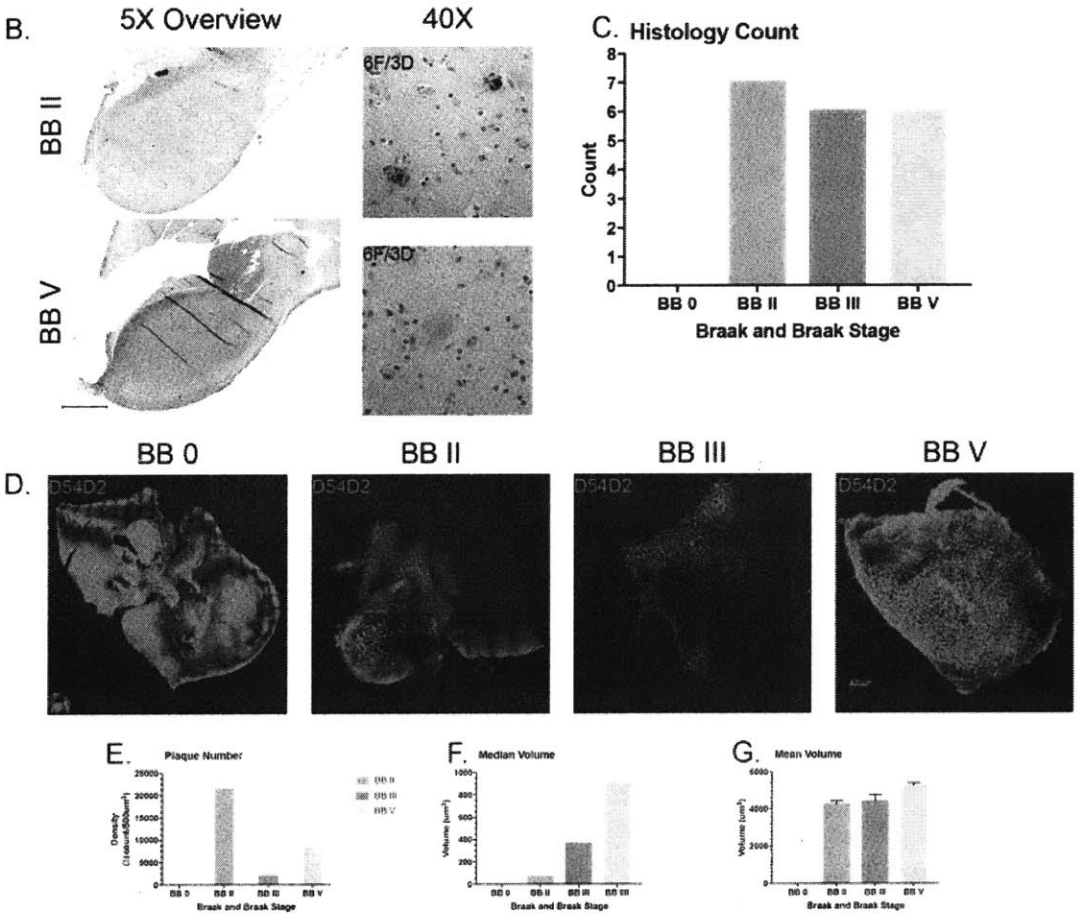

Figure 7: Human mammillary body and associated white matter show AD-related amyloid burden. A) Information on the patient samples used for the experiments in this figure. B) Representative images of 5X tile scans showing the overall MM structure (left) and representative high-magnification image of the plaque types used for quantification (right). C) Quantification of histologically identified plaques from pathology slide sections. D) Representative images of the large-volume MB samples labeled with D54D2. E) The plaque count does not reflect the severity of the disease, however the F) median and G) mean plaque volumes increase with disease severity in this small cohort.

Conclusions and Future Directions

In this thesis I have optimized emerging whole-brain proteomic-profiling techniques to reveal early hubs of pathological seeding in Alzheimer's mouse brain. The data demonstrate that critical subcortical nodes of the Papez memory circuit show unique vulnerability to amyloid aggregation, and analyses of precisely aged mouse brains reveals within-network similarities in regional burden that develop sequentially over time. By showing that regions within the circuit have abnormal neuroinflammatory responses and weakened long-range projections, we begin to understand how the susceptibility may form and spread from a few key vulnerable hubs to the rest of the connectome. Because we also confirm pathology in a small cohort of patient mammillary bodies, we can link the animal models to the human disease and make predictions about what we might expect in patient populations. From our network susceptibility model, we expect a stereotypical progression of cognitive symptoms that correlates well with the patient literature.[195,267,308] However, because this framework does not depend on regional susceptibility, it is possible, and very likely, that the origins of human disease are more diverse than the regions we observe in our mice. The model I propose may account for the seemingly multifaceted etiology of the disease, wherein any region within the susceptible network may be vulnerable due to underlying genetic or lifestyle factors, which may precipitate pathology in any part of the circuit, from which it can spread to other regions. The hypothesis I propose from my data, that the Papez circuit is a critical hub of early disease, has been postulated before,[267,298,198] however none of the proposals have been able to provide concrete molecular evidence for the possibility, and have been unable to link white and gray matter pathologies.[198] With the ability to identify amyloid specifically throughout the whole brain, we can rectify many of the controversies that arise in patient imaging and thin-slice sectioning, however, like most good science, the work in this thesis raises more questions than for those it provides answers. Some of the potential new directions that the research opens are profoundly important for the Alzheimer's field, and are also at the core of understanding how memory sits in the brain.

The first major question to come from this work is whether the mammillary body is the key seed node, or if it acts as a dumping ground for amyloid from elsewhere. APP is trafficked to the synapse,[225,70] and thus it is likely to travel long distances, however it is fiercely debated whether amyloid peptides themselves accumulate within cells. If the proteolysis does not primarily happen in mammillary body neurons, then a major question is where it does come from. Because the projections to and from this region are poorly understood, it is first important to know to where the region connects. This may also shed light on the propagation patterns that we see in the mouse. With the widespread use of optogenetics,[250] coupling

mammillary body tracing to functional manipulation can reveal not only its physical, but also its functional, connectome.

From a different perspective all-together, a major question in the field of AD is whether amyloid peptides propagate physically like prions. Resources have been devoted to this question,[278] and initial studies do seem to suggest that aggregates can physically propagate between connected regions.[246,96] However, these studies do not address whether functional alterations of high amyloid input into a region may cause a functional propagation and thus the question remains open. With the data I present showing amyloid accumulation within and along white matter tracts, we have the first glimpse of physical propagation of the pathogenic proteins. Furthermore, by seeing amyloid within axonal tracts, we may begin to understand how it disrupts tau leading to the other major hallmark of AD. Significantly, because we see the tract development months after the initial burden, this may be a potential mechanism to explain the long temporal lag between initiating amyloid events and cognitive impairment. Together, these are intriguing ideas at the core of the AD field, and a multitude of correlational follow-up studies can now use our tools and observations to provide strong evidence in favor of this propagation. However, one reason we still do not know the answer is that physical and functional disruption of circuits are inextricably linked, and without tools to watch the aggregates travel and manipulate their paths, the direct evidence seems untenable. In the interim while molecular tools for *in vivo* long-range projection tracking are under development, forging ahead with the idea that network disruption may be equally responsible for the impairments seen in AD patients is a way to extend our understanding of both the disease and the brain, while potentially moving towards novel treatments for brain disorders.

One of the major consequences of amyloid aggregation has been shown to be the induction of hyperexcitability and sub-seizure like neural activity.[21] This type of activity certainly has detrimental effects on the networks that underlie cognition, yet our understanding of circuit- and systems- level neuroscience is nascent. Exactly how aberrant activity translates to cognitive disruption is far from our understanding as a field, but we can make progress towards this knowledge-producing goal through disease interrogation. In 2015, I worked with Li-Huei to write a set of guidelines for the 2015 Alzheimer's Disease Sumit (Appendix D). In these, we suggested that circuit-level investigation will be critical for solving brain disease, and thus basic neuroscience of behavior, circuits, systems, and cells is important for our advancement. With the abundance of large-scale –omics techniques revealing new genetic and molecular information daily, it seemed like a computational revolution had taken over experimental science, towards *in silico* analyses of the –omics data. In the pursuit of disease research, I

think it is incredibly important not to lose sight of the key mechanistic and academic questions that drive science forward. In the intervening time since Li-Huei presented our ideas, a good deal of progress has been made in using network activity to halt and, in some cases, reverse Alzheimer's disease. Excitingly for the conclusion of this thesis, a group of neurologists are using deep brain stimulation of the fornix- right near the mammillary body -to enhance memory performance and slow the progression of the disease.[199] Because these treatments can also restore cellular health, using stimulating tools may provide promising avenues for intervention and bring us closer towards a cure.

In conclusion, the work I present in this thesis begins to address multiple questions about the initiation and spread of key pathologies that have been plaguing the Alzheimer's field for many years. The data has demonstrated the importance of subcortical hubs in memory and Alzheimer's, and provided useful tools and concrete scientific avenues to follow up on the questions. By showing that the mammillary body has amyloid across stages of Alzheimer's in human patients, we can hopefully provide important links between animal and clinical research, and emphasize the importance of these types of preclinical studies for advancing disease knowledge. Our findings can immediately translate to the clinic, where investigators may be able to find novel imaging biomarkers to identify patients at the earliest prodromal stages, when some hope remains for efficacious treatments. Taking this first step to identify patients and slow the disease significantly will be a major, and much needed, milestone on the path to a cure.

Appendix A: Protocol for iSWITCH labeling thick tissue sections

Solutions:

SWITCH Fixative	1% glutaraldehyde 4% paraformaldehyde in 1X PBS
Inactivation Solution	1% acrylamide 1M glycine 0.1% triton- X100 in 1X PBS
PBST	0.1% triton- X100 in 1X PBS
Clearing Solution (pH 8.5 - 9.0)	200mM sodium dodecylsulfate 20mM lithium hydroxide monohydrate 4mM boric acid in ddH_2O
Blocking Buffer	2% bovine serum albumin in PBST
Weak Binding Solution (pH 10.5)	37.75mM Na_2HPO_4 3.53mM KH_2PO_4 0.02% sodium azide in PBST
Reversal Buffer (pH 7.4)	37.75mM Na_2HPO_4 3.53mM KH_2PO_4 0.02% sodium azide in PBST
Hoechst solution	1mg/ml Hoechst 33258 in ddH_2O
Refractive index matching solution (RIMS)	75g Histodenz 20mL 0.1M phosphate buffer 60mL ddH_2O

Abbreviations:

h	hours
C	degrees Celcius
m	minutes

Pre-steps if clearing:

I. Perfuse with ice-cold PBS immediately followed by SWITCH fixative.
II. Post-fix brains in SWITCH fixative for 72h at 4C on rocker.
III. Inactivate brains by incubating in inactivation solution for 48h at room temperature.
IV. Wash 3 x 15m in PBST, shaking at room temperature.
V. Slice brains at room temperature.
VI. Clear sections by incubating in clearing solution at 37-55C until white matter tracts are translucent.
VII. Wash for 1-12h at room temperature in PBST.

SWITCH labeling (for 40um sections[e]):

I. Block by incubating in blocking buffer for 2h at room temperature.
II. Wash 3 x 15m in PBST, shaking at room temperature.
III. Incubate sections in weak binding solution for 1h.
IV. Put directly into 400uL[f] of weak binding solution and add concentrated primary.[g]
V. Leave shaking for at least 12h[h] at 37C[i].
VI. Calculate the volume of primary incubation solution. Add extra to account for the volume of solution in the tissue.[j]
VII. Add ⅙ of the volume calculated in step VI of reversal buffer[k] each hour for 6h.
VIII. After final addition, let samples incubate in primary for at least 1h at room temperature.[l]
IX. Wash 3 x 1h in PBST, shaking at room temperature.
X. Use a secondary antibody[m] at the same dilution as the primary antibody. Dilute in PBST, shaking at room temperature for at least 4h.
XI. Wash 2 x 1h in 1XPBS, shaking at room temperature.
XII. Incubate in Hoechst diluted 1:1000[n] in 1XPBS to label nuclei for 1h at room temperature.
XIII. Wash 2 x 15m in 1XPBS, shaking at room temperature.
XIV. Wash overnight in 1XPBS, shaking at room temperature.
XV. (If cleared, incubate in RIMS for 2h at room temperature.)
XVI. Mount samples for imaging.

---

[e] For 100um sections multiply times by 4; for 250um sections multiply long incubations by 6 and shorter washes by 4.

[f] For 100um 400ul + more concentrated antibody; for 250um sections likely 500uL - 750uL with concentrated antibody.

[g] Primary should be concentrated into weak binding solution using **insert filter name.** NB: Not concentrating antibody will change the composition of the weak binding solution and it may not work as well.

[h] 12 hours is the absolute minimum for 40um. For 100um, 24 hours is the minimum. For 250, 48 hours is the minimum. Longer is almost always better with a sweet-spot between 48 and 72 hours.

[i] If the antibody is very specific and/or lower affinity, 38C will work very well. If the antibody is a bit dirty or very high affinity, you should leave it at room temperature or 4C.

[j] For example, if you have 400uL weak binding + 5uL primary antibody per well, assume 425uL volume per sample.

[k] For a 40um sample, you would have 425uL total volume and add 71ul every hour for 6 hours. The volume and the time should be scaled for tissue thickness, up to 8 hours for 250um.

[l] For 100um sections 2h minimum, for 250um 4h minimum. This is the only step where longer *isn't* always better. You want enough time for the ionic concentration to fully equalize and allow antibody binding, but you don't want to leave it too long or you will get strong signal on the surface. If you don't leave it long enough, you might get weak signal, especially if there wasn't much labeling during the weak binding incubation. The timing on this step likely needs to be empirically tested.

[m] For 100um sections and larger, use fragment Alexafluor antibodies (I use Cell Signaling Technologies or AbCam). For 40um sections, normal AlexaFluor conjugated antibodies from LifeTechnologies are best.

[n] For 100uM sections and larger, use 1:100 Hoechst dilution.

Appendix B: Protocol for iSWITCH labeling intact tissue samples

Solutions:

SWITCH Fixative	1% glutaraldehyde 4% paraformaldehyde in 1X PBS
Inactivation Solution	1% acrylamide 1M glycine 0.1% triton- X100 in 1X PBS
PBST	0.1% triton- X100 in 1X PBS
Clearing Solution (pH 8.5 - 9.0)	200mM sodium dodecylsulfate 20mM lithium hydroxide monohydrate 4mM boric acid in ddH_2O
Blocking Buffer	2% bovine serum albumin in PBST
Weak Binding Solution (pH 10.5)	37.75mM Na_2HPO_4 3.53mM KH_2PO_4 0.02% sodium azide in PBST
Reversal Buffer (pH 7.4)	37.75mM Na_2HPO_4 3.53mM KH_2PO_4 0.02% sodium azide in PBST
Hoechst solution	1mg/ml Hoechst 33258 in ddH_2O
Refractive index matching solution (RIMS)	75g Histodenz 20mL 0.1M phosphate buffer 60mL ddH_2O

Abbreviations:

h	hours
C	degrees Celcius
m	minutes
d	days

Pre-steps if clearing:

I. Perfuse with ice-cold PBS immediately followed by SWITCH fixative.
II. Post-fix brains in SWITCH fixative for 72h at 4C on rocker.
III. Inactivate brains by incubating in inactivation solution for 48h at room temperature.
IV. Wash brains 12h in PBST, shaking at room temperature.
V. (Cut whole-brains into hemispheres)[o]
VI. Clear brains by incubating in clearing solution at 37-55C until white matter tracts are translucent.
VII. Wash for 48h at room temperature in PBST.

SWITCH labeling (for hemispheres[p]):

I. Incubate sections in weak binding solution for 24h.
II. Put directly into 1mL[q] of weak binding solution and add concentrated primary.[r]
III. Leave shaking for at least 72 hours[s] at 37C.
IV. Calculate the volume of primary incubation solution. Add extra to account for the volume of solution in the tissue.[t]
V. Add ⅛ of the volume calculated in step IV of reversal buffer[u] each hour for 8 hours.
VI. After final addition, let samples incubate in primary for at least 12h at 37C.[v]
VII. Wash 24h in PBST, shaking at 37C.
VIII. Use a secondary antibody[w] at the same dilution as the primary antibody. Dilute in PBST, shaking at 37C for the same duration as step III.
IX. Wash 24h in 1XPBS, shaking at room temperature.
X. Incubate in Hoechst diluted 1:100 in 1XPBS to label nuclei for 12h at room temperature.
XI. Wash 48h in 1XPBS, shaking at room temperature.
XII. Incubate in RIMS for 24h at room temperature.
XIII. Mount samples for imaging.

---

[o] Hemispheres will clear more quickly, so if you plan to cut them, doing it in advance is advantageous. If not, brains can be cut into hemispheres or other large (imprecise) chunks after clearing.

[p] For whole brain, multiply weak binding incubation and secondary incubation by 2. Washes and other incubation times remain the same or should be empirically tested.

[q] Solution should just cover the tissue. Volume may be different for whole brain or depending on the tube.

[r] Primary should be concentrated into weak binding solution using **insert filter name.** NB: Not concentrating antibody will change the composition of the weak binding solution and it may not work as well.

[s] 72h is the absolute minimum for a hemisphere and is likely not enough time for most experiments. 5d is usually very good for a hemisphere. For whole brain, scale accordingly.

[t] For example, if you have 1mL weak binding + 25uL concentrated primary antibody + 250uL volume in sample = 1275uL

[u] For the hemisphere with 1275 total, you add 160ul every hour for 8 hours. The volume will scale with the size of the tissue.

[v] This is the only step where longer *isn't* always better. You want enough time for the ionic concentration to fully equalize and allow antibody binding, but you don't want to leave it too long or you will get strong signal on the surface. If you don't leave it long enough, you might get weak signal, especially if there wasn't much labeling during the weak binding incubation. This can also be done at 37C. The specifics for this step likely need to be empirically tested. It can be tested on smaller chunks and scaled.

[w] Use fragment AlexaFluor antibodies (Cell Signaling Technologies or AbCam).

Appendix C: Protocol for iSWITCH labeling human autopsy specimens.

Solutions:

SWITCH Fixative	1% glutaraldehyde in 1X PBS
Inactivation Solution	1% acrylamide 1M glycine 0.1% triton- X100 in 1X PBS
PBST	0.1% triton- X100 in 1X PBS
Clearing Solution (pH 8.5 - 9.0)	200mM sodium dodecylsulfate 20mM lithium hydroxide monohydrate 4mM boric acid in ddH_2O
Blocking Buffer	2% bovine serum albumin in PBST
Weak Binding Solution (pH 10.5)	37.75mM Na_2HPO_4 3.53mM KH_2PO_4 0.02% sodium azide in PBST
Reversal Buffer (pH 7.4)	37.75mM Na_2HPO_4 3.53mM KH_2PO_4 0.02% sodium azide in PBST
Hoechst solution	1mg/ml Hoechst 33258 in ddH_2O
Refractive index matching solution (RIMS)	75g Histodenz 20mL 0.1M phosphate buffer 60mL ddH_2O

Abbreviations:

h	hours
C	degrees Celcius
m	minutes
d	days

Pre-steps if paraffin embedded:

I. Place blocks into Xylene for 8d. Switch Xylene solution twice per day.

II. Rehydrate blocks[x]:

Chemical	Timing
100% Ethanol	1 hour 20 minutes
100% Ethanol	1 hour 20 minutes
100% Ethanol	1 hour 20 minutes
95% Ethanol	1 hour
95% Ethanol	1 hour
Running dH_2O from tap	10 minutes
dH_2O	Storage

Pre-steps if clearing:

I. Post-fix tissue in SWITCH fixative for 10d at 4C on rocker.

II. Inactivate tissue by incubating in inactivation solution for 72h at room temperature.

III. Wash tissue 24h in PBST, shaking at room temperature.

IV. Clear brains by incubating in clearing solution at 37-55C until sample appears translucent.

V. Wash for 72h at room temperature in PBST.

SWITCH labeling:

I. Incubate tissue in weak binding solution for 24h.

II. Put directly into 5mL[y] of weak binding solution and add concentrated primary.[z]

III. Leave shaking for at least 5d[aa] at 37C.

IV. Calculate the volume of primary incubation solution. Add extra for the volume in the tissue.[bb]

V. Add ⅛ of the volume calculated in step IV of reversal buffer[cc] each hour for 8 hours.

VI. After final addition, let samples incubate in primary for at least 12h at 37.[dd]

VII. Wash 24h in PBST, shaking at 37C.

VIII. Use a secondary antibody[ee] at the same dilution as the primary antibody. Dilute in PBST, shaking at 37C for the same duration as step III.

---

[x] This protocol works on paraffinized blocks that are 2-5mm thick. These steps should be tested depending on the brand of paraffin and the size of the blocks.

[y] Solution should just cover the tissue. Volume may be different depending on the tube or dish.

[z] Primary should be concentrated into weak binding solution using **insert filter name.** NB: Not concentrating antibody will change the composition of the weak binding solution and it may not work as well.

[aa] 5d is the absolute minimum and is likely not enough time for most experiments. Test this timing empirically.

[bb] For example, if you have 5mL weak binding + 25uL concentrated primary antibody + 500uL volume in sample = 5525uL

[cc] For the hemisphere with 5525 total, you add 690uL every hour for 8 hours. The volume will scale with the size of the tissue.

[dd] This is the only step where longer *isn't* always better. You want enough time for the ionic concentration to fully equalize and allow antibody binding, but you don't want to leave it too long or you will get strong signal on the surface. If you don't leave it long enough, you might get weak signal, especially if there wasn't much labeling during the weak binding incubation. This can also be done at 37C. The specifics for this step likely need to be empirically tested. It can be tested on smaller chunks and scaled.

IX. Wash 24h in 1XPBS, shaking at room temperature.
X. Incubate in Hoechst diluted 1:100 in 1XPBS to label nuclei for 12h at room temperature.
XI. Wash 48h in 1XPBS, shaking at room temperature.
XII. Incubate in RIMS for 24h at room temperature.

[ee] Use fragment AlexaFluor antibodies (Cell Signaling Technologies or AbCam).

Appendix D: Recommendations to the NIA-AA 2015 AD Summit

(Recommendations)

Interdisciplinary Research to Understand the Heterogeneity and Multifactorial Etiology of Alzheimer's Disease: Optogenetics

Introduction to recommendations:

The human brain evolved to interact with dynamic internal and external environments. Changes in each affect functioning of neural circuits and brain systems. In understanding the biological basis for the onset and progression of Alzheimer's disease, researchers need to elaborate the interaction between brain, environmental stimuli, and pathology. This requires the use of advanced tools for testing causality, as correlative evidence will not provide the mechanistic insights necessary for advancing understanding of the disease to create a cure.

Optogenetics is the use of light-controllable, genetically encoded tools to probe neural functioning at the systems, circuit, cellular, and molecular levels. (5)

Recommendations

- *Create a holistic understanding of how neural circuit functioning changes in Alzheimer's using 'classical' opsin-channels (e.g. channelrhodopsin) and genetic tricks for circuit tagging. Note: 'Circuit' here to be interpreted as both long-range region-to-region communicating circuits, and microcircuitry of multiple cells and cell types within a brain region. (1a,1c,1d)*
  - *Define neural circuits crucial in disease based on pathological affliction, relevance to patient behavioral outcomes, connectivity. (2) (7)*
  - *Identify basic principles of how these circuits respond to stimuli when healthy. (4) (5) (9)*
  - *Observe changes in circuit function in response to known Alzheimer's pathology. (2) (5)*
  - *Probe how circuit activity affects Alzheimer's progression. (2) (5)*
  - *Investigate whether optogenetic manipulation influences how the defined circuits respond to the environment and influence disease progression. (4)*

- *Use advanced, optically responsive molecular tools to probe causality of cellular activities in Alzheimer's at the receptor, enzymatic, protein-protein interaction, and transcriptional levels in multiple cell types including astrocytes, microglia, and oligodendrocytes.*
  - *Identify ideal transgenic vectors for non-neuronal cell-types to which these molecular tools could be targeted. (5) (6)*
  - *Use optically controllable transcriptional machinery to probe the role of big-data identified genetic mutations in iPSC and animal models using within-subject conditions to control for heterogeneous genetic backgrounds and developmental experiences. (1b) (4) (7)*

- *Develop alternative treatment methods based on successful deep brain stimulation models and optogenetic specificity for testing circuit intervention as a safe alternative or addition to drug therapeutics. (10)*
  - *Support research programs to design non-invasive, circuit-specific stimulation paradigms such as far-red sensitive channels, transcranial magnetic stimulation, and implantable microLED technologies. (5) (6) (10)*

- *Use non-invasive technologies, along with opto-transgenic animals and large-volume imaging technologies to causally study how rodent models' behavior, circuit function, and pathological outcomes vary with focal changes in neural, molecular, or genetic activity. (4)*

Appendix D continued: Recommendations to the NIA-AA 2015 AD Summit (Slide)

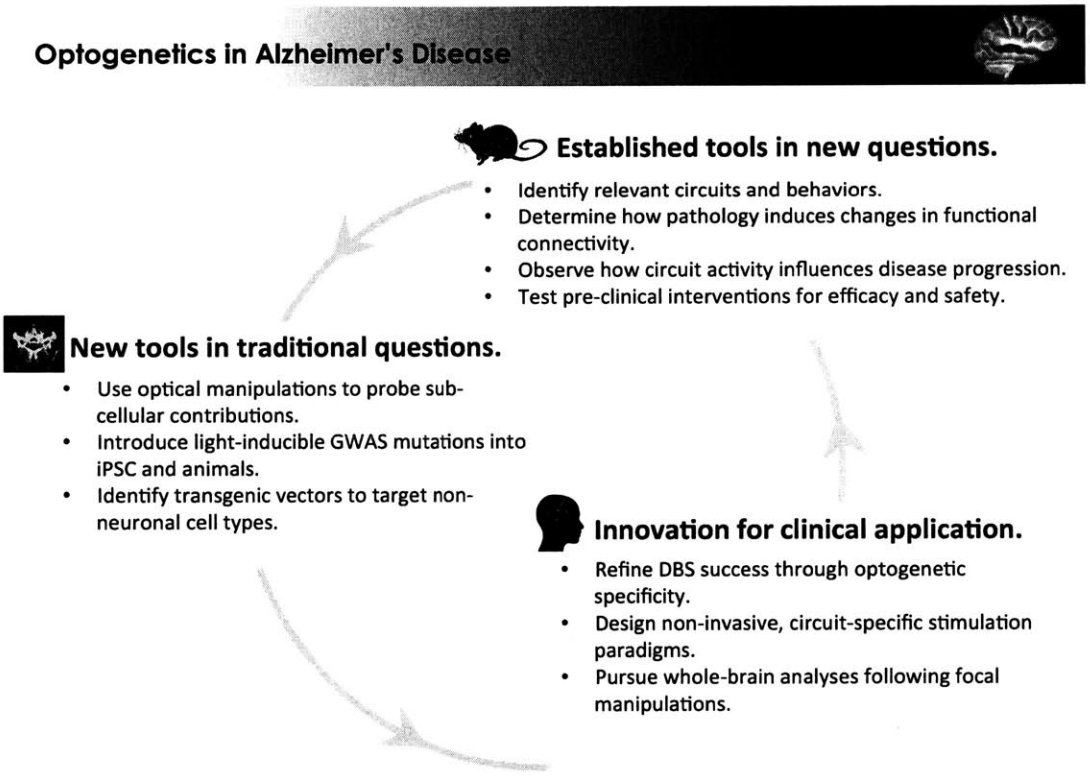

Appendix D continued: Recommendations to the NIA-AA 2015 AD Summit (Talking Points)

Interdisciplinary Research to Understand the Heterogeneity and Multifactorial Etiology of Alzheimer's Disease: Optogenetics

Talking points:

INTRO:

Neural circuits are essential to behavior, and Alzheimer's is ultimately a behavioral disease, where learning and memory behaviors are disrupted.

Current emphasis needs to include:

- *Understanding the circuit disruptions behind the memory impairments,*
- *Developing advanced tools for testing causality, and*
- *Translating these findings into clinical applications.*

Optogenetics are advanced tools ideally suited for this task. They are light-controllable, genetically encoded proteins that enable us to probe neural functioning at the systems, circuit, cellular, and molecular levels.

MOUSE PICTURE:

These tools have revolutionized the field of neuroscience over the past decade. Most well known are light-activated ion channels -- channelrhodopsin and halorhodopsin -- that allow millisecond control over neuronal activity.

As a first step to understand the circuit disruptions behind the memory impairments, we can use these established tools in new questions in AD research.

This includes (read bullet points)

By integrating basic behavioral neuroscience with key symptomatic alterations in AD, we can begin to understand how the brain functions and why AD manifests as a memory disorder.

CELL PICTURE:

We can also use new optogenetic tools in traditional questions. Decades of molecular research have contributed to our current understanding of the mechanisms of AD. However, until now, functional experiments have been limited by the available tools. It is now within our grasp to:

(read bullet points)

Ultimately we will be able to take subcellular observations and correlate them to circuit disruptions and get a more complete, or holistic understanding of the pathophysiology of the disease.

BRAIN PICTURE:
A critical consideration in this process is innovation for clinical application. Optogenetics allow targeted interventions which alone may be efficacious but may also be useful when paired with system-wide therapeutics.

We need to: (read bullet points)

With safer tools, and an understanding of manipulations prior to human use, we may finally deliver viable options for treatment.

Each of these approaches can and should inform each other. Optogenetics are poised to play a key role across all areas of Alzheimer's research. By implementing these tools across multiple levels of investigation, we remove translational barriers and speed our quest for the cure.

References

1. Bloom, D. E. *et al.* The Global Economic Burden of Noncommunicable Diseases. *World Econ. Forum* 1–46 (2011).

2. Kinch, M. S. & Patridge, E. An analysis of FDA-approved drugs for psychiatric disorders. *Drug Discov. Today* **20,** 3–6 (2015).

3. Bandelow, B. *et al.* Efficacy of treatments for anxiety disorders: a meta-analysis. *Int. Clin. Psychopharmacol.* 1–10 (2015). doi:10.1097/YIC.0000000000000078

4. Kesselheim, A. S., Hwang, T. J. & Franklin, J. M. Two decades of new drug development for central nervous system disorders. *Nat. Rev. Drug Discov.* **14,** 815–816 (2015).

5. McKhann, G. M. *et al.* The diagnosis of dementia due to Alzheimer's disease: Recommendations from the National Institute on Aging-Alzheimer's Association workgroups on diagnostic guidelines for Alzheimer's disease. *Alzheimer's Dement.* **7,** 263–269 (2011).

6. Hurd, M. D., Martorell, P., Delavande, A., Mullen, K. J. & Langa, K. M. Monetary costs of dementia in the United States. *N. Engl. J. Med.* **368,** 1326–34 (2013).

7. Alzheimer Association. 2016 Alzheimer ' S Disease Facts and Figures. 1–5 (2016).

8. Hardy, J. & Higgins, G. Alzheimer's Disease : The Amyloid Cascade Hypothesis. *Science (80-.).* **256,** 184–185 (1992).

9. Hardy, J. & Selkoe, D. J. The amyloid hypothesis of Alzheimer's disease: progress and problems on the road to therapeutics. *Science* **297,** 353–356 (2002).

10. Montine, T. J. *et al.* National institute on aging-Alzheimer's association guidelines for the neuropathologic assessment of Alzheimer's disease: A practical approach. *Acta Neuropathol.* **123,** 1–11 (2012).

11. Jack, C. R. *et al.* Introduction to the recommendations from the National Institute on Aging-Alzheimer's Association workgroups on diagnostic guidelines for Alzheimer's disease. *Alzheimer's Dement.* **7,** 257–262 (2011).

12. Holmes, C. *et al.* Long-term effects of Abeta42 immunisation in Alzheimer's disease: follow-up of a randomised, placebo-controlled phase I trial. *Lancet* **372,** 216–23 (2008).

13. Vellas, B. *et al.* Long-term follow-up of patients immunized with AN1792: reduced functional decline in antibody responders. *Curr. Alzheimer Res.* **6,** 144–51 (2009).

14. De Strooper, B. & Karran, E. The Cellular Phase of Alzheimer's Disease. *Cell* **164,** 603–615 (2016).

15. Dubois, B. *et al.* Advancing research diagnostic criteria for Alzheimer's disease: The IWG-2 criteria. *Lancet Neurol.* **13,** 614–629 (2014).

16. Papp, K. V. *et al.* Free and cued memory in relation to biomarker-defined Abnormalities in clinically normal older Adults and those at risk for Alzheimer's disease. *Neuropsychologia* **73,** 169–175 (2015).

17. Irish, M., Piguet, O., Hodges, J. R & Hornberger, M. Common and unique gray matter correlates of episodic memory dysfunction in frontotemporal dementia and alzheimer's disease. *Hum. Brain Mapp.* **35,** 1422–1435 (2014).

18. Ray, N. J. *et al.* Cholinergic Basal Forebrain Structure Influences the Reconfiguration of White Matter Connections to Support Residual Memory in Mild Cognitive Impairment. *J. Neurosci.* **35,** 739–747 (2015).

19. Mattson, M. P. Late-onset dementia: a mosaic of prototypical pathologies modifiable by diet and lifestyle. *npj Aging Mech. Dis.* **1,** 15003 (2015).

20. Palop, J. J. *et al.* Aberrant Excitatory Neuronal Activity and Compensatory Remodeling of Inhibitory Hippocampal Circuits in Mouse Models of Alzheimer's Disease. *Neuron* **55,** 697–711 (2007).

21. Vossel, K. A. *et al.* Seizures and epileptiform activity in the early stages of Alzheimer disease. *JAMA Neurol.* **70,** 1158–66 (2013).

22. Verret, L. *et al.* Inhibitory interneuron deficit links altered network activity and cognitive dysfunction in alzheimer model. *Cell* **149,** 708–721 (2012).

23. Bakker, A., Albert, M. S., Krauss, G., Speck, C. L. & Gallagher, M. Response of the medial temporal lobe network in amnestic mild cognitive impairment to therapeutic intervention assessed by fMRI and memory task performance. *NeuroImage Clin.* **7,** 688–698 (2015).

24. Jack, C. R. *et al.* Brain beta-amyloid measures and magnetic resonance imaging atrophy both predict time-to-progression from mild cognitive impairment to Alzheimer's disease. *Brain* **133,** 3336–3348 (2010).

25. Morris, M. C. *et al.* MIND diet associated with reduced incidence of Alzheimer's disease. *Alzheimer's Dement.* **11,** 1007–1014 (2015).

26. Wilson, R. S. *et al.* Early life socioeconomic status and late life risk of Alzheimer's disease. *Neuroepidemiology* **25,** 8–14 (2005).

27. Profenno, L. A., Porsteinsson, A. P. & Faraone, S. V. Meta-Analysis of Alzheimer's Disease Risk with Obesity, Diabetes, and Related Disorders. *Biol. Psychiatry* **67,** 505–512 (2010).

28. Hyman, B. T. *et al.* National Insitute on Aging- Alzheimer's Association guidelines for the neuropathologic assessment of Alzheimer's disease. *Alzheimer's Dement.* **8,** 1–13 (2013).

29. Tanzi, R. *et al.* Amyloid-beta Protein Gene: cDNA, mRNA Distribution, and Genetic Linkage Near the Alzheimer Locus. **235,** (1987).

30. St George-Hyslop, P. H. *et al.* The genetic defect causing familial Alzheimer's Disease maps on Chromosome 21. *Science (80-.).* **235,** 885–890 (1987).

31. Kang, J. *et al.* The precursor of Alzheimer's disease amyloid A4 protein resembles a cell-surface receptor. *Nature* **325,** 733–736 (1987).

32. Goldgaber, D., Lerman, M., McBride, O. W., Saffiotti, U. & Gajdusek, D. C. Characterization and Chromosomal Localization of a cDNA Encoding Brain Amyloid of Alzheimer ' s Disease. *Science (80-.).* **235,** 877–880 (1987).

33. Sherrington, R. *et al.* Cloning of a gene bearing missense mutations in early-onset familial Alzheimer's disease. *Nature* **375,** 754–760 (1995).

34. Levy-Lahad, E. *et al.* Candidate Gene for the Chromosome 1 Familial Alzheimer's Disease Locus. *Science (80-.).* **269,** 973–977 (1995).

35. Schellenberg, G. *et al.* Genetic linkage evidence for a familial Alzheimer's disease locus on chromosome 14. *Science (80-.).* **258,** 668–671 (1992).

36. De Strooper, B. Lessons from a failed gamma-secretase Alzheimer trial. *Cell* **159,** 721–726 (2014).

37. Karran, E. & Hardy, J. A critique of the drug discovery and phase 3 clinical programs targeting the amyloid hypothesis for Alzheimer disease. *Ann. Neurol.* **76,** 185–205 (2014).

38. Lambert, J. C. *et al.* Meta-analysis of 74,046 individuals identifies 11 new susceptibility loci for Alzheimer's disease. *Nat. Genet.* **45,** 1452–8 (2013).

39. Palop, J. J. & Mucke, L. Amyloid-[beta]-induced neuronal dysfunction in Alzheimer's disease: from synapses toward neural networks. *Nat. Neurosci.* **13,** 812–818 (2010).

40. Selkoe, D. J. Alzheimer's Disease: Genes, Proteins, and Therapy. *Physiol. Rev.* **81,** 741–766 (2001).

41. Hardy, J. The Alzheimer family of diseases: many etiologies, one pathogenesis? *Proc. Natl. Acad. Sci. U. S. A.* **94,** 2095–2097 (1997).

42. De Jonghe, C. *et al.* Pathogenic APP mutations near the gamma-secretase cleavage site differentially affect Abeta secretion and APP C-terminal fragment stability. *Hum. Mol. Genet.* **10,** 1665–71 (2001).

43. Rovelet-Lecrux, A. *et al.* APP locus duplication causes autosomal dominant early-onset Alzheimer disease with cerebral amyloid angiopathy. *Nat. Genet.* **38,** 24–26 (2006).

44. Sleegers, K. *et al.* APP duplication is sufficient to cause early onset Alzheimer's dementia with cerebral amyloid angiopathy. *Brain* **129,** 2977–2983 (2006).

45. Wisniewski, K. E., Wisniewski, H. M. & Wen, G. Y. Occurrence of Neuropathological Changes and Dementia of Alzheimer ' s Disease in Down' s Syndrome. *Ann. Neurol.* **17,** 278–282 (1984).

46. Glenner, G. G. & Wong, C. W. Alzheimer's disease and Down's syndrome: Sharing of a unique cerebrovascular amyloid fibril protein. *Biochem. Biophys. Res. Commun.* **122,** 1131–1135 (1984).

47. Hutton, M. *et al.* Association of missense and 5'-splice-site mutations in tau with the inherited dementia FTDP-17. *Nature* **393,** 702–705 (1998).

48. Spillantini, M. G., Crowther, R. A., Kamphorst, W., Heutink, P. & van Swieten, J. C. Tau pathology in two Dutch families with mutations in the microtubule-binding region of tau. *Am. J. Pathol.* **153,** 1359–63 (1998).

49. Poorkaj, P. *et al.* Tau is a candidate gene for chromosome 17 frontotemporal dementia. *Ann. Neurol.* **43,** 815–825 (1998).

50. Jonsson, T. *et al.* A mutation in APP protects against Alzheimer's disease and age-related cognitive decline. *Nature* **488,** 96–99 (2012).

51. Nedergaard, M. & Verkhratsky, A. Artifact versus reality-How astrocytes contribute to synaptic events. *Glia* **60,** 1013–1023 (2012).

52. Schafer, D. P., Lehrman, E. K. & Stevens, B. The 'quad-partite' synapse: Microglia-synapse interactions in the developing and mature CNS. *Glia* **61,** 24–36 (2013).

53. Boyles, J. K., Pitas, R. E., Wilson, E., Mahley, R. W. & Taylor, J. M. Apolipoprotein E associated with astrocytic glia of the central nervous system and with nonmyelinating glia of the peripheral nervous system. *J. Clin. Invest.* **76,** 1501–1513 (1985).

54. Stone, D. J. *et al.* Astrocytes and microglia respond to estrogen with increased apoE mRNA in vivo and in vitro. *Exp. Neurol.* **143,** 313–8 (1997).

55. Zhang, Y. *et al.* An RNA-sequencing transcriptome and splicing database of glia, neurons, and vascular cells of the cerebral cortex. *J. Neurosci.* **34,** 11929–11947 (2014).

56. Castellano, J. M. *et al.* Human APOE Isoforms Differentially Regulate Brain Amyloid-β Peptide Clearance. *Sci Transl Med* **3,** 89ra57 (2011).

57. Reiman, E. M. *et al.* Fibrillar amyloid-beta burden in cognitively normal people at 3 levels of genetic risk for Alzheimer's disease. *Proc. Natl. Acad. Sci. U. S. A.* **106,** 6820–6825 (2009).

58. Crotti, A. & Ransohoff, R. M. Microglial Physiology and Pathophysiology: Insights from Genome-wide Transcriptional Profiling. *Immunity* **44,** 505–515 (2016).

59. Wang, Y. *et al.* TREM2-mediated early microglial response limits diffusion and toxicity of amyloid plaques. *J. Exp. Med.* jem.20151948 (2016). doi:10.1084/jem.20151948

60. Wang, Y. *et al.* TREM2 lipid sensing sustains the microglial response in an Alzheimer's disease model. *Cell* **160,** 1061–1071 (2015).

61. Mandrekar, S. *et al.* Microglia Mediate the Clearance of Soluble A through Fluid Phase Macropinocytosis. *J. Neurosci.* **29,** 4252–4262 (2009).

62. Liao, M. C., Ahmed, M., Smith, S. O. & Van Nostrand, W. E. Degradation of amyloid-beta protein by purified myelin basic protein. *J. Biol. Chem.* **284,** 28917–28925 (2009).

63. Yankner, B. A., Duffy, L. K. & Kirschner, D. A. Neurotrophic and Neurotoxic Effects of Amyloid Beta Protein: Reversal by Tachykinin Neuropeptides. **421,** (1988).

64. Terry, R. D. *et al.* Physical basis of cognitive alterations in Alzheimer's disease: Synapse loss is the major correlate of cognitive impairment. *Ann. Neurol.* **30,** 572–580 (1991).

65. DeKosky, S. T. & Scheff, S. W. Synapse loss in frontal cortex biopsies in Alzheimer's disease: Correlation with cognitive severity. *Ann. Neurol.* **27,** 457–464 (1990).

66. Siskova, Z. *et al.* Dendritic structural degeneration is functionally linked to cellular hyperexcitability in a mouse model of alzheimer's disease. *Neuron* **84,** 1023–1033 (2014).

67. Wu, J. *et al.* Arc/Arg3.1 Regulates an Endosomal Pathway Essential for Activity-Dependent Beta-Amyloid Generation. *Cell* **147,** 615–628 (2011).

68. Cirrito, J. R. *et al.* Synaptic activity regulates interstitial fluid amyloid-beta levels in vivo. *Neuron* **48,** 913–922 (2005).

69. Wei, W. *et al.* Amyloid beta from axons and dendrites reduces local spine number and plasticity. *Nat. Neurosci.* **13,** 190–196 (2009).

70. Das, U. *et al.* Activity-induced convergence of app and bace-1 in acidic microdomains via an endocytosis-dependent pathway. *Neuron* **79,** 447–460 (2013).

71. Koo, E. H. *et al.* Precursor of amyloid protein in Alzheimer disease undergoes fast anterograde axonal transport. *Proc. Natl. Acad. Sci. U. S. A.* **87,** 1561–1565 (1990).

72. Dougherty, J. J., Wu, J. & Nichols, R. a. Beta-amyloid regulation of presynaptic nicotinic receptors in rat hippocampus and neocortex. *J. Neurosci.* **23,** 6740–6747 (2003).

73. Abramov, E. *et al.* Amyloid-beta as a positive endogenous regulator of release probability at hippocampal synapses. *Nat. Neurosci.* **12,** 1567–1576 (2009).

74. Snyder, E. M. *et al.* Regulation of NMDA receptor trafficking by amyloid-beta. *Nat. Neurosci.* **8,** 1051–8 (2005).

75. Roselli, F. *et al.* Soluble beta-amyloid1-40 induces NMDA-dependent degradation of postsynaptic density-95 at glutamatergic synapses. *J. Neurosci.* **25,** 11061–11070 (2005).

76. Walsh, D. M. *et al.* Naturally secreted oligomers of amyloid beta protein potently inhibit hippocampal long-term potentiation in vivo. *Nature* **416,** 535–539 (2002).

77. Li, S. *et al.* Soluble Oligomers of Amyloid Beta Protein Facilitate Hippocampal Long-Term Depression by Disrupting Neuronal Glutamate Uptake. *Neuron* **62,** 788–801 (2009).

78. Chapman, P. F. *et al.* Impaired synaptic plasticity and learning in aged amyloid precursor protein transgenic mice. *Nat. Neurosci.* **2,** 271–276 (1999).

79. Hsieh, H. *et al.* AMPAR Removal Underlies ABeta-Induced Synaptic Depression and Dendritic Spine Loss. *Neuron* **52,** 831–843 (2006).

80. Volicer, L., Smith, S. & Volicer, B. J. Effect of seizures on progression of dementia of the alzheimer type. *Dement. Geriatr. Cogn. Disord.* **6,** 258–263 (1995).

81. Busche, M. A. *et al.* Rescue of long-range circuit dysfunction in Alzheimer's disease models. *Nat. Neurosci.* **18,** 1623–30 (2015).

82. Thal, D. R., Rüb, U., Orantes, M. & Braak, H. Phases of A beta-deposition in the human brain and its relevance for the development of AD. *Neurology* **58,** 1791–1800 (2002).

83. Klunk, W. E. *et al.* Imaging Brain Amyloid in Alzheimer's Disease with Pittsburgh Compound-B. *Ann. Neurol.* **55,** 306–319 (2004).

84. Wong, D. F. *et al.* In vivo imaging of amyloid deposition in Alzheimer disease using the radioligand 18F-AV-45 (florbetapir [corrected] F 18). *J. Nucl. Med.* **51,** 913–920 (2010).

85. Forsberg, A. *et al.* PET imaging of amyloid deposition in patients with mild cognitive impairment. *Neurobiol. Aging* **29,** 1456–1465 (2008).

86. Albert, M. S. *et al.* The diagnosis of mild cognitive impairment due to Alzheimer's disease: Recommendations from the National Institute on Aging-Alzheimer's Association workgroups on diagnostic guidelines for Alzheimer's disease. *Alzheimer's Dement.* **7,** 270–279 (2011).

87. Greicius, M. D., Srivastava, G., Reiss, A. L. & Menon, V. Default-mode network activity distinguishes Alzheimer's disease from healthy aging: evidence from functional MRI. *Proc. Natl. Acad. Sci. U. S. A.* **101,** 4637–42 (2004).

88. Buckner, R. L. Molecular, Structural, and Functional Characterization of Alzheimer's Disease: Evidence for a Relationship between Default Activity, Amyloid, and Memory. *J. Neurosci.* **25,** 7709–7717 (2005).

89. Sperling, R., LaViolette, P. & O'Keefe, K. Amyloid deposition is associated with impaired default network function in older persons without dementia. *Neuron* **63,** 178–188 (2009).

90. Hedden, T. *et al.* Cognitive Profile of Amyloid Burden and White Matter Hyperintensities in Cognitively Normal Older Adults. *J. Neurosci.* **32,** 16233–16242 (2012).

91. Mormino, E. C. *et al.* Cognitive Profile of Amyloid Burden and White Matter Hyperintensities in Cognitively Normal Older Adults. *JAMA Neurol.* **71,** 1379–85 (2014).

92. Villemagne, V. L. *et al.* Longitudinal assessment of Abeta and cognition in aging and Alzheimer disease. *Ann. Neurol.* **69,** 181–192 (2011).

93. Kadir, A. *et al.* Dynamic changes in PET amyloid and FDG imaging at different stages of Alzheimer's disease. *Neurobiol. Aging* **33,** 198.e1–198.e14 (2012).

94. Koivunen, J. *et al.* Amyloid PET imaging in patients with mild cognitive impairment: A 2-year follow-up study. *Neurology* **76,** 1085–1090 (2011).

95. Jack, C. R. *et al.* Serial PIB and MRI in normal, mild cognitive impairment and Alzheimers disease: Implications for sequence of pathological events in Alzheimer's disease. *Brain* **132,**

1355–1365 (2009).

96. Harris, J. A. *et al.* Transsynaptic Progression of Amyloid-beta-Induced Neuronal Dysfunction within the Entorhinal-Hippocampal Network. *Neuron* **68,** 428–441 (2010).

97. Jucker, M. & Walker, L. C. Self-propagation of pathogenic protein aggregates in neurodegenerative diseases. *Nature* **501,** 45–51 (2013).

98. Fleisher, A. S. *et al.* Phase 2 safety trial targeting amyloid beta production with a gamma-secretase inhibitor in Alzheimer disease. *Arch. Neurol.* **65,** 1031–1038 (2008).

99. May, P. C. *et al.* The Potent BACE1 Inhibitor LY2886721 Elicits Robust Central ABeta Pharmacodynamic Responses in Mice, Dogs, and Humans. *J. Neurosci.* **35,** 1199–1210 (2015).

100. Vassar, R. BACE1 inhibitor drugs in clinical trials for Alzheimer's disease. *Alzheimers. Res. Ther.* **6,** 89 (2014).

101. Doody, R. S. *et al.* A phase 3 trial of semagacestat for treatment of Alzheimer's disease. *N. Engl. J. Med.* **369,** 341–50 (2013).

102. Orgogozo, J. M. *et al.* Subacute meningoencephalitis in a subset of patients with AD after Abeta42 immunization. *Neurology* **61,** 46–54 (2003).

103. Farlow, M. R. *et al.* Long-term treatment with active Aβ immunotherapy with CAD106 in mild Alzheimer's disease. *Alzheimers. Res. Ther.* **7,** 23 (2015).

104. Siemers, E. R. *et al.* Phase 3 solanezumab trials: Secondary outcomes in mild Alzheimer's disease patients. *Alzheimer's Dement.* **12,** 1–11 (2015).

105. Ratner, M. Biogen's early Alzheimer's data raise hopes, some eyebrows. *Nat. Biotechnol.* **33,** 438–438 (2015).

106. van der Kant, R. & Goldstein, L. S. B. Cellular Functions of the Amyloid Precursor Protein from Development to Dementia. *Dev. Cell* **32,** 502–515 (2015).

107. Duggan, S. P. & McCarthy, J. V. Beyond gamma-secretase activity: The multifunctional nature of presenilins in cell signalling pathways. *Cell. Signal.* **28,** 1–11 (2016).

108. Müller, U. *et al.* Behavioral and anatomical deficits in mice homozygous for a modified β-amyloid precursor protein gene. *Cell* **79,** 755–765 (1994).

109. Dawson, G. R. *et al.* Age-related cognitive deficits, impaired long-term potentiation and reduction in synaptic marker density in mice lacking the beta-amyloid precursor protein. *Neuroscience* **90,** 1–13 (1999).

110. Xia, D. *et al.* Presenilin-1 knockin mice reveal loss-of-function mechanism for familial alzheimer's disease. *Neuron* **85,** 967–981 (2015).

111. Nelson, O. *et al.* Familial Alzheimer disease-linked mutations specifically disrupt Ca 2+ leak function of presenilin 1. *J. Clin. Invest.* **117,** 1230–1239 (2007).

112. Strittmatter, W. J. *et al.* Apolipoprotein E: high-avidity binding to beta-amyloid and increased frequency of type 4 allele in late-onset familial Alzheimer disease. *Proc. Natl. Acad. Sci. U. S. A.* **90,** 1977–81 (1993).

113. Corder, E. H. *et al.* Gene dose of apolipoprotein E type 4 allele and the risk of Alzheimer's disease in late onset families. *Science* **261,** 921–923 (1993).

114. Morris, J. C. *et al.* APOE predicts amyloid-beta but not tau Alzheimer pathology in cognitively normal aging. *Ann. Neurol.* **67,** 122–131 (2010).

115. Fabelo, N. *et al.* Altered lipid composition in cortical lipid rafts occurs at early stages of sporadic Alzheimer's disease and facilitates APP/BACE1 interactions. *Neurobiol. Aging* **35,** 1801–1812 (2014).

116. Lambert, J.-C. *et al.* Genome-wide association study identifies variants at CLU and CR1 associated with Alzheimer's disease. *Nat. Genet.* **41,** 1094–1099 (2009).

117. Harold, D. *et al.* Genome-wide association study identifies variants at CLU and PICALM associated with Alzheimer's disease , and shows evidence for additional susceptibility genes. *Nat. Genet.* **41,** 1088–1093 (2009).

118. Hollingworth, P. *et al.* Common variants at ABCA7, MS4A6A/MS4A4E, EPHA1, CD33 and CD2AP are associated with Alzheimer's disease. *Nat. Genet.* **43,** 429–35 (2011).

119. Naj, A. C. *et al.* Common variants at MS4A4/MS4A6E, CD2AP, CD33 and EPHA1 are associated with late-onset Alzheimer's disease. *Nat. Genet.* **43,** 436–441 (2011).

120. Guerreiro, R. *et al.* TREM2 variants in Alzheimer's disease. *N. Engl. J. Med.* **368,** 117–27 (2013).

121. Jonsson, T. *et al.* Variant of TREM2 associated with the risk of Alzheimer's disease. *N. Engl. J. Med.* **368,** 107–16 (2013).

122. Rogaeva, E. *et al.* The neuronal sortilin-related receptor SORL1 is genetically associated with Alzheimer's Disease. *Nat Genet* **39,** 168–177 (2007).

123. Sakae, N. *et al.* ABCA7 Deficiency Accelerates Amyloid-beta Generation and Alzheimer's Neuronal Pathology. *J Neurosci.* **36,** 3848–3859 (2016).

124. Miller, S. E. *et al.* CALM Regulates Clathrin-Coated Vesicle Size and Maturation by Directly Sensing and Driving Membrane Curvature. *Dev. Cell* **33,** 163–175 (2015).

125. Hong, S. *et al.* Complement and microglia mediate early synapse loss in Alzheimer mouse models. *Science (80-.).* **8373,** 1–9 (2016).

126. Millecamps, S. & Julien, J.-P. Axonal transport deficits and neurodegenerative diseases. *Nat. Rev. Neurosci.* **14,** 161–76 (2013).

127. LaFerla, F. M. Calcium dyshomeostasis and intracellular signalling in Alzheimer's disease. *Nat. Rev. Neurosci.* **3,** 862–872 (2002).

128. Treusch, S. *et al.* Functional Links Between Abeta Toxicity, Endocytic Trafficking, and Alzheimer's Disease Risk Factors in Yeast. *Science (80-.).* **334,** 1241–1245 (2011).

129. Iwata, A. *et al.* Altered CpG methylation in sporadic alzheimer's disease is associated with APP and MAPT dysregulation. *Hum. Mol. Genet.* **23,** 648–656 (2014).

130. De Jager, P. L. *et al.* Alzheimer's disease: early alterations in brain DNA methylation at ANK1, BIN1, RHBDF2 and other loci. *Nat Neurosci* **17,** 1156–1163 (2014).

131. Yu, L. *et al.* Association of Brain DNA methylation in SORL1, ABCA7, HLA-DRB5, SLC24A4, and BIN1 with pathological diagnosis of Alzheimer disease. *JAMA Neurol.* **72,** 15–24 (2015).

132. Gjoneska, E. *et al.* Conserved epigenomic signals in mice and humans reveal immune basis of Alzheimer's disease. *Nature* **518,** 365–9 (2015).

133. Guan, J.-S. *et al.* HDAC2 negatively regulates memory formation and synaptic plasticity. *Nature* **459,** 55–60 (2009).

134. Gräff, J. *et al.* An epigenetic blockade of cognitive functions in the neurodegenerating brain. *Nature* **483,** 222–6 (2012).

135. Lu, T. *et al.* REST and stress resistance in ageing and Alzheimer's disease. *Nature* **507,** 448–54 (2014).

136. Nho, K. *et al.* Protective variant for hippocampal atrophy identified by whole exome sequencing. *Ann. Neurol.* **77,** 547–552 (2015).

137. Mecocci, P., MacGarvey, U. & Beal, M. F. Oxidative damage to mitochondrial DNA is increased in Alzheimer's disease. *Ann. Neurol.* **36,** 747–751 (1994).

138. Jo, D.-G. *et al.* Evidence that gamma-secretase mediates oxidative stress-induced beta-secretase expression in Alzheimer's disease. *Neurobiol. Aging* **31,** 917–25 (2010).

139. Praticò, D., Uryu, K., Leight, S., Trojanoswki, J. Q. & Lee, V. M.-Y. Increased lipid peroxidation precedes amyloid plaque formation in an animal model of Alzheimer amyloidosis. *J. Neurosci.* **21,** 4183–4187 (2001).

140. Rhein, V. *et al.* Amyloid-beta and tau synergistically impair the oxidative phosphorylation system in triple transgenic Alzheimer's disease mice. *Proc. Natl. Acad. Sci. U. S. A.* **106,** 20057–62 (2009).

141. Salminen, A. *et al.* Impaired mitochondrial energy metabolism in Alzheimer's disease: Impact on pathogenesis via disturbed epigenetic regulation of chromatin landscape. *Prog. Neurobiol.* **131,** 1–20 (2015).

142. Lu, T. *et al.* Gene regulation and DNA damage in the ageing human brain. *Nature* **429,** 883–891 (2004).

143. Frost, B., Hemberg, M., Lewis, J. & Feany, M. B. Tau promotes neurodegeneration through global chromatin relaxation. *Nat. Neurosci.* **17,** 357–366 (2014).

144. Kim, D. *et al.* Deregulation of HDAC1 by p25/Cdk5 in Neurotoxicity. *Neuron* **60,** 803–817 (2008).

145. Anderson, A. J., Stoltzner, S., Lai, F., Su, J. & Nixon, R A. Morphological and biochemical assessment of DNA damage and apoptosis in Down syndrome and Alzheimer disease, and effect of postmortem tissue archival on TUNEL. *Neurobiol. Aging* **21,** 511–524 (2000).

146. Suberbielle, E. *et al.* Physiologic brain activity causes DNA double-strand breaks in neurons, with exacerbation by amyloid-β. *Nat. Neurosci.* **16,** 613–621 (2013).

147. Madabhushi, R. *et al.* Activity-Induced DNA Breaks Govern the Expression of Neuronal Early-Response Genes. *Cell* **43,** 118–125 (2007).

148. Xie, H. *et al.* Mitochondrial alterations near amyloid plaques in an Alzheimer's disease mouse model. *J Neurosci* **33,** 17042–17051 (2013).

149. Seo, J. *et al.* Activity-dependent p25 generation regulates synaptic plasticity and abeta-induced cognitive impairment. *Cell* **157,** 486–498 (2014).

150. Cruz, J. C., Tseng, H. C., Goldman, J. A., Shih, H. & Tsai, L. H. Aberrant Cdk5 activation by p25 triggers pathological events leading to neurodegeneration and neurofibrillary tangles. *Neuron* **40,** 471–483 (2003).

151. Pigino, G. *et al.* Alzheimer's Presenilin 1 Mutations Impair Kinesin-Based Axonal Transport. **23,** 4499–4508 (2003).

152. Decker, H., Lo, K. Y., Unger, S. M., Ferreira, S. T. & Silverman, M. A. Amyloid-β peptide oligomers disrupt axonal transport through an NMDA receptor-dependent mechanism that is mediated by glycogen synthase kinase 3β in primary cultured hippocampal neurons. *J. Neurosci.* **30,** 9166–9171 (2010).

153. Lindwall, G. & Cole, R. D. Phosphorylation affects the ability of tau protein to promote microtubule assembly. *J. Biol. Chem.* **259,** 5301–5305 (1984).

154. Bramblett, G. T. *et al.* Abnormal tau phosphorylation at Ser396 in Alzheimer's disease recapitulates development and contributes to reduced microtubule binding. *Neuron* **10,** 1089–1099 (1993).

155. Sontag, E., Nunbhakdi-Craig, V., Lee, G., Bloom, G. S. & Mumby, M. C. Regulation of the phosphorylation state and microtubule-binding activity of tau by protein phosphatase 2A. *Neuron* **17,** 1201–1207 (1996).

156. Vogelsberg-Ragaglia, V., Schuck, T., Trojanowski, J. Q. & Lee, V. M. PP2A mRNA expression is quantitatively decreased in Alzheimer's disease hippocampus. *Exp. Neurol.* **168,** 402–12 (2001).

157. Sontag, J.-M. & Sontag, E. Protein phosphatase 2A dysfunction in Alzheimer's disease. *Front. Mol. Neurosci.* **7,** 16 (2014).

158. Dixit, R., Ross, J. L., Goldman, Y. E. & Holzbaur, E. L. F. Differential Regulation of Dynein and Kinesin Motor Proteins by Tau. *Science* **319,** 8–11 (2008).

159. Rui, Y., Tiwari, P., Xie, Z. & Zheng, J. Q. Acute Impairment of Mitochondrial Trafficking by Beta-Amyloid Peptides in Hippocampal Neurons. *J. Neurosci.* **26,** 10480–10487 (2006).

160. Busciglio, J., Lorenzo, A., Yeh, J. & Yankner, B. A. Beta-Amyloid fibrils induce tau phosphorylation and loss of microtubule binding. *Neuron* **14,** 879–888 (1995).

161. Hoover, B. R. *et al.* Tau Mislocalization to Dendritic Spines Mediates Synaptic Dysfunction Independently of Neurodegeneration. *Neuron* **68,** 1067–1081 (2010).

162. Yamada, K. *et al.* Neuronal activity regulates extracellular tau in vivo. *J. Exp. Med.* **211,** 387–93 (2014).

163. Pooler, A. M., Phillips, E. C., Lau, D. H. W., Noble, W. & Hanger, D. P. Physiological release of endogenous tau is stimulated by neuronal activity. *EMBO Rep.* **14,** 389–94 (2013).

164. Moreau, K. *et al.* PICALM modulates autophagy activity and tau accumulation. *Nat. Commun.* **5,** 4998 (2014).

165. Min, S. W. *et al.* Acetylation of tau inhibits its degradation and contributes to tauopathy. *Neuron* **67,** 953–966 (2010).

166. Cohen, T. J. *et al.* The acetylation of tau inhibits its function and promotes pathological tau aggregation. *Nat. Commun.* **2,** 252 (2011).

167. Tracy, T. E. *et al.* Acetylated Tau Obstructs KIBRA-Mediated Signaling in Synaptic Plasticity and Promotes Tauopathy-Related Memory Loss. *Neuron* **90,** 245–260 (2016).

168. Xiao, G. & Gan, L. S. Receptor-mediated endocytosis and brain delivery of therapeutic biologics. *Int. J. Cell Biol.* **2013,** (2013).

169. Nixon, R. A. *et al.* Extensive Involvement of Autophagy in Alzheimer Disease: An Immuno-Electron Microscopy Study. *J. Neuropathol. Exp. Neurol.* **64,** 113–122 (2005).

170. Kononenko, N. L. & Haucke, V. Molecular mechanisms of presynaptic membrane retrieval and synaptic vesicle reformation. *Neuron* **85,** 484–496 (2015).

171. Orre, M. *et al.* Isolation of glia from Alzheimer's mice reveals inflammation anddysfunction. *Neurobiol. Aging* **35,** 2746–2760 (2014).

172. Chen, Z. *et al.* Microglial displacement of inhibitory synapses provides neuroprotection in the adult brain. *Nat. Commun.* **5,** 4486 (2014).

173. Cacucci, F., Yi, M., Wills, T. J., Chapman, P. & O'Keefe, J. Place cell firing correlates with memory deficits and amyloid plaque burden in Tg2576 Alzheimer mouse model. *Proc. Natl. Acad. Sci. U. S. A.* **105,** 7863–8 (2008).

174. Zhao, R., Fowler, S. W., Chiang, A. C. A., Ji, D. & Jankowsky, J. L. Impairments in experience-dependent scaling and stability of hippocampal place fields limit spatial learning in a mouse model of Alzheimer's disease. *Hippocampus* **24,** 963–978 (2014).

175. Ciupek, S. M., Cheng, J., Ali, Y. O., Lu, H.-C. & Ji, D. Progressive Functional Impairments of Hippocampal Neurons in a Tauopathy Mouse Model. *J. Neurosci.* **35,** 8118–8131 (2015).

176. Morris, R. G., Garrud, P., Rawlins, J. N. & O'Keefe, J. Place navigation impaired in rats with hippocampal lesions. *Nature* **297,** 681–683 (1982).

177. Wilson, M. a & McNaughton, B. L. Dynamics of the hippocampal ensemble code for space. *Science* **261,** 1055–1058 (1993).

178. Wallenstein, G. V & Hasselmo, M. E. GABAergic modulation of hippocampal population activity: sequence learning, place field development, and the phase precession effect. *J. Neurophysiol.* **78,** 393–408 (1997).

179. Whitehouse, P. J., Price, D. L., Clark, a W., Coyle, J. T. & DeLong, M. R. Alzheimer disease: evidence for selective loss of cholinergic neurons in the nucleus basalis. *Ann Neurol* **10,** 122–126 (1981).

180. Metherate, R., Cox, C. L. & Ashe, J. H. Cellular bases of neocortical activation: modulation of neural oscillations by the nucleus basalis and endogenous acetylcholine. *J. Neurosci.* **12,** 4701–4711 (1992).

181. Mesulam, M., Shaw, P., Mash, D. & Weintraub, S. Cholinergic nucleus basalis tauopathy emerges early in the aging-MCI-AD continuum. *Ann. Neurol.* **55,** 815–828 (2004).

182. Bartus, R. T., Dean, R. L., Beer, B. & Lippa, A. The cholinergic hypothesis of geriatric memory dysfunction. *Science* **217,** 408–414 (1982).

183. Hangya, B., Ranade, S. P., Lorenc, M. & Kepecs, A. Central Cholinergic Neurons Are Rapidly Recruited by Reinforcement Feedback. *Cell* **162,** 1155–1168 (2015).

184. Zhu, C. W. *et al.* Long-term associations between cholinesterase inhibitors and memantine use and health outcomes among patients with Alzheimer's disease. *Alzheimers. Dement.* **9,** 733–40 (2013).

185. Mattson, M. P. Pathways towards and away from Alzheimer's disease. *Nature* **430,** 631–639 (2004).

186. Braak, H. & Del Tredici, K. The pathological process underlying Alzheimer's disease in individuals under thirty. *Acta Neuropathol.* **121,** 171–181 (2011).

187. Braak, H. & Braak, E. Neuropathological stageing of Alzheimer-related changes. *Acta Neuropathol.* **82,** 239–259 (1991).

188. Johnson, K. A *et al.* Tau positron emission tomographic imaging in aging and early Alzheimer disease. *Ann. Neurol.* **79,** 110–119 (2016).

189. Steffenach, H. A., Witter, M., Moser, M. B. & Moser, E. I. Spatial memory in the rat requires the dorsolateral band of the entorhinal cortex. *Neuron* **45,** 301–313 (2005).

190. Vargha-Khadem, F. *et al.* Differential effects of early hippocampal pathology on episodic and semantic memory. *Science (80-.).* **277,** 376–380 (1997).

191. Schöll, M. *et al.* PET Imaging of Tau Deposition in the Aging Human Brain. 971–982 (2016). doi:10.1016/j.neuron.2016.01.028

192. Ossenkoppele, R. *et al.* Tau PET patterns mirror clinical and neuroanatomical variability in Alzheimer's disease. 1–17 (2016). doi:10.1093/brain/aww027

193. Ye, L. *et al.* Progression of Seed-Induced Abeta Deposition within the Limbic Connectome. *Brain Pathol.* **25,** 743–752 (2015).

194. Braak, H. & Braak, E. Alzheimer's disease affects limbic nuclei of the thalamus. *Acta Neuropathol.* **81,** 261–268 (1991).

195. Bruen, P. D., McGeown, W. J., Shanks, M. F. & Venneri, A. Neuroanatomical correlates of neuropsychiatric symptoms in Alzheimer's disease. *Brain* **131,** 2455–2463 (2008).

196. Iba, M. *et al.* Tau pathology spread in PS19 tau transgenic mice following locus coeruleus (LC) injections of synthetic tau fibrils is determined by the LC's afferent and efferent connections. *Acta Neuropathol.* **130,** 349–362 (2015).

197. Nestor, P. J., Fryer, T. D., Smielewski, P. & Hodges, J. R. Limbic hypometabolism in Alzheimer's disease and mild cognitive impairment. *Ann. Neurol.* **54,** 343–351 (2003).

198. Fletcher, E., Carmichael, O., Pasternak, O., Maier-Hein, K. H. & DeCarli, C. Early Brain Loss in Circuits Affected by Alzheimer's Disease is Predicted by Fornix Microstructure but may be Independent of Gray Matter. *Front. Aging Neurosci.* **6,** 106 (2014).

199. Laxton, A. W. *et al.* A phase I trial of deep brain stimulation of memory circuits in Alzheimer's disease. *Ann. Neurol.* **68,** 521–534 (2010).

200. Spires-Jones, T. L. & Hyman, B. The Intersection of Amyloid Beta and Tau at Synapses in Alzheimer's Disease. *Neuron* **82,** 756–771 (2014).

201. Reitz, C. & Mayeux, R. Alzheimer disease: Epidemiology, diagnostic criteria, risk factors and biomarkers. *Biochem. Pharmacol.* **88,** 640–651 (2014).

202. McEwen, B. S. Central effects of stress hormones in health and disease: Understanding the protective and damaging effects of stress and stress mediators. *Eur. J. Pharmacol.* **583,** 174–185 (2008).

203. Diano, S. *et al.* Ghrelin controls hippocampal spine synapse density and memory performance. *Nat. Neurosci.* **9,** 381–8 (2006).

204. Lupien, S. J. *et al.* Cortisol levels during human aging predict hippocampal atrophy and memory deficits. *Nat. Neurosci.* **1,** 69–73 (1998).

205. Baglietto-Vargas, D. *et al.* Short-term modern life-like stress exacerbates Aβ-pathology and synapse loss in 3xTg-AD mice. *J. Neurochem.* **134,** 915–926 (2015).

206. Rei, D. *et al.* Basolateral amygdala bidirectionally modulates stress-induced hippocampal learning and memory deficits through a p25/Cdk5-dependent pathway. *Proc. Natl. Acad. Sci.* 201415845

(2015). doi:10.1073/pnas.1415845112

207. Shytle, R. D *et al.* Cholinergic modulation of microglial activation by α7 nicotinic receptors. *J. Neurochem.* **89,** 337–343 (2004).

208. Talantova, M. *et al.* Aβ induces astrocytic glutamate release, extrasynaptic NMDA receptor activation, and synaptic loss. *Proc. Natl. Acad. Sci.* **110,** E2518–E2527 (2013).

209. Pedersen, J. T. & Sigurdsson, E. M. Tau immunotherapy for Alzheimer's disease. *Trends Mol. Med.* **21,** 394–402 (2015).

210. Aisen, P. S. *et al.* Effects of rofecoxib or naproxen vs placebo on Alzheimer disease progression: a randomized controlled trial *JAMA* **289,** 2819–2826 (2003).

211. Porrini, V. *et al.* CHF5074 (CSP-1103) induces microglia alternative activation in plaque-free Tg2576 mice and primary glial cultures exposed to beta-amyloid. *Neuroscience* **302,** 112–120 (2014).

212. Kuhn, J. *et al.* Deep brain stimulation of the nucleus basalis of meynert in early stage of Alzheimer's dementia. *Brain Stimul.* **8,** 838–839 (2015).

213. Sankar, T. *et al.* Deep brain stimulation influences brain structure in Alzheimer's disease. *Brain Stimul.* **8,** 645–654 (2015).

214. Roy, D. S. *et al.* Memory retrieval by activating engram cells in mouse models of early Alzheimer's disease. *Nature* (2016) doi:10.1038/nature17172

215 Fischer, A., Sananbenesi, F., Wang, X., Dobbin, M. & Tsai, L.-H. Recovery of learning and memory is associated with chromatin remodelling. *Nature* **447,** 178–82 (2007).

216. Hamelin, L. *et al.* Early and protective microglial activation in Alzheimer's disease: a prospective study using 18 F-DPA-714 PET imaging. 1–13 (2016). doi:10.1093/brain/aww017

217. Nhan, H. S., Chiang, K. & Koo, E. H. The multifaceted nature of amyloid precursor protein and its proteolytic fragments: friends and foes. *Acta Neuropathol.* **129,** 1–19 (2014).

218. Lammich, S. *et al.* Constitutive and regulated alpha-secretase cleavage of Alzheimer's amyloid precursor protein by a disintegrin metalloprotease. *Proc. Natl. Acad. Sci. U. S. A.* **96,** 3922–3927 (1999).

219. Willem, M. *et al.* η-Secretase processing of APP inhibits neuronal activity in the hippocampus. *Nature* **526,** 443–447 (2015).

220. Markram, H. *et al.* Reconstruction and Simulation of Neocortical Microcircuitry. *Cell* **163,** 456–492 (2015).

221. Zeisel, A. *et al.* Cell types in the mouse cortex and hippocampus revealed by single-cell RNA-seq. *Science (80-.).* **347,** 1138–42 (2015).

222. Beyeler, A. *et al.* Divergent Routing of Positive and Negative Information from the Amygdala

during Memory Retrieval. *Neuron* **90,** 348–361 (2016).

223. Oakley, H. *et al.* Intraneuronal β-Amyloid Aggregates, Neurodegeneration, and Neuron Loss in Transgenic Mice with Five Familial Alzheimer's Disease Mutations: Potential Factors in Amyloid Plaque Formation. *J. Neurosci.* **26,** 10129–10140 (2006).

224. Espina, V., Milia, J., Wu, G., Cowherd, S. & Liotta, L. A. Laser capture microdissection. *Methods Mol. Biol.* **319,** 213–229 (2006).

225. Haass, C., Kaether, C., Thinakaran, G. & Sisodia, S. Trafficking and proteolytic processing of APP. *Cold Spring Harb. Perspect. Med.* **2,** 1–25 (2012).

226. Richardson, D. S. & Lichtman, J. W. Clarifying Tissue Clearing. *Cell* **162,** 246–257 (2015).

227. Kim, S. Y., Chung, K. & Deisseroth, K. Light microscopy mapping of connections in the intact brain. *Trends in Cognitive Sciences* **17,** 596–599 (2013).

228. Renier, N. *et al.* IDISCO: A simple, rapid method to immunolabel large tissue samples for volume imaging. *Cell* **159,** 896–910 (2014).

229. Murray, E. *et al.* Simple, Scalable Proteomic Imaging for High-Dimensional Profiling of Intact Systems. *Cell* **163,** 1500–1514 (2015).

230. Yang, B. *et al.* Single-cell phenotyping within transparent intact tissue through whole-body clearing. *Cell* **158,** 945–958 (2014).

231. Tianqing, L., Rong, G. & Genping, S. Determination of the Diffusion Coefficient for SDS Micelle with Different Shape and the Effects of Ethanol by Cyclic Voltammetry Without Probes. *J. Dispers. Sci. Technol.* **17,** 509–526 (1996).

232. Huisken, J., Swoger, J., Bene, F. Del, Wittbrodt, J. & Stelzer, E. H. K. Live Embryos by Selective Plane Illumination Microscopy. 13–16

233. Gage, G. J., Kipke, D. R. & Shain, W. Whole animal perfusion fixation for rodents. *J. Vis. Exp.* e3564 (2012). doi:10.3791/3564

234. Goodpaster, T. & Randolph-Habecker, J. A Flexible Mouse-On-Mouse Immunohistochemical Staining Technique Adaptable to Biotin-Free Reagents, Immunofluorescence, and Multiple Antibody Staining. *J. Histochem. Cytochem.* **62,** 197–204 (2014).

235. Chung, K. *et al.* Structural and molecular interrogation of intact biological systems. *Nature* **497,** 332–7 (2013).

236. Qualtiere, L. F., Anderson, a G. & Meyers, P. Effects of ionic and nonionic detergents on antigen-antibody reactions. *J. Immunol.* **119,** 1645–1651 (1977).

237. Reverberi, R. & Reverberi, L. Factors affecting the antigen-antibody reaction. *Blood Transfus.* **5,** 227–240 (2007).

238. Kutten, K. S. *et al.* Deformably Registering and Annotating Whole CLARITY Brains to an Atlas

via Masked LDDMM. **9896,** 1–9 (2016).

239. Despotovic, I., Goossens, B. & Philips, W. MRI Segmentation of the Human Brain : Challenges , Methods , and Applications. **2015,** (2015).

240. Li, Q. *et al.* Establishing brain functional laterality in adult mice through unilateral gene manipulation in the embryonic cortex. *Cell Res.* **23,** 1147–1149 (2013).

241. Stafford, J. M. *et al.* Large-scaie topology and the default mode network in the mouse connectome. *Proc. Natl. Acad. Sci. U. S. A.* **111,** 18745–50 (2014).

242. Lu, H. *et al.* Rat brains also have a default mode network. *Proc. Natl. Acad. Sci.* **109,** 3979–3984 (2012).

243. Sokolowski, K. & Corbin, J. G. Wired for behaviors: from development to function of innate limbic system circuitry. *Front. Mol. Neurosci.* **5,** 1–15 (2012).

244. Catani, M., Dell'Acqua, F. & Thiebaut de Schotten, M. A revised limbic system model for memory, emotion and behaviour. *Neurosci. Biobehav. Rev.* **37,** 1724–1737 (2013).

245. Jansen, W. J. *et al.* Prevalence of Cerebral Amyloid Pathology in Persons Without Dementia: A Meta-analysis. *JAMA* **313,** 1924–1938 (2015).

246. Ye, L. *et al.* Progression of Seed-Induced A?? Deposition within the Limbic Connectome. *Brain Pathol.* **25,** 743–752 (2015).

247. Venter, J. C. *et al.* The sequence of the human genome. *Science (80-.).* **291,** 1304–1351 (2001).

248. Bero, A. W. *et al.* Early remodeling of the neocortex upon episodic memory encoding. *Proc. Natl. Acad. Sci.* **111,** 11852–11857 (2014).

249. Aebersold, R. & Mann, M. Mass spectrometry-based proteomics. *Nature* **422,** 198–207 (2003).

250. Boyden, E. S. Optogenetics and the future of neuroscience. *Nat. Neurosci.* **18,** 1200–1201 (2015).

251. Susaki, E. A. *et al.* Advanced CUBIC protocols for whole-brain and whole-body clearing and imaging. *Nat. Protoc.* **10,** 1709–27 (2015).

252. Erturk, A. *et al.* Three-dimensional imaging of solvent-cleared organs using 3DISCO. *Nat Protoc* **7,** 1983–1995 (2012).

253. Schindelin, J. *et al.* Fiji: an open-source platform for biological-image analysis. *Nat. Methods* **9,** 676–82 (2012).

254. Eichenbaum, H., Sauvage, M., Fortin, N., Komorowski, R. & Lipton, P. Towards a functional organization of episodic memory in the medial temporal lobe. *Neuroscience and Biobehavioral Reviews* **36,** 1597–1608 (2012).

255. Jack, C. R. *et al.* Prediction of AD with MRI-based hippocampal volume in mild cognitive impairment. *Neurology* **52,** 1397–1403 (1999).

256. Dickerson, B. C. *et al.* MRI-derived entorhinal and hippocampal atrophy in incipient and very mild Alzheimer's disease. *Neurobiol. Aging* **22,** 747–754 (2001).

257. Jack, C. R. *et al.* Rates of beta-amyloid accumulation are independent of hippocampal neurodegeneration. *Neurology* **82,** 1605–1612 (2014).

258. Braak, H., Braak, E., Bohl, J. & Lang, W. Alzheimer's disease: amyloid plaques in the cerebellum. *J. Neurol. Sci.* **93,** 277–287 (1989).

259. Hedden, T. *et al.* Disruption of functional connectivity in clinically normal older adults harboring amyloid burden. *J Neurosci* **29,** 12686–12694 (2009).

260. Serrano-Pozo, A. *et al.* Thal Amyloid Stages Do Not Significantly Impact the Correlation Between Neuropathological Change and Cognition in the Alzheimer Disease Continuum. *J. Neuropathol. Exp. Neurol.* **0,** 1–11 (2016).

261. Seo, J. *et al.* Activity-dependent p25 generation regulates synaptic plasticity and a??-induced cognitive impairment. *Cell* **157,** 486–498 (2014).

262. Hsai, A. Y. *et al.* Plaque-independent disruption of neural circuits in Alzheimer's disease mouse models. *Proc. Natl. Acad. Sci. U. S. A.* **96,** 3228–33 (1999).

263. Robin, J. *et al.* Functional connectivity of hippocampal and prefrontal networks during episodic and spatial memory based on real-world environments. *Hippocampus* **25,** 81–93 (2015).

264. Jost, B. C. & Grossberg, G. T. The evolution of psychiatric symptoms in Alzheimer's disease: A natural history study. *J. Am. Geriatr. Soc.* **44,** 1078–1081 (1996).

265. Sperling, R. Functional MRI studies of associative encoding in normal aging, mild cognitive impairment, and Alzheimer's disease. *Ann. N. Y. Acad. Sci.* **1097,** 146–155 (2007).

266. Buckner, R. L., Andrews-Hanna, J. R. & Schacter, D. L. The brain's default network: Anatomy, function, and relevance to disease. *Ann. N. Y. Acad. Sci.* **1124,** 1–38 (2008).

267. Aggleton, J. P., Pralus, A., Nelson, A. J. D. & Hornberger, M. Thalamic pathology and memory loss in early Alzheimer's disease: moving the focus from the medial temporal lobe to Papez circuit. *Brain* aww083 (2016). doi:10.1093/brain/aww083

268. Zaborszky, L., van den Pol, A. N. & Gyengesi, E. *The Basal Forebrain Cholinergic Projection System in Mice. The Mouse Nervous System* (2012). doi:10.1016/B978-0-12-369497-3.10028-7

269. Mufson, E. ., Counts, S. E., Perez, S. E. & Ginsberg, S. D. Cholinergic system during the progression of Alzheimer's disease: therapeutic implications. *Expert Rev. Neurother.* **8,** 1703–1718 (2009).

270. Fletcher, E. *et al.* Beta-amyloid, hippocampal atrophy and their relation to longitudinal brain change in cognitively normal individuals. *Neurobiol. Aging* **40,** 173–180 (2016).

271. Eimer, W. A. & Vassar, R. Neuron loss in the 5XFAD mouse model of Alzheimer's disease correlates with intraneuronal Aβ42 accumulation and Caspase-3 activation. *Mol. Neurodegener.* **8,**

2 (2013).

272. Falke, E. *et al.* Subicular dendritic arborization in Alzheimer's disease correlates with neurofibrillary tangle density. *Am. J. Pathol.* **163,** 1615–21 (2003).

273. Carlesimo, G. A. *et al.* Atrophy of presubiculum and subiculum is the earliest hippocampal anatomical marker of Alzheimer's disease. *Alzheimer's Dement. Diagnosis, Assess. Dis. Monit.* **1,** 24–32 (2015).

274. Vann, S. D. Dismantling the papez circuit for memory in rats. *Elife* **2013,** 1–21 (2013).

275. Vann, S. D. & Aggleton, J. P. The mammillary bodies: two memory systems in one? *Nat. Rev. Neurosci.* **5,** 35–44 (2004).

276. Jung, Y. C., Chanraud, S. & Sullivan, E. V. Neuroimaging of Wernicke's encephalopathy and Korsakoff's syndrome. *Neuropsychol Rev.* **22,** 170–180 (2012).

277. Sullivan, E. V *et al.* In vivo mammillary body volume deficits in amnesic and nonamnesic alcoholics. *Alcohol. Clin. Exp. Res.* **23,** 1629–36 (1999).

278. Jucker, M. & Walker, L. C. Pathogenic protein seeding in Alzheimer disease and other neurodegenerative disorders. *Ann. Neurol.* **70,** 532–540 (2011).

279. Kayed, R. & Lasagna-Reeves, C. Molecular Mechanisms of Amyloid Oligomers Toxicity. *J. Alzheimers Dis.* **33,** S67–S78 (2013).

280. Yuan, P. *et al.* TREM2 Haplodeficiency in Mice and Humans Impairs the Microglia Barrier Function Leading to Decreased Amyloid Compaction and Severe Axonal Dystrophy. *Neuron* **90,** 724–739 (2016).

281. Canobbio, I., Abubaker, A. A., Visconte, C., Torti, M. & Pula, G. Role of amyloid peptides in vascular dysfunction and platelet dysregulation in Alzheimer's disease. *Front Cell Neurosci* **9,** 65 (2015).

282. De La Torre, J. C. Is Alzheimer's disease a neurodegenerative or a vascular disorder? Data, dogma, and dialectics. *Lancet Neurol.* **3,** 184–190 (2004).

283. Lee, L., Kosuri, P. & Arancio, O. Picomolar amyloid-β peptides enhance spontaneous astrocyte calcium transients. *J. Alzheimer's Dis.* **38,** 49–62 (2014).

284. Kuchibhotla, K. V, Lattarulo, C. R., Hyman, B. T. & Bacskai, B. J. Astrocytes in Alzheimer. *Science (80-.).* **323,** 1143d–1143d (2009).

285. Kimbrough, I. F., Robel, S., Roberson, E. D. & Sontheimer, H. Vascular amyloidosis impairs the gliovascular unit in a mouse model of Alzheimer's disease. *Brain* **138,** 3716–3733 (2015).

286. Deane, R. *et al.* apoE isoform – specific disruption of amyloid β peptide clearance from mouse brain. *J. Clin. Invest.* **118,** 4002–4013 (2008).

287. Uchihara, T., Kondo, H., Akiyama, H. & Ikeda, K. White matter amyloid in Alzheimer's disease

brain. *Acta Neuropathol.(Berl)* **90,** 51–56 (1995).

288. Iwamoto, N., Nishiyama, E., Ohwada, J. & Arai, H. Distribution Of Amyloid Deposits In the Cerebral White Matter Of the Alzheimers Disease Brain - Relationship to Blood Vessels. *Acta Neuropathol.* **93,** 334–340 (1997).

289. Kamenetz, F. *et al.* APP processing and synaptic function. *Neuron* **37,** 925–937 (2003).

290. Zhang, Y., Thompson, R., Zhang, H. & Xu, H. APP processing in Alzheimer ' s disease. *Brain* 1–13 (2011). doi:10.1186/1756-6606-4-3

291. McDuff, T. & Sumi, S. M. Subcortical degeneration in Alzheimer's disease. *Neurology* **35,** 123–126 (1985).

292. Grossi, D., Lopez, O. L. & Martinez, A. J. Mamillary bodies in Alzheimer's disease. *Acta Neurol.Scand.* **80,** 41–45 (1989).

293. Aggleton, J. P. & Mishkin, M. Mamillary-body lesions and visual recognition in monkeys. *Exp. brain Res.* **58,** 190–7 (1985).

294. Saunders, R. C. & Weiskrantz, L. The effects of fornix transection and combined fornix transection, mammillary body lesions and hippocampal ablations on object-pair association memory in the rhesus monkey. *Behav. Brain Res.* **35,** 85–94 (1989).

295. Parker, A. & Gaffan, D. Mamillary Body Lesions in Monkeys Impair Object-in-Place Memory: Functional Unity of the Fornix-Mamillary System. *J. Cogn. Neurosci.* **9,** 512–21 (1997).

296. Tsivilis, D. *et al.* A disproportionate role for the fornix and mammillary bodies in recall versus recognition memory. *Nat. Neurosci.* **11,** 834–842 (2008).

297. Yoder, R. M., Peck, J. R. & Taube, J. S. Visual landmark information gains control of the head direction signal at the lateral mammillary nuclei. *J. Neurosci.* **35,** 1354–67 (2015).

298. Hornberger, M. *et al.* In vivo and post-mortem memory circuit integrity in frontotemporal dementia and Alzheimer's disease. *Brain* **135,** 3015–3025 (2012).

299. Arendt, T., Bigl, V., Arendt, A. & Tennstedt, A. Loss of neurons in the nucleus basalis of Meynert in Alzheimer's disease, paralysis agitans and Korsakoff's disease. *Acta Neuropathol.* **61,** 101–108 (1983).

300. Sechi, G. & Serra, A. Wernicke ' s encephalopathy : new clinical settings and recent advances in diagnosis and management. *Lancet Neurol.* **6,** 442 – 455 (2007).

301. Zahr, N. M. *et al.* Associations between in vivo neuroimaging and postmortem brain cytokine markers in a rodent model of Wernicke's encephalopathy. *Exp. Neurol.* **261,** 109–119 (2014).

302. Heneka, M. T. *et al.* Neuroinflammation in Alzheimer's disease. *Lancet Neurol.* **14,** 388–405 (2015).

303. Kristensen, P. *et al.* Hypothalamic CART is a new anorectic peptide regulated by leptin. *Nature*

393, 72–76 (1998).

304. Mao, P., Meshul, C. K., Thuillier, P., Goldberg, N. R. S. & Reddy, P. H. CART peptide is a potential endogenous antioxidant and preferentially localized in mitochondria. *PLoS One* **7,** (2012).

305. M O, J., I M, M. & M J, K. CART Peptides Regulate Psychostimulants and May be Endogenous Antidepressants. *Curr. Neuropharmacol.* **9,** 12–16 (2011).

306. Gribkoff, V. K. & Kaczmarek, L. K The Need for New Approaches in CNS Drug Discovery: Why Drugs Have Failed, and What Can Be Done to Improve Outcomes. *Neuropharmacology* (2016). doi:10.1016/j.neuropharm.2016.03.021

307. Gondard, E. *et al.* Rapid modulation of protein expression in the rat hippocampus following deep brain stimulation of the fornix. *Brain Stimul.* **8,** 1058–1064 (2015).

308. Rosenberg, P. B., Nowrangi, M. A. & Lyketsos, C. G. Neuropsychiatric symptoms in Alzheimer's disease: What might be associated brain circuits? *Molecular Aspects of Medicine* **43-44,** 25–37 (2015).

309. Diffusion Time Calculator. *PhysiologyWeb.com*

310. Stigter, D., Williams, R. & Mysels, K. Micellar self diffusion of sodium lauryl sulfate. **59,** 330–335 (1954).

311. Lein, E. S. *et al.* Genome-wide atlas of gene expression in the adult mouse brain. *Nature* **445,** 168–176 (2007).